

**GROWTH AND CHARACTERISATION OF
CERTAIN ORGANIC CRYSTALS**

S. K. PREMACHANDRAN M. Sc.

THESIS SUBMITTED IN
PARTIAL FULFILMENT OF THE REQUIREMENTS
FOR THE DEGREE OF
DOCTOR OF PHILOSOPHY

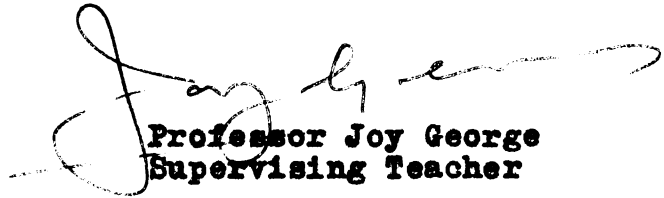
**SOLID STATE PHYSICS LABORATORY
DEPARTMENT OF PHYSICS
UNIVERSITY OF COCHIN**

1981

CERTIFICATE

Certified that the work reported in the present thesis is based on the bona fide work done by S.K. Premachandran, research scholar, under my guidance in the Department of Physics, University of Cochin, and has not been included in any other thesis submitted previously for the award of any degree.

Cochin-22
January 17, 1981



Professor Joy George
Supervising Teacher

DECLARATION

Certified that the work presented in this thesis is based on the original work done by me under the guidance of Professor Joy George in the Department of Physics, University of Cochin, and has not been included in any other thesis submitted previously for the award of any degree.

Cochin-22
January 17, 1981



S.K. Premachandran

SYNOPSIS

GROWTH AND CHARACTERISATION OF CERTAIN ORGANIC CRYSTALS

The thesis presents the results of the investigations on the crystallisation behaviour, defect structure and electrical properties of certain organic crystals--phthalic anhydride and potassium acid phthalate.

Hollow crystals of phthalic anhydride were grown from vapour. The morphology of these hollow crystals were studied in detail and a mechanism for their growth has been proposed. A closed crystal-vapour system was used to study the basal plane growth of the whiskers and the sequential growth observed, confirmed the mechanism suggested for hollow crystals. The dendritic crystals of phthalic anhydride were grown, both from the melt and solution. The observed morphologies of these dendrites are described.

Spherulites of phthalic anhydride have been grown by the artificial initiation of nucleation, from melt and solution. The variation of the substructure of these spherulites with the growth temperature was investigated. The spherulitic films having ribbon substructure were etched to reveal dislocations. A mechanism for the formation of the observed etch

pattern has been suggested. The slip occurring in these ribbons were studied and the results are presented.

Large single crystals of phthalic anhydride were grown by the Bridgman method. The shape of the growth tube, pull rate and temperature profile suitable for growing good single crystals were determined by trial and error. Potassium acid phthalate single crystals were grown from aqueous solutions. The addition of thiourea has been found to promote growth in the $\langle 001 \rangle$ direction.

Phthalic anhydride crystals were cleaved along the $\{110\}$ planes and cut perpendicular to it. The potassium acid phthalate crystals were cleaved along the $\{001\}$ plane and cut into slabs having $\{010\}$ and $\{100\}$ faces. The cleavage surfaces of phthalic anhydride and potassium acid phthalate crystals were examined by optical techniques and surface topography has been studied.

Of the various etchants used, $\text{NH}_4\text{OH} : \text{H}_2\text{O}$ in the ratio 1 : 3 by volume have been found to delineate dislocations on the $\{001\}$ and $\{110\}$ surfaces

of phthalic anhydride. The morphology of etch pits on these faces have been studied in detail and the dislocation densities on them have been determined. On potassium acid phthalate cleavage surfaces, an etchant consisting of one part of water in five parts of acetone by volume was found suitable to reveal the dislocations. The dislocation configurations on these crystals have been examined by successive etching. The effect of annealing on these crystals has been discussed in the light of the observed dislocation configurations. Pyramidal indentations were made on the different faces of these crystals and the slip traces observed were used to identify the slip planes.

The anisotropy of electrical conduction in phthalic anhydride and potassium acid phthalate single crystals were investigated by measuring the conductivity in the various directions at different temperatures and the activation energies have been calculated.

CONTENTS

		Page
SYNOPSIS	1
INTRODUCTION	1
CHAPTER ONE	PHYSICS OF CRYSTAL GROWTH	
1.1	Introduction	7
1.2	Theory of Crystal Growth	7
1.3	Dissolution of Crystal Faces	20
CHAPTER TWO	TECHNOLOGY OF CRYSTAL GROWTH	
2.1	Introduction	24
2.2	Growth from Melt	24
2.3	Growth from Vapour	33
2.4	Growth from Solution	38
2.5	Hydrothermal Growth	40
2.6	Flux Growth	41
2.7	Growth from Gels	43
CHAPTER THREE	MORPHOLOGY OF CRYSTALS	
3.1	Introduction	45
3.2	Morphology and Structure	46
3.3	Morphology and Bonding	47
3.4	Crystal Habits	48
CHAPTER FOUR	DISLOCATIONS IN CRYSTALS	
4.1	Introduction	66
4.2	The Strain and Stress fields around Dislocations	67
4.3	Dislocation Reactions	72
4.4	Cleavage	76
4.5	Plastic Deformation	78
4.6	Direct Observation of Dislocations	80

		Page
CHAPTER FIVE	ELECTRICAL CONDUCTIVITY OF ORGANIC CRYSTALS	
5.1	Introduction	92
5.2	Observable Parameters	94
5.3	Conductivity Measurements	97
5.4	Charge-Transfer Complexes	100
CHAPTER SIX	EXPERIMENTAL TECHNIQUES	
6.1	Introduction	103
6.2	Material Preparation	103
6.3	Growth of Crystals and Specimen Preparation	104
6.4	Defect Structure	112
6.5	Surface Topography of Crystal Cleavages	113
6.6	Investigations on Slip Systems	116
6.7	Conductivity Measurements	117
CHAPTER SEVEN	RESULTS AND DISCUSSION	
7.1	Introduction	119
7.2	Growth of Crystals	120
7.3	Dislocation Etch Studies	139
7.4	Investigations on Slip	149
7.5	Topography of Crystal Surface	150
7.6	D.C. Conductivity of Phthalic Anhydride and Potassium Acid Phthalate Crystals	151
CONCLUSION	160
REFERENCES	162
ACKNOWLEDGEMENTS		

INTRODUCTION

Organic crystals provide a variety of solids with interesting electrical properties. The properties include ferroelectricity (Thiourea [1], Guanidinium Uranyl Sulfate trihydrate [2]), piezoelectricity (Phenanthrene [3]) and photoconductivity (Anthracene [4]). One dimensional conductors (TTF-TCNQ [5]) and semiconductors of organic origin have been reported.

The industrial interest in this field is mainly due to the existence of a large variety of molecular species and the possibility of synthesising new materials with specific properties, once the link between the structure and properties is known. It has long been recognised that the entrance to the field of 'molecular electronics' is possible only through the production of complex molecules in a high degree of purity and growth of large single crystals of high perfection.

The following comment on the growth of single crystals by Spedding [6] seems to be pertinent here. 'If a certain property is to be measured, 80% of the effort and ingenuity will either be spent on producing pure metals and alloys, in growing single crystals,

without contaminating them or in characterising the crystals, so that one knows what one is measuring. Only about 20% of the effort will be spent on measuring the property'.

The growth of single crystals of organic compounds is rather difficult, unlike the inorganic counterpart. The non-availability of suitable solvents often forbid the use of solution growth techniques. Vapour growth usually result in either small crystals or crystalline aggregates. The supercooling tendency of organic materials, their low thermal conductivities and thermal decomposition often make the use of melt growth techniques difficult. Organic materials always contain some impurities and hence extensive purification procedures are to be applied before growth. A combination of chromatographic, zone-refining, sublimation and recrystallisation techniques are often to be applied. The usual growth techniques are to be modified to grow organic crystals. Both anthracene [7] and anthraquinone [8] have been thus grown by the Bridgman method. Also Bleay et al [9] have successfully grown benzil and benzophenone single crystals by the Czochralski pulling method.

The perfection of organic crystals are even less investigated than the growth. Only a limited number of organic crystals have been studied by techniques such as X-ray topography, neutron topography, decoration,

chemical and thermal etching. The volatility of organic crystals prevents the use of electron microscopy which would otherwise have been a very valuable technique.

The electrical properties of organic crystals have been investigated from the point of view of their insulating rather than their conducting properties. The characteristic resistivities vary from 10^{14} ohm cm to 10^{-2} ohm cm with a carrier concentration of 10^6 to 10^{19} carriers per cm^3 . The typical mobilities vary from 10^2 to 10^{-6} $\text{cm}^2 \text{ volt}^{-1} \text{ sec}^{-1}$. The lack of published data on conductivity is largely due to the difficulties encountered in the measurement of very low voltages in very high impedance circuits. The activation energy for conduction measured in organic crystals by various workers shows a relative scatter in the values--from 1.0 to 2.8 eV for anthracene [10,11,12] and 0.72 to 3.7 eV for naphthalene [13]. This may be due to the difference in the degree of purity of crystals or the different electrode configurations used by workers in the field.

The exact conduction mechanism of organic crystals is not well established. Theoretical progress in the area of electrical conduction in organic crystals has been limited compared to the experimental data available. The majority of studies on organic crystals

have been conducted on aromatic compounds due to the availability of data on their structure and the low activation energy for semiconduction in these materials.

Phthalic anhydride, a member of the aromatic acid anhydrides and potassium acid phthalate, the potassium salt of phthalic acid, were studied as a part of the investigations carried out in this laboratory on the growth and characterisation of organic crystals.

Phthalic anhydride is extensively used as the primary material for the production of cellophane [14] and as a curing agent in epoxy resins [15]. The vibrational spectra of this material have been reported by Hase [16]. Phthalic anhydride forms a large number of donor-acceptor complexes. Complexes with phthalic anhydride as the acceptor have been investigated in diethyl ether-isopentane glass [17]. Recently Rastogi et al [18] have detected the formation of a 1 : 1 complex of phthalic anhydride with 8-hydroxyquinoline. The most promising result of this and other related materials have been the preparation of a series of more than hundred new polymers with specific resistivities distributed over a wide range [19,20,21]. The material has been found to possess triboluminescent properties [22,23,24], and the triboluminescence spectrum of phthalic anhydride measured at room temperature has been found to differ markedly from the photoluminescence spectrum unlike other materials.

All the reported studies were conducted on pressed pellets, in diethyl ether-isopentane glass or on powders. It is hoped that the growth and characterisation of large single crystals will lead to a better understanding of the different properties of this crystal.

Potassium acid phthalate, crystallises in the orthorhombic class [25] like phthalic anhydride. But the structure is ionic. The material in powder form has been reported to be piezoelectric [26]. The crystal is currently used in the field of ultra soft X-ray spectroscopy due to the large 2d-spacings [27]. Though Bearden et al [28] have reported that the crystals were free from twinning and other flaws, not much work has been reported on the growth and properties of potassium acid phthalate crystals. And it was felt, it would be interesting to study in detail the growth, defect structure and electrical properties of this material also.

Part of these investigations have been published in the form of following papers:

1. Growth and morphology of phthalic anhydride crystals
(1977) J. Crystal Growth 37, 189.
2. Dendritic growth of phthalic anhydride crystals
(1977) J. Crystal Growth 41, 325.

3. Growth of phthalic anhydride in a closed crystal-vapour system
(1978) *J. Crystal Growth* 43, 126.
4. Growth of phthalic anhydride spherulites
(1979) *J. Crystal Growth* 46, 297.
5. Growth and perfection of phthalic anhydride single crystals
(1979) *J. Phys. D: Appl. Phys.* 12, 1129
6. Growth and characterisation of potassium acid phthalate single crystals
Presented in the National Conference on Crystallography, 1980.

CHAPTER ONE

PHYSICS OF CRYSTAL GROWTH

1.1. Introduction

The industrial demand for better crystals and crystals of new materials with extraordinary properties, promoted research in the science of crystal growth and their characterisation both in the academic and technological fields. In the last decade the science of crystal growth has developed into a multi-disciplinary subject. The basic concepts have been formulated and the observations on the growth process of many crystals have been successfully explained. Yet the theoretical progress is far from being able to point out a successful set of parameters to grow crystals of a particular material.

1.2. Theory of Crystal Growth

The evolution of crystal growth theory can be conveniently outlined under two separate sections, one dealing with the growth of perfect crystals and the other on the growth of imperfect crystals.

a) Growth of perfect crystals

The first attempt to study the growth of crystals on thermodynamical grounds was made by Gibbs [29]. He considered the phase transformation

from vapour to solid resulting in crystals and formulated the minimum free energy criterion which states that

$$\sum_{i=1}^n \sigma_i F_i \text{ is a minimum, where } \sigma_i \text{ is the}$$

surface free energy of the i^{th} face of area F_i , for a crystal surface in equilibrium with its vapour. The theory was further developed by Curie [30] and Wulff [31] and others.

If P_i is the perpendicular distance of the i^{th} crystal face from an interior point of the crystal, then the volume of the crystal is

$$V = 1/3 \sum_i P_i F_i \quad (1)$$

with an energy

$$E = \sum_{i=1}^n \sigma_i F_i \quad (2)$$

For an infinitesimal change in volume,

$$dV = \sum_{i=1}^n F_i dP_i \quad (3)$$

Comparing the equations we get

$$P_i \propto \sigma_i \quad (4)$$

Bravais [32] attacked the problem by considering the growth velocities of various crystal faces and the densities of lattice points on them. This so called

theory of reticular densities, predicted the disappearance of fast growing faces and the survival of slow growing ones. Soehncke [33] introduced the idea of surface free energies and showed that the faces with greatest reticular densities are those with minimum surface free energy.

An atomic theory of crystal growth was put forward by Kossel [34] and Stranski [35] in the nineteenth century. In this model the atoms constituting the crystal are arranged in three dimensional order so as to give each atom a specific structural environment. A cubic crystal can be thought as made up of small cubes which represents unit cells. The interaction with cubes is through two different bonds of strength ϕ_1 and ϕ_2 . ϕ_1 is the strength of the nearest neighbor bond while ϕ_2 is the strength of the second nearest neighbor bond. According to this picture the various atomic sites on a closed packed surface can be assigned different energies.

The surface of such a crystal will appear atomically smooth at absolute zero or partially covered by another layer. In the latter case the difference in level is an atomic spacing and is called a step. As the temperature is raised, the atoms on the surface of the

crystal will get thermally agitated and will gain an energy sufficient enough to overcome the binding energy. This process will introduce vacant sites on smooth faces and create kinks along the step. On reaching the dynamic equilibrium, the surface gets active with the production of kinks, adsorbed atoms and vacancies. Atoms get absorbed on the crystal faces and they migrate towards a step and moves along it to a kink position to get incorporated or re-evaporated. The energies at a surface site, on a step and on a kink are $\phi_1 + 4\phi_2$, $2\phi_1 + 6\phi_2$ and $-4\phi_1 - 6\phi_2$ respectively, and are related to each other as

$$\phi_1 + 4\phi_2 > 2\phi_1 + 6\phi_2 > -4\phi_1 - 6\phi_2 \quad (5)$$

To commence growth, the saturation is to be increased. Now more and more atoms get absorbed and they get deposited on the step kinks. As a result the step advances with a certain velocity. Soon the step disappears after completing the surface. Further growth requires a step which in turn requires nucleation on an atomically smooth surface. This requires an additional energy. Thus the rate of growth will depend not on the velocity of step advance but on the frequency of nucleation.

1) Surface migration of adsorbed molecules

An adsorbed molecule on an atomically smooth crystal face can migrate considerable distances before it get incorporated in the crystal. The migration distance x_s of the adsorbed molecule is given by the Einstein's formula

$$x_s^2 = D_s \tau_s \quad (6)$$

where D_s is the diffusion coefficient and τ_s the mean life on the surface. In the Kossel-Stranski model

$$x_s \sim a \exp (3\phi_1/2KT) \quad (7)$$

where ϕ_2 , the second neighbor bonding is neglected.

2) Advance of steps

The migrating molecules get incorporated at kink sites on the steps. According to Burton, Cabrera and Frank [36] there exist a finite number of kinks in the steps at any temperature. The mean distance between kinks is taken as x_0 which is several orders of the lattice constant 'a' and much shorter than the migration distance.

$$x_0 \sim \frac{1}{2} a \exp (\phi_1/2KT) \quad (8)$$

The supersaturation,

$$\sigma = \alpha - 1 \quad (9)$$

where $\alpha = P/P_0$, is the ratio of the actual vapour pressure to that at equilibrium. Similarly the supersaturation of adsorbed atoms is given by

$$\sigma_s = \alpha_s - 1 \quad (10)$$

where

$$\alpha_s = n_s/n_{s_0} \quad (11)$$

n_s is the actual and n_{s_0} the equilibrium concentration on the surface.

For a straight step extending in the x-direction of the orthogonal Cartesian system, the steady state condition can be written as

$$x_s^2 \nabla^2 \psi = \psi \quad (12)$$

where $\psi = \sigma - \sigma_s$ (13)

Near a step,

$$\sigma_s = \sigma \quad (14)$$

and far away from the step,

$$\sigma(y) = \sigma [1 - \exp(-|y|/x_s)] \quad (15)$$

The rate of advance of steps is given as

$$v = 2\sigma x_s \exp(-W/KT) \quad (16)$$

where the diffusion from either side of the step is

taken into consideration, ν is a frequency factor and W , the evaporation energy.

For a parallel flow of steps separated by a distance y_0 the velocity of steps is given by

$$v(y_0) = v \tanh(y_0/2x_g) \quad (17)$$

and for a circular surface step of radius ρ ,

$$v(\rho) = v (1 - \rho_0/\rho) \quad (18)$$

where ρ_0 is the radius of the critical nucleus.

3) Nucleation on a surface

Due to the thermodynamic fluctuations on the crystal surface, steps may be created. Once the step has spread along the whole surface, further growth is arrested due to the absence of a step. Hence a nucleation of a monomolecular island is necessary. This requires an additional energy. A cluster of molecules formed on the surface will either disintegrate or grow depending upon the radius of the island. If we assume that only a single nuclei of monomolecular height is formed and it has a circular shape with radius ρ then the excess free energy g of the system is given by

$$g(\rho) = -KT \log \alpha \pi \rho^2/a^2 + \gamma 2\pi\rho/a \quad (19)$$

where α is the supersaturation and γ the surface tension at the interface. Once the nucleus is formed

due to the thermodynamic fluctuations it will spread and again leave it smooth. For further growth a fresh nucleation is necessary. Thus the growth is a microscopically discontinuous function of time. The growth rate of crystals is governed by nucleation rate rather than the growth velocity of surface steps.

The thermodynamic probability of nucleation is

$$\exp(-g_0/KT) = \exp[-\pi(\gamma/KT)^2/\log \alpha] \quad (20)$$

where g_0 is the excess free energy for a nucleus of critical radius r_0 . The rate of nucleation I per unit area per unit time thus becomes

$$I = \nu N_0 \exp(-g_1/KT) \quad (21)$$

where ν is the number of molecules approaching the nucleus per second and N_0 is the number of available surface sites per unit area. The kinetic approach of Becker and Doring [37] and Frank [38] yields a similar equation for nucleation rate.

The rate of growth of a singular surface is controlled by the rate of nucleation I and the surface step velocity v . If the average time for nucleation

$$t_n \sim 1/IS \quad (22)$$

and the time for a surface step to sweep the complete

surface is

$$t_n \sim \sqrt{s/v} \quad (23)$$

Then the rate of growth of a singular surface is given by

$$R_n \sim a S I \quad (24)$$

where a is constant and S is the surface area.

The two dimensional growth model [39] discussed above takes into consideration only the possibility of existence of single nucleus. Hillig [40], Hayashi-Shichiri [41] and others considered the probability of nucleation of more than one nucleus and found that the growth rate is given by

$$R \sim a I^{1/3} V^{2/3} \quad (25)$$

which is independent of S unlike equation (24). In real crystals however the observed growth rates are far greater than that predicted by this model. Against a supersaturation of about 25 % to 50% predicted necessary for growth by this model, crystals have been known to grow at such small supersaturations as 1% or lower.

b) Growth of imperfect crystals

The discrepancy between the observed growth rate and that predicted by the two-dimensional growth theories mainly arises from the difficulty of nucleation

on an atomically smooth surface. The necessity of creation of a new step, after a step has swept a crystal face, was circumvented by Frank [42], by assuming the presence of screw dislocations in real crystals. The screw dislocations emerging on a crystal surface produces a spiral step anchored at the dislocation. This mechanism thus provides steps with kinks. To an observer from above the spiral will appear as rotating.

The mathematical treatment of such a spiral is outlined below. If ω is the rotational velocity in radians/second, the growth rate is given by

$$R = (\omega / 2\pi)h \quad (26)$$

where h is the step height of the spiral. Taking as constant with time, the step velocity of the curved steps may be calculated. The velocity of a curved step of radius ρ is greater than the straight step by

$$v = v_g(1 - \rho_c/\rho) \quad (27)$$

where ρ_c and ρ are the radius of the critical nuclei and real nuclei.

1) The radius of curvature of steps (ρ)

Considering a portion of a circular step $y = f(x)$, such as RPQ in figure (1), the point P is

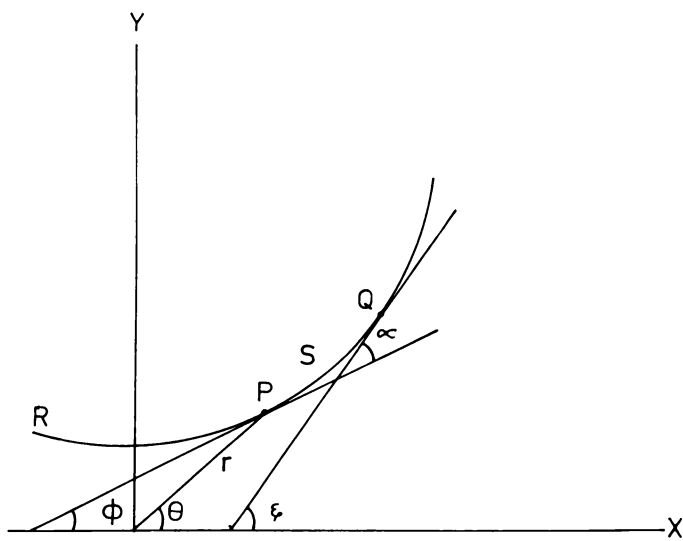


Fig.(1) A portion of a circular step.

represented by $P(r, \theta)$ in polar coordinates. The tangents to P and Q cut the x-axis at angles ϕ and ξ and make themselves an angle of α . Now the average curvature of the arc PQ ($=S$) is given by

$$\frac{\xi - \phi}{S} = \frac{[(\phi + \alpha) - \phi]}{S} \quad (28)$$

as $S \rightarrow 0$ the curvature at P is given by

$$\begin{aligned} K_c &= \lim_{S \rightarrow 0} [(\phi + \alpha) - \phi] / S \\ &= d\phi / ds \end{aligned} \quad (29)$$

The radius of curvature is thus

$$\rho = 1/K_c = ds/d\phi \quad (30)$$

In Cartesian coordinates

$$\tan \phi = dy/dx = y' \quad (31)$$

$$\frac{d}{ds}(\tan \phi) = [1+(y')^2] d\phi/ds \quad (32)$$

$$y'' dx/ds = [1+(y')^2][1/\rho] \quad (33)$$

$$\text{and } dx/ds = [1+(y')^2]^{-1/2} \quad (34)$$

$$\begin{aligned} \text{Solving for } \rho & \\ \rho &= \frac{[1+(y')^2]^{3/2}}{y''} \end{aligned} \quad (35)$$

In polar coordinates

$$[1+(y')^2]^{3/2} = (dr/dx)^3 [1+r^2(d\theta/dr)^2]^{3/2} \quad (36)$$

$$\text{and } y'' = (dr/dx)^3 [d^2y/dr^2](dx/dr) - (d^2x/dr^2)(dy/dr) \quad (37)$$

The value of ρ is thus

$$\rho = \frac{[1+r^2(\theta')^2]^{3/2}}{2+r^2(\theta')^3+r\theta''} \quad (38)$$

where $\theta' = d\theta/dr$ and $\theta'' = d^2\theta/dr^2$

2) Velocity normal to a rotating spiral step

To derive an expression for the velocity of step, consider a portion of the spiral step RPQ as shown in figure (2). The point P(r, θ) has a radius of curvature ρ . The radius vector r is rotating anticlockwise or clockwise with an angular velocity ω . Resolving the tangential and radial velocities, let PA represent $r\omega$ and PC the radial component V_ρ . In the completed parallelogram ADGP, $\angle APD = \alpha = \angle PDC$ and $\sin \alpha = PC/CD = PC/AP = V_\rho/r\omega$.

For an infinitesimal rotation $d\theta$ the radius changes by dr and

$$\sin \alpha = EF/PF = \frac{1}{[1+r^2(d\theta/dr)^2]^{1/2}} \quad (39)$$

Equating these equations (38) and (39)

$$V_\rho = \frac{r\omega}{[1+r^2(d\theta/dr)^2]^{1/2}} \quad (40)$$

3) The spiral

If the growing step is curved and has a velocity V_p along the radius of curvature, the velocity of the curved step is related to that of a straight step on the surface by equation (27). Thus equating V_p from equations (40) and (27)

$$r\omega/[1+r^2(d\theta/dr)]^{1/2} = V_a(1 - \rho_c/\rho) \quad (41)$$

The solution of (41) determines the relation between r and θ . For large values of r equation (41) reduces to give

$$\theta = (\omega/V_a)r + \text{constant} \quad (42)$$

and for small values of r

$$\theta = (1/2\rho_c)r + \text{constant} \quad (43)$$

Both equations (42) and (43) represent an Archimedean spiral, with a constant step spacing Y_0 , ($Y_0 = 19\rho_c$).

4) Experimental observations of growth spirals

The observation of spiral steps on beryl crystals by Griffin [43] with the aid of bright field microscopy strongly supported the theory of Burton, Cabrera and Frank. Since then, growth spirals have been observed on SiC and other mineral and synthetic crystals [44]. The spiral step appears either as circular or as

polygonal depending upon the number of kinks available at the steps. Spirals have been observed on NaCl [45] FeCr_2S_4 [46] and $n\text{-C}_{28}\text{H}_{58}$ [47]. Nakada et al [48] have observed unit cell steps occurring from a screw dislocation with Burgers vector normal to the surface. Thus the Frank mechanism can be considered to be correct. The various forms of spirals and the forms resulting from the interaction of two or more spirals have been discussed in detail by Verma [49] and Amelinckx [50].

1.3. Dissolution of Crystal Faces

Dissolution of crystals is an important crystal processing technology as well as a means to study the fundamentals of crystal growth. The dissolution process is either used to dissolve semiconductor crystals in localised areas defined by a masking film or to reveal dislocations, by the preferential dissolution at their emergence points.

Dissolution of crystals, which is essentially the reverse phenomenon of growth, can be understood in terms of the same concepts involved in the growth of crystals. The surface steps, along with the active kinks in them, sweep across the vicinal faces during growth. In dissolution these normal steps will recede and disappear. In the two dimensional theories of

crystal growth this disappearance of steps will leave an atomically smooth surface. The difficulty of removal of a molecule from these surfaces makes the process a microscopically discontinuous function of time.

In the BCF model, the receding steps, on intercepting an emergent screw dislocation, becomes curved. Dissolution, now takes place preferentially at those points which leaves a spiral depression instead of a spiral hill on growth. Cabrera and Levine [51] have proposed a theory for the dissolution process in crystals having screw dislocations. If v is the normal velocity of a step located at a distance r from the screw dislocation which has a radius of curvature ρ , then v is given by

$$v = v_{\infty} [1 - (\rho_c/\rho) - (r_0 \rho_c/r^2)] \quad (44)$$

where v_{∞} is the normal velocity of a step located at large distance and ρ_c is the radius of the critical nuclei. The value of ρ_c is given by

$$\rho_c = \gamma \Omega / \Delta \mu_0 \quad (45)$$

where γ is the surface free energy, Ω is the volume occupied by one molecule and $\Delta \mu_0$ the difference in the chemical potential of the surrounding medium and the crystal. In equation (44) r_0 is expressed as

$$r_0 = \mu b^2 / 8\pi^2 \gamma \quad (46)$$

where \bar{b} is the Burgers vector of the screw dislocation. Equation (46) gives a measure of the strain energy around the dislocation.

The rotating steps associated with a screw dislocation can be represented by

$$\theta = f(r) - \omega t \quad (47)$$

In polar coordinates the normal velocity v and radius of curvature are given by

$$v = -r \dot{\theta} / [1 + (r \theta')^2]^{\frac{1}{2}} \quad (48)$$

and

$$\rho = [1 + (r \theta')^2]^{\frac{3}{2}} [2 \theta' + r \theta'' + r^2 \theta'^3] \quad (49)$$

where $\dot{\theta} = \frac{\partial \theta}{\partial t} = -\omega$

$$\theta' = \frac{\partial \theta}{\partial r} \quad \text{and} \quad \theta'' = \frac{\partial^2 \theta}{\partial r^2}$$

Introducing $r = s \rho_c$

$$r (\partial \theta / \partial t) = s (\partial \theta / \partial s) = \tan \phi \quad (50)$$

where ϕ is the angle between the radius vector and the tangent to the step

$$= [1 - (s_0/s)^2] \sec \phi - (1/s) \tan \phi - \omega_1 s \quad (51)$$

Solving for $\phi(s)$

$$\phi(s) = \frac{1}{2}\pi - 1/\omega_1 s + \frac{1}{\omega_1 s^2} - \dots + \dots \quad (52)$$

for $s \gg 1$.

Depending upon the values of s_0 , being greater than zero or less than zero, growth or dissolution will take place. The direct observation of spiral depressions have been able to confirm the mechanism [52].

CHAPTER TWO

TECHNOLOGY OF CRYSTAL GROWTH

2.1. Introduction

The demand for large and perfect single crystals for devices, initiated a search for understanding the basic parameters involved in the process of crystal growth. This resulted in considerably improving the technology of producing highly perfect crystals. The present chapter deals with the technological aspects of the different growth methods currently employed.

2.2. Growth from Melt

For the growth of single crystals from melt, the transition from an equilibrium state in which the substance is completely molten to a state where the substance is completely solid, is to be controlled effectively. The portion of the grown crystal serves as a conducting path for the latent heat and the conductivities often coincide with the direction of easy growth. The growth from melt thus essentially involves the control of temperatures. The various methods described below achieves this by a variety of techniques.

a) Czochralski pulling

This technique proposed in 1918 still remains the most reliable method for the growth of large single crystals in a relatively short time. In this method the material to be grown as single crystal is melted in a crucible. A seed crystal is introduced into the melt and then withdrawn slowly. The seed crystal is often rotated while pulling to attain thermal symmetry and to stir the melt.

The various parameters that can be controlled are the rotation and pulling speeds, atmosphere of growth and temperature of growth. The efficiency of the method thus depends upon the smooth rotation and pull rates as well as the constancy of temperature of the melt.

The ideal materials suitable for pulling are those having a congruent melting point, a low vapour pressure and low viscosity. The absence of a phase change in the range of room temperature and growth temperature is desirable.

(1) Crucibles

The crucible material is to be so selected that it is insoluble or slightly soluble in the melt. Crucibles should be readily cleanable so that

impurities can be easily removed. Since crystal pulling often involves high temperatures, crucibles should have high strength and low porosity. If r.f. heating is used the resistance of the container is of importance. The non-uniformity of the crucibles will develop hot-spots and the temperature of the melt will vary laterally producing a non-circular cross section in the pulled crystal.

(ii) Methods of heating

The melt from which the crystal is being pulled should be heated upto an appropriate temperature and held constantly. A variety of techniques have been used to heat the charge. Resistance heating, in which the heating element is wires or tapes of nichrome, kanthal, tungsten or stainless steel [53], is widely used. Machined graphite or silicon carbide heaters which forms self-supporting heaters are used in the high temperature region [54]. Radio frequency heating is the most commonly used method of heating which has the advantages of ease of control and operation [55]. R.f. heating only heats the outside layer of the susceptor. The depth of this layer D called the skin depth is given by

$$D = \frac{3570}{\sqrt{f\mu}} \text{ cms} \quad (53)$$

where f is the frequency and ρ is the resistivity. As the frequency is reduced the skin depth is increased resulting in the uniform heating of the crucible. Frequencies of the order of 10KHz to 500KHz have been found to be the most useful.

(iii) Seeds

The chief advantage of Czochralski pulling method is that crystals of desired orientation can be grown by using a suitably oriented seed. Seeds of low dislocation density should be selected and etched to remove the work damaged outer layer. The seed is usually annealed to reduce the dislocation content. If a suitable seed crystal is not available polycrystalline material, single crystals of another material, a capillary tube or wires of non-reactive metals may be used. In order to grow better quality crystals the diameter of the crystal is reduced and then increased to the desired diameter. This necking operation, helps to eliminate the propagating dislocations from the seed and to select a single grain from the polycrystalline seed for further growth.

(iv) Pull and rotation rates

The rotation of seeds provide effective stirring of the melt decreasing the thermal gradient present in it. The quality of crystals is dependent

on the nature of the solid-liquid interface. A flat interface avoids both non-uniform impurity distribution and facet formation. The study of flow patterns [56] have shown that alternate stopping and/or reversing the rotation prevents the incorporation of impurities into the crystal.

The pulling rate controls the diameter of the crystal. The pull rate if increased will result in the reduction of the diameter of the growing crystal. The same effect can also be produced by increasing the temperature of the melt. Often control of both is required to perform the necking operation. An increase in diameter of the crystal increases the strain and result in the production of dislocations. Often a compromise is to be made between the ultimate crystal diameter, melt temperature and dislocation density.

(v) Modifications on the Czochralski system

The conventional apparatus have been modified by many workers to suit the different requirements for growing specific materials. Miyazawa et al [57] have effectively controlled the diameter of the growing crystals automatically by the use of an analogue control coupled with a crystal weighing system. Mateika et al [58] have described the details of a typical Czochralski

crystal puller with automatic diameter control. For InSe [59] a floating disc with a rectangular slit over the melt have been found to improve the crystal quality.

The liquid encapsulated Czochralski (LEC) method [60] uses a thick blanket of molten boric oxide and a sufficiently high pressure over the melt to prevent the decomposition and escape of vapours. The need for high pressures to prevent the loss of vapours of volatile compounds have resulted in the design of chambers which can withstand such pressures [61].

b) Bridgman method

In this method the control of the transition from melt to solid is effected by controlling the temperature at the melt-solid interface. The furnace often has two halves separated by an insulating disc. The upper half is maintained at a temperature higher than the melting point of the material while the lower at a temperature below it. The material in a tubular container is held in the upper zone so as to melt completely. The container, suspended from a wire is then lowered to the second zone with the help of a reduction motor. Spontaneous nucleation occurs at the tip of the container as it traverses the gradient. For specific materials the tip shape [62], temperature

gradient [63] and the lowering rate are found to be of importance. To select a single grain out of the many formed during the spurious nucleation a constriction in between the main body of the container and tip, is found to be effective.

(i) Containers

The containers vary from glass, silica and quartz to refractory materials [64]. For low melting point materials glass containers can be conveniently used. This may be evacuated and then sealed. For high melting point materials graphite, carbon, platinum and some refractory oxides have been used. The bulk of the heat of fusion liberated on solidification is to be removed by conduction along the container and through the grown crystal. For materials having low temperature conductivities silica tubes coated with graphite have been found successful.

(ii) Furnaces

Depending upon the temperature required, the furnaces can be made from tubes of glass or graphite wound with kanthal wire. R.f. heated furnaces can also be used. The temperature profile is to be carefully shaped by proper winding or through the reduction

of tube diameters. The general profile of temperature depends upon whether both ends of the furnace tubes are closed or opened.

(iii) Traverse mechanism

Many variants of this method exists in which either the crucible is lowered or the heater is raised, slowly. In the former case rotation of the crucible while lowering have been found to increase the probability of strain-free single crystal growth. The movement of either crucible or furnace can be made by a simple clockwork mechanism or other complex rotation lowering systems [65].

The method has several disadvantages. The crystal, being confined to the crucible, will be highly strained. Solids which expands on solidification cannot be grown by this method. The orientation of the crystal cannot be controlled.

For materials having low melting points and low decomposition pressures externally supported crucibles have been used to prevent the thermoelastic expansion and subsequent explosion [65]. Other variants of this method have been discussed in detail by Fischer [66].

c) Zone melting

In zone melting, a small portion of the relatively large ingot is melted and the molten zone is

made to travel along the length of the charge. This method, suggested by Pfann [67] is mainly intended for the purification of materials. The technique can be used to grow single crystals as well.

(1) Zoning in a container

For successful zoning, the container for the charge should have a good lateral heat transfer and a poor longitudinal heat transfer. To achieve this, the container walls are made as thin as possible and in special cases, tubes made up of alternate rings of good and poor conductors pressed together have been designed. For horizontal zone melting the cross-sections of the container vary from semi-circular to trapezoidal. The longitudinal shape should be selected so as to minimise the strain due to solidification. Radial, helical and spiral models have been described by Pfann [68].

The molten zone should preferably have a constant length, a stable solid-liquid interface and a well defined thermal gradient. For materials having low thermal conductivities, the zone width tends to vary. This has been overcome by slowly rotating the container about its axis. Intermittent rotation has been found to be more effective [69].

(ii) Zone refining without containers

Materials which are reactive at their melting point cannot be purified or grown as single crystals by zoning in a container due to the container contamination. The need for a container in such cases have been avoided by using a compacted rod of the material held vertically. A small heater produces a molten zone, which holds the two vertical colinear rods by the surface tension. The molten zone is made to traverse the rod slowly in one direction and fast in the other direction. This method called the Floating Zone Method (FZM) has been successfully used for the growth of LaB_6 [70] and other materials [71,72].

2.3. Growth from Vapour

Growth from vapour phase is the most versatile growth process, for the production of pure crystals. Vapour growth of epitaxial films on similar or foreign substrates has immense application potentialities in the semiconductor, opto-electronic and acousto-electric devices.

Any substance, which has appreciable vapour pressure, may be grown as single crystals by condensation on a comparatively cold surface. During growth, molecules

or atoms get incorporated into the kinks on a step after the adsorption and diffusion. A fraction get reevaporated after diffusion.

a) Physical transport techniques

In this technique the polycrystalline source material is heated to appropriate temperatures and the vapour is made to condense on an externally cooled substrate. The problem of crucible material contamination can be avoided in this method by using an electron-beam, focussed on the charge. High power lasers may also be used [73]. Flash evaporation of stoichiometric powders [74] and molecular beam techniques [75] can also be considered as physical transport methods.

Single crystals can be grown by sublimation where the substance is converted directly from the solid to vapour and back again to solid. This may be assisted by vacuum. To obtain flawless crystals the growth rate is to be controlled by working under low supersaturations. The temperature difference between the source and substrate may be conveniently controlled to produce optimum supersaturations. The rate of transfer of molecules, may be further restricted by the use of an inert gas, which then becomes diffusion controlled.

Travelling containers or heaters have also been used satisfactorily for the growth of crystals from vapour. In this technique a quartz ampoule filled at one end with the source material is passed through a furnace whose temperature profile has a single peak. The ampoule can either be closed or plugged with a loose fitting plug. The presence of a tapered end at the growth end has been found to often promote the growth of single crystals. Both horizontal and vertical pulling of heater or container have been found effective for specific materials.

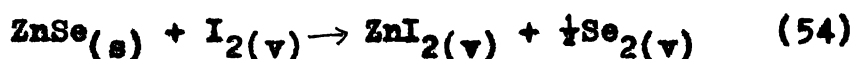
Excellent crystals of hexamethylene tetramine and urotropine have been grown by Honingman [77] and Heyer [78]. The heating was achieved by a metal block thermostat and nucleation was promoted by a cold spot. The latter incorporated provision for the measurement of growth rates of individual crystal faces.

b) Chemical transport techniques

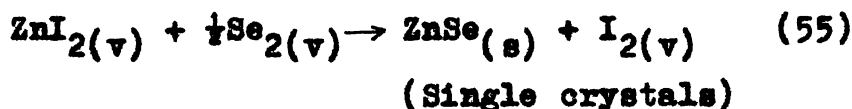
In chemical transport technique, the material to be grown as single crystals is made to react with a transporting agent to convert the same into a volatile material and deposition is made by inducing the reverse chemical reaction. The process is mainly used in

systems which has low vapour pressures by themselves and can undergo a reversible chemical reaction.

For the growth of ZnSe, the material is enclosed in a tube with a small amount of iodine gas. At a temperature T_1 , the material kept at one end of the tube reacts with iodine to form ZnI_2



The vapours travel by convection to the other end kept at a temperature T_2 favourable for the reverse reaction,



The ZnSe is deposited in the solid form in this region. Under controlled conditions single crystals have been found to form.

In general the overall reaction for the transport of an element A by an agent Y may be written as



The equilibrium constant K is given by

$$K = \frac{P(AY_y)}{(PY)^y} = \frac{1}{\alpha_A} \quad (57)$$

where α_A is the equilibrium activity of A. If the

value of α_A is below unity, volatilisation will result and if above unity, deposition. This can either be brought out by changing the pressure or the temperature of the system. Due to the convenience the latter is always preferred wherever possible.

c) Chemical vapour deposition (CVD)

CVD is one of the many techniques used, by which a solid material can be deposited on a support. In this method a chemical reaction is used to produce a solid deposit from the gaseous reactants. Currently three different types of reactions are used for the production of single crystal films, viz- 1) the pyrolysis of hydrides, 2) halide reduction and 3) the direct chemical reaction between volatile species to form the desired compound.

For the growth of silicon the reduction of SiH_4 or the reduction of SiCl_4 [79] in presence of hydrogen gas can be used. GaAs, GaP or $\text{GaAs}_{(1-x)}\text{P}_x$ can be grown by the direct reaction of the type



where M is either As or P.

Tietjen et al [80] have grown $\text{GaAs}_{(1-x)}\text{P}_x$ by passing HCl over a gallium source kept at 775°C . The volatile gallium chloride which is carried to the

reaction zone at 850°C , reacts with phosphine and arsine. The deposition is made on a suitable substrate kept at 750°C . Bloem et al [81] have reviewed the CVD techniques for silicon. The CVD technique have been used to deposit scandium hydride [82], A-15 superconductors [83] and similar compounds.

2.4. Growth from Solution

Single crystals of materials which have a structural phase transition near their melting points can be conveniently grown from solutions. In this method a saturated solution is prepared in a suitable solvent and crystallisation is initiated by the slow cooling of the solution or by the slow evaporation of the solvent. In the former case the solutions are prepared at a higher temperature and cooled slowly to a lower temperature to produce the supersaturation necessary for growth. This requires a positive coefficient of solubility. A compact arrangement for the growth from solution by slow cooling has been described by James et al [84]. The saturated solution is kept in a tank, heated by an infrared lamp. The seeds are fixed on a seed holder attached to a rotating shaft which enters to the tank through the lid of the container. The temperature of the solution is reduced

at a rate of $0.1^{\circ}\text{C}/\text{day}$ or lower with a Beckman type thermometer and a suitable programmer. Large α -sulfur crystals have been grown by this method [85]. Large and perfect crystals of industrially important crystals like ethylene diamine tartrate (EDT), ammonium di-hydrogen phosphate (ADP) and potassium di-hydrogen phosphate (KDP) crystals are grown by this method. The designs of solution growth apparatus vary from the simple laboratory model described above to complex industrial models.

The substances which have less marked variation of solubility with temperature can be grown by the constant temperature method. The saturated solution is allowed to evaporate at a constant temperature to produce the supersaturation by solvent depletion. A solution prepared in a beaker covered by a filter paper or placed in a desiccator is enough for the growth of crystals. Better control of the evaporation rate have been achieved by Robinson [86]. Forno [87] have designed an apparatus for the growth of hexamine crystals, which involves a vapour recycling principle with suitable stirring mechanism.

Various models of the apparatus used for solution growth have been reported [88]. Delfino [89] have modified the apparatus to grow crystals of ionic

salts not by the temperature change but by the electrolytic solvent-decomposition.

2.5. Hydrothermal Growth

The hydrothermal growth mainly used to grow crystals of quartz [90], utilises the increased solubility of materials in water at very high temperatures above the boiling point of H_2O . The apparatus required for the method is a thick walled autoclave which can withstand the pressure of the superheated water. A temperature gradient is produced along the length of the autoclave so that the upper portion is at a temperature lower than the bottom. The autoclave is filled with the nutrient and water and closed by self-sealing seals [91]. The seeds crystals, introduced into the upper portion, begins to grow as the nutrient dissolves and moves up the gradient.

Usually, to increase the solubility, a mineraliser like NaOH is to be added in different proportions. Thus for quartz an addition of 0.5N NaOH solution has been found to increase the solubility considerably [92]. Zircon single crystals have been grown by Uhrin et al [93]. They have reported that KF-lm LiF is a suitable mineraliser for zircon. Addition of KOH and K_2CO_3 solutions have been reported to increase the solubility

of tri-octahedral mica in water [94]. Single crystals of a large number of materials like VO_2 , $\text{Y}_3\text{Fe}_5\text{O}_{12}$ and Al_2O_3 have been grown by this method [95,96,97].

2.6. Flux Growth

Flux growth technique is one of the most versatile of the current techniques used to grow crystals. Flux growth is mainly used to grow crystals of materials, whose melting point is too high. The method utilises the lowering of the melting point of materials in molten salts. In the actual growth, the material is melted with a suitable salt, preferably having the material itself as one of the constituents. If the material has a positive coefficient of solubility in the flux, the solution prepared at a high temperature is slowly cooled. In other materials a slow evaporation akin to the solution growth is commonly used.

Platinum crucibles are used wherever possible due to the low reactivity. The crucibles are either closed by a lid and welded together or partially covered. The crucibles are embedded in the hollows made in a refractory brick, and packed with alumina powder. The whole assembly is then placed in a muffle furnace. The growth run is usually performed with the help of a temperature programmer which can be programmed for different cooling rates ranging from 1°C per hour to 40°C per minute.

After the growth, the grown crystals can be removed by washing in a suitable acid which dissolves the flux and not the crystals. The different fluxes suitable for particular materials have been listed in the various reviews [98,99,100]. New fluxes for new materials can be selected from the known phase diagrams [101] or in the absence of a phase diagram by trial and error.

A large number of important crystals have been satisfactorily grown by this method. Beryllia [102], garnet Crystals [103] and corundum [104] have been grown, to quote a few. The advantages of flux growth are

- 1) the low growth temperature compared to the melting point of the pure material
- 2) the easy doping facility
- 3) control of stoichiometry, and
- 4) simple apparatus and control.

The main disadvantages of this method are that

- 1) the nucleation is spontaneous
- 2) the exact measurement of the growth temperature is not possible.

2.7. Growth from Gels

The gel method offers reasonable prospects of success in the growth of single crystals of materials which cannot be grown from melt, vapour and solution, due to the decomposition before melting, low vapour pressure or low solubility. Other materials [105,106,107] can also be grown by this method to avoid the thermal strain often introduced during growth from melt and vapour. In the gel method the growth takes place at low temperatures. The gel can be prepared in different ways. In one method a solution of sodium silicate of suitable specific gravity [106] is mixed with a component of the final compound to be grown. On the top of this the other reactant is placed in the form of a solution. This supplies the other component of the material to be crystallised and also keeps the gel from drying out. The components slowly diffuse and react to form the compound. Crystals start to nucleate at the micro-flaws in the gel or at the dust particles, inherently present in them. Another variant of the method uses a U-tube. The gel is kept at the centre of the vertically kept U-tube. The reactants, in the form of solutions, are kept above the gel in the two limbs of the U-tube.

The nucleation and growth of crystals in the gel matrix is controlled by several parameters. The concentration of the feed solution and the pH of the gel have been found to affect the nucleation. The ageing of the gel and gel density also influences the growth and perfection of crystals [108,109]. The optimum values of the various parameters for a particular material is to be found out by trial and error.

The disadvantages of this method are the slow growth rate, which is essentially diffusion limited, the inability to control the nucleation and the relatively small sizes of the crystals obtained.

CHAPTER THREE

MORPHOLOGY OF CRYSTALS

3.1. Introduction

The macroscopic form and structure exhibited by a crystal is its morphology. It has long been known that the interplanar angles of a crystal remains the same irrespective of the habit. Haiiy [110] observed that the different habits of calcite crystals can be regenerated by stacking the small crystal units obtained by cleaving. The study of the geometrical shape of crystals later led Hessel [111] to the conclusion that only 32 classes of symmetry are alone possible in crystals. The attempts made by Gibbs [29] to describe the morphology of crystals from a thermodynamical point of view resulted in the formulation of the minimum energy criterion. If γ_s is the surface energy per unit area of the face having an area A , then the morphology of a crystal is determined by the integral $\int \gamma_s dA$ summed over all the faces. The equilibrium habit is that for which the integral has a minimum value. Wulff [31] devised a method for the construction of the equilibrium forms of a crystal. In this construction normals are drawn to every face of a crystal from an interior point. Taking the length of the normal proportional to the

surface free energy of the respective faces a polar plot of surface free energy can be drawn. The surface thus generated exhibit maxima and minima. If planes are now drawn perpendicular to the normals passing through the minima, the morphology of the crystal can be regenerated. The Wulff construction of crystals usually result either in surfaces having a sharp minima or gradual minima. In the former case a slight change of orientation requires rather large energies and thus correspond to smooth surfaces. In the latter case the energy changes involved in misorientation is small and the surfaces are rough.

The study of the shape of a growing crystal is difficult compared to the analysis of the equilibrium form. A large number of parameters invariably appear such as the crystal structure [112], supersaturation, presence of impurities and the presence of imperfections.

3.2. Morphology and Structure

The morphology of a crystal is closely related to the crystal form $\{hkl\}$ and the interplanar spacings d_{hkl} . The Bravais-Friedel law [113] states that the most prominent faces of a crystal are those with the largest lattice spacings. For a cubic crystal with a primitive lattice, the interplanar spacings d_{hkl} decrease with the $\{100\}$, $\{110\}$, $\{111\}$, $\{200\}$... etc. faces. Centering

the primitive cell, result in a doubling of the lattice planes thus halving the interplanar spacings. It has been found that there exist crystals which violates the Bravais-Friedel law. This violation has been traced back to the presence of glide planes, screw axes [114] and pseudo-symmetric features [115].

3.3. Morphology and Bonding

The growth of crystals involves the formation of strong bonds between the crystallising units. Kink sites on crystal faces offers a more probable deposition site than an atomically smooth surface, since they offers at least one more bond than the free surface. Thus there exist a periodic bond chain (PBC) [116] between the building units. Layer growth is possible only when there is strong bonds between periodic bond chains. Each layer is repeated at a distance of d_{hkl} . Such faces, with strong bonds are called F-faces. In the absence of a bonding the nucleation probability at all sites is the same and layer growth is impossible. In this case the surface will appear stepped and is called a S-face. In addition, kinked faces also exist, called the K-faces, due to the total absence of PBC's. The different nature of bonding that exist in the various faces of a crystal thus promotes or prevents growth to give the crystal, the observed morphology.

3.4. Crystal Habits

Of the various external habits exhibited by crystals, only that of whiskers, dendrites and spherulites are dealt with in this section, since only these morphologies are of direct interest in the present context.

a) Whiskers

Whiskers are filamentary crystals which have negligible dimensions compared to its length. Whiskers of a large number of substances have been reported [117,118,119]. The interest in whiskers is two fold. Whiskers exhibit mechanical strength and behaviour close to that predicted by theories. The enhanced mechanical stability of whiskers have been found to be due to the low dislocation content. The academic interest in whiskers have been centered around the different growth mechanisms and structures. The technological interest in this morphology has been due to the direct application potentialities, circumventing the need for the costly and tedious cutting and polishing procedures.

Whiskers can be grown, by the solid-solid transformation [120], from vapour [121], from solution [122] and by electromigration [123]. The morphology of the whiskers have been found to depend upon the material, growth method and temperature of growth. The various

forms of whiskers range from uniform crystals to scrolls and other complex forms [124,125,126].

The observations on the whisker growth of various substances show that some of them grow from the base whereas others grow at the tip. Theoretical models to explain both these modes of growth have been proposed. For the growth from the base, Frank [127] and Eshelby [128] assumes the presence of a hump on the surface of the substrate, with a constraining collar at the base, of a growing whisker. The surface tractions facilitate the growth by supplying material at the base. The essential mechanism is a Frank-Read source which operates below the surface, with the Burgers vector normal to the surface. Under the tensile stress of the whisker, the source climbs forming sheets of interstitial atoms, which subsequently climb towards the root of the whisker adding one atomic layer. The growth rate is thus limited by the rate of migration of vacant sites from the climbing dislocation.

In the dislocation model of Frank, the existence of a spiral dislocation with one end meeting the free surface and the other running as a screw into the main mass, is assumed. Amelinckx et al [129], on the basis of the direct observations of helical dislocations have

proposed another mode which presumes the occurrence of helical dislocations.

The theory developed for the whiskers growing at the tip parallels to that of bulk crystals. If the axis of whisker growth is the direction of high density and if the faces that bind the whisker are low energy surfaces, the nucleation on the whisker tip will be easier compared to the other faces. But the subsequent growth, once a layer is completed on the whisker tip, requires an additional energy. This difficulty warrants higher supersaturations for the growth of whiskers at the observed rates. To overcome this nucleation barrier Sears [130] applied the screw dislocation model of Frank [42] which presents a self perpetuating spiral step. In this model the atoms are more easily accommodated at the spiral steps enhancing the growth along the axis of the whisker. Thus the theory predicts a single dislocation in a whisker. Actual observations on the whiskers after etching and decoration have verified the existence of axial dislocations, incapable of multiplication [131]. The various observations of dislocation loops, spirals and helices show that the dislocation model is acceptable. The dislocation model has also been successful to account for the branchings and kinkings observed in whiskers.

In several materials the growth of dislocation free whiskers were observed. In these materials the axial dislocation is not essential [132,133]. Observations on these whiskers showed that selected impurities alone were able to induce whisker growth, and the whiskers always carried a hemispherical cap at the growing tip. The investigations on these whiskers led Wagner and Ellis [134] to the formulation of the vapour-liquid-solid (VLS) mechanism. In this, the specific impurities added form a globule of liquid on the substrate which is kept in equilibrium with the vapours of the material to be grown as whiskers. The atoms dissolve in the liquid globule and condense in turn from the liquid phase on to the crystal substrate, causing the whisker crystal to rise with the hemispherical cap.

The stability criterions for the liquid droplet impose restrictions on the size of the whiskers. The minimum radius required is given by

$$r_{\text{mini}} = \frac{2\gamma_{LV}V_L}{RT\log\sigma} \quad (59)$$

where γ_{LV} is the liquid-vapour interfacial energy and V_L the molar volume of the liquid.

The plausibility of this mechanism has been verified, on several materials [135]. The V-L-S mechanism offers control over the location of growth, diameter of

crystal and ultimate length. By this growth it has been possible to grow arrays of crystals by placing the impurities on holes made on a mask of pyrolytic graphite kept on the substrate. The growth starts when the crystal substrate is placed in an atmosphere of its own vapour, after alloying and removal of the mask. Crystals of silicon [136] have been grown as whiskers by coating the substrate with a gold film. The gold dissolves silicon to form a Si-Au alloy in the form of globules which initiates the whisker growth. The V-L-S mechanism has been found to operate on a series of important materials [137,138,139,140].

Thus at present both the dislocation model and the V-L-S mechanism are found satisfactory to explain the various morphological modifications found in whiskers of specific materials. The occasional branching and kinking effects during the growth of whiskers have been accounted for, in both these models. In crystals growing by the dislocation mechanism the kinking has been attributed to the branching of dislocations and have been observed in NaCl and other materials [131]. In whiskers growing by the V-L-S mechanism, the kinking is produced due to the change in the interface direction [141] and branches develop

due to rupture of the alloy droplet during the kinking sequence.

b) Hollow whiskers

The morphology of hollow whiskers and hopper crystals have been observed in crystals grown by various methods, and from various substances [142,143,144,145]. Hollow crystals have a void through the center of a cylindrical or prismatic needle. For NiF_2 , the morphology is that of a hollow cylinder while for SbS_3 , it is a hollow prism [146,147]. Though the occurrence of a hollow crystal has been often related to the conditions of growth, temperature and supersaturation, a general qualitative theory has not been evolved. Developments in this field upto 1976 have been reviewed by Simov [148]. Many authors have reported the induced hollow crystal formation on the addition of impurities [149]. On ZnS the presence of impurity have been recognised as essential for hollow crystal formation [150]. But the observations of Paorici [151,152] on various other materials showed that hollow whiskers can also grow in the absence of an impurity. At present the only inference that can be made is that, the presence of impurities is an important, though not necessarily an essential factor in promoting the formation of hollow crystals.

The outer surfaces of hollow crystals are usually smooth and inner surfaces are stepped. Maeda et al [153] have described the growth of a hollow crystal at the bottom of which a column exist with a spiral at top. The hollow crystals reported by Iwanaga and Shibata [154] have an opening on one of the prismatic walls. Hollow cones have been reported by Chandrasekharaiyah et al [155]. The crystals of Fujisaki et al [156] have the shape of a winding spiral of hexagonal cross section. Most of the hollow crystals have been found to be single. But the hollow crystals reported by Mckee et al [157] were found to give rise to even powder pattern under X-ray diffraction, indicating the polycrystalline nature of these crystals. The defects on hollow crystals have been investigated by Fujisaki [156] by a polarisation microscope and reports a strain free crystal. Soxman [158] has also observed strain free hollow crystals of ZnS. The etching technique has been applied to hollow crystals [153] and the upper surfaces have been found to have a higher density of dislocations.

The mechanism of growth of hollow crystals was investigated by Frank [159]. His theory, applicable only for specific materials having specific morphology, is not generally applicable. Sharma et al [160] and Iwanaga et al [154] have proposed that the prismatic

faces of a hollow crystal are developed by the clustered growth of whiskers and space-filling between them. The opening left on the crystal face has been attributed to the abrupt cessation of growth of a whisker. Their mechanism is substantiated by the observation of a large number of striations parallel to the axis of hollow crystals. But the polygonised faces of a hollow crystal requires a regular nucleation at the nucleation stage. Amelinckx [161], Chandrasekharaiyah et al [155] and Maeda et al [153] proposed a hollow dislocation model. In this model a narrow step expanding from the center outward promotes growth of the outer rim alone, by diffusion. This model fails to give any rational explanation for the expansion of the step outwards. Yoshida [143] proposed that hollow crystals are formed by the capillary rise of the nutrient along an axial channel to the top. This is restricted to only special cases and is not applicable to the majority.

The skeletal form theory developed by Lemmalain et al [162] assumes the presence of a screw dislocation. At low supersaturations the steps offered by the screw provides sites for nucleation. At higher supersaturations the nucleation rate at apexes and edges are the highest due to the enhanced heat transfer and supersaturation. This mode of growth result in

hollows with steps inside. Iwanaga et al [163] also suggests of the operation of a skeleton formation in the hollow crystals. Of the different theories put forward the mechanism of skeletal development is found to be most satisfactory to explain the observed morphology of hollow crystals.

c) Dendrites

The dendritic morphology of crystals is a highly branched structure with the different branches oriented in crystallographic directions. This kind of morphology has been observed in cast metals [164], organic materials [165] and in ionic salts [166]. The observation of this morphology, during the crystallisation of a large number of materials from all the three states of matter, showed that the dendritic growth is a widespread phenomenon.

The dendritic morphology is thermodynamically unstable since it requires an increase in surface energy due to its extended surfaces, compared to the equilibrium shape. The occurrence of dendrites show that there exist some driving force which promotes the morphology. Theoretical attempts have been mainly directed to find out the critical parameters.

Any satisfactory theory dealing with dendrites should be able to explain the following general observations. The dendritic growth usually start with the development of a fibre. The fibre tip growing into the melt or solution soon develops instabilities which subsequently grow out as primary branches. The process repeats often systematically, producing secondary and tertiary branches, all of which are oriented crystallographically.

The origin of dendrites have been traced to result from the kinetics of crystal growth, as the sharp tip offers a diffusion controlled growth process by the diffusion of either latent heat or solute [167]. Tiller et al [168] recognised the importance of the local constitutional undercooling in the unidirectional crystal growth. The constitutional supercooling if small, produces cellular perturbations on the crystal surface and if large, lead to the formation of dendrites [164]. The model was extended by Mullins and Sekerka [169] who showed that sinusoidal perturbations develop at the planar interface of a growing needle and that these perturbations will grow in a manner predicted by theory. The theory of the morphological stability has been applied on ice cylinders growing in water with minute impurity and excellent agreement between theory and experiment have been

found [170,171,172]. The Mullins-Sekerka theory is applicable only in the initial stages of the perturbation and has not yet been extended to account for the completely developed dendrite. Jackson's [173] investigations on the structure of interface revealed that the different materials can be classified as those having rough interface with high mobility and as those having a smooth interface with low mobility. The low mobility materials grow with faceted morphology while those with high mobility grow dendritically. The surface tension at the interface is another constraint which determines the dendritic growth of a material [174].

Once the perturbations have grown into dendrites, new parameters like the velocity of dendrites and the arm spacing etc. enter into the analysis. Attempts to predict the growth velocity of a dendrite in terms of the supercooling were made by Ivatsev [175] Temkin [176] and Trivedi [177].

The theories assume the tip of a growing dendrite to be a parallel sided needle with a hemispherical cap of radius ρ . The needle having a composition C_g is at solute equilibrium with an adjacent liquid having a concentration C_β , at the interface and C_∞ away from it. The growth velocity v requiring a

material, equal to $v\pi\rho^2(C_\beta - C_\alpha)$ is given by

$$v\pi\rho^2(C_\beta - C_\alpha) = [D(C_\beta - C_0) 2\pi\rho^2]/\rho \quad (60)$$

$$\text{ie } v = (2D/\rho) \Omega_0 \quad (61)$$

where Ω_0 is the supersaturation defined by

$$\Omega_0 = (C_\beta - C_0) / C_\beta - C_\alpha \quad (62)$$

The equation (61) shows that the growth velocity increases with the decrease of the dendritic radius. Purdy [178] has shown that as the radius ρ becomes small, the capillary effect of the surface tension γ also have to be taken into the analysis.

Introduction of the capillary constant G modifies the equation (61) as

$$v = 2D/\rho [\Omega_0 - (G/\rho)] \quad (63)$$

Now the velocity of growth exhibits a maxima at a critical radius ρ_0 . The maximum growth velocity v_{\max} occurs at $dv/d\rho = 0$ and is given by

$$v_{\max} = D \Omega_0^2 / 2G \quad (64)$$

The incorporation of the other constraints into this equation further reduces the velocity. The interface mobility [173] thus influences the growth velocity according to the equation

$$v = (2D/\rho) \left\{ 1 - \left(\rho_c/\rho \right) - v/[m(C_\beta - C_0)] \right\} \quad (65)$$

Observations on a large number of dendrites showed that the dendritic tip in reality had the shape of a paraboloid of revolution [175]. Due to the curvature at the tip, the interface now is no more iso-concentrate and this reduces the velocity. The models of Temkin [176] and Trivedi [177] takes these into consideration. A detailed theoretical discussion on the formation of dendrites has been given in the review of Langer [179].

Glicksman [180] comparing the different analysis finds that they all result in the same relation between velocity and supercooling differing only in numerical constants. All relations contains a constant

$$G = \alpha \Delta S_f / C_p \gamma_{SL} \quad (66)$$

where α is the thermal diffusivity S_f is the entropy of fusion, L is the enthalpy of fusion, C_p is the specific heat of the liquid and γ_{SL} is the solid-liquid interfacial energy. He further shows that the theories of Trivedi [177] and Nash-Glicksman [181] are more successful than the theory of Ivatsov, with an universal value for the growth rate exponent. Langer et al [182] have proposed that the maximum velocity criterion is to be replaced by the condition that, $v \rho^2 = \text{a constant}$. Their measurement of v and ρ as functions of the supercooling $\Delta\theta$ show close agreement with the Glicksman's result. Langer et al

assuming a tip shape of a paraboloid of revolution successfully explained the sinusoidal surface instabilities oscillating on the surface of the tip.

Though the majority of constraints involved in dendritic growth has been identified and evidence for the existence of a universal law of the dendritic growth has been obtained [183], a satisfactory theory which can be rigorously verified experimentally is yet to be evolved.

d) Spherulites

The spherulitic morphology, exhibited by minerals [184], polymers [185] and other materials [186], consists of spherically symmetric crystalline aggregates. This macroscopic spherical symmetry is in violation with the uniform packing of microscopic units. The spherulites thus radiate, from a nucleus with the substructure of needles, with small angle branchings, to fill the area created by the outwardly increasing volume. A satisfactory elucidation of the factors, which give rise to and control the anomalous and exceptional growth of spherulites, has been a long-standing problem in the theory of crystal growth.

The experimental findings on the spherulitic crystallisation show that this mode of growth is restricted

to melts having high viscosities. The extinction behaviour under crossed polaroids [187] and the study of micro beam X-ray diffraction [188] of spherulites indicate that the substructure is oriented along some preferred crystallographic direction and lies parallel to or almost parallel to the radial direction. The small angle branching has been observed to result by the splitting of the parent fiber in non-crystallographic directions. The radial growth rate under isothermal conditions remains constant, once the growth starts from a heterogeneously nucleated centre. The cross sectional area of substructure depends on the temperature of crystallisation being very small at large undercooling and prismatic needles with isometric cross sections at small undercoolings.

According to Keith and Padden [185], the steady state growth of a spherulite at a constant radial rate, though resembles the dendritic mode of growth with side branches, differs from it in various ways. Whereas the dendritic growth proceeds with the branching in crystallographic directions due to the instabilities at the growing tip, the spherulites grow by small angle branching in non-crystallographic directions. The dendritic growth rate, solely controlled

by the diffusion of heat and matter, is considered to be non-linear. The spherulitic growth obeys a linear growth law of the form $G = f(T)$. Keith et al argues that the growth rate and periodic splitting is essentially controlled by the presence of impurities and by the rate of heat transfer at the interface.

A crystal growing into the melt containing impurities, will reject the impurities so as to result in an increased impurity concentration at the growing interface. The impurity concentration in the steady-state for a crystal growing with a velocity G is given by

$$C(x) = C_0 \exp(-Gx/D) + C_G \quad (67)$$

where C_0 is the concentration of excess impurity at the interface, C_G is the concentration of the impurity in the bulk melt and D is the diffusion coefficient for impurity in the melt. In non-stirred melt the rejection of impurities will result in a layer of impurity of thickness $\delta = D/G$. Considering a spherical nucleus, it is thus covered by a thin layer of impurities. In the interface there will exist a high impurity concentration and low temperature gradient producing a slow linear growth. But due to the high viscosity, the bulk liquids has a large supercooling and a low diffusion coefficient, D . This reduces the impurity layer thickness and any

accidental projections into the melt will result in rapid growth. This instabilities of the growing surface does not result in the production of thermal dendrites since the value of $G/\Delta T$ is very small, where ΔT is the undercooling. Due to the instability the planar interface breaks up into a series of fibrous projections leaving the inter-fiber region impurity rich.

The branching of the fibers should be the result of some singularities like dislocations and temperature gradients. The growing interface of a fiber is persistent only if δ is small. If δ increases to great values the growing fiber will develop singularities invariably resulting in the growth of branches. These branches thus have the same crystallographic orientation as the parent fiber but will be oriented slightly to it.

The theory developed by Keith and Padden, though superficially accounts for the growth of spherulites of different materials, is not rigorous in the sense that it cannot explain the various complex features exhibited. The role of impurities in spherulitic growth have been questioned [189]. The morphology of spherulites often depart from the ideal case of identical substructure orientation. In selenium cylindrites [186] an arm to

arm variation of orientation has been reported. In conclusion it may be stated that though the basic parameters involved in spherulitic growth has been identified, theoretical and experimental investigations are yet to be done to ascertain the mechanism of growth particularly in substances other than polymers.

CHAPTER FOUR

DISLOCATIONS IN CRYSTALS

4.1. Introduction

Dislocations are line defects present in an otherwise perfect crystal. A dislocation is characterised by two components namely, 1) the path of the line in the crystal and 2) the 'Burgers vector', which is a measure of the strength of the dislocation. A dislocation line is surrounded by strongly disturbed material while far away from the line the crystal is perfect. The Burgers vector is defined by comparing the defect crystal with a perfect crystal. If a closed circuit is drawn on the surface of a perfect crystal by atom-to-atom steps, it will form a closed path. The same sequence, if followed in the defect crystal, around a dislocation exhibit a closure failure. This closure failure can be described by means of a vector pointing from the end to the beginning of the circuit, called the Burgers vector. This vector will have a magnitude equal to the multiples of the translation vector.

The Burgers vector can make any angle with the dislocation line, between the two limiting cases of the vector being perpendicular to the dislocation line and being parallel to it. In the former case the

dislocation is called an edge dislocation and in the latter a screw dislocation. The atomic arrangements at an edge dislocation and screw dislocation are shown in figures (3) and (4). In general the dislocations are curved and exhibits a mixed character.

4.2. The Strain and Stress fields around Dislocations

The material, surrounding the dislocation, is highly strained. The different forces that the surroundings exert on the dislocation line can be analysed by assuming the crystal to be an elastic solid and excluding a cylinder having a radius of atomic dimensions around the dislocation line from it.

For an elastically isotropic material the strain field around a straight dislocation can be discussed accurately. For a dislocation that extend in the Z-direction in cylindrical polar coordinates (r, θ, z) , the deviation from the initial position, x_0 in the imperfect crystal can be expressed as,

$$\mathbf{x} = \mathbf{x}_0 + \mathbf{u}(\mathbf{x}_0) \quad (68)$$

where \mathbf{x} is the position of a point in the imperfect crystal and \mathbf{x}_0 is the corresponding point in the perfect crystal. $\mathbf{u}(\mathbf{x}_0)$ is a vector with components (uvw) .

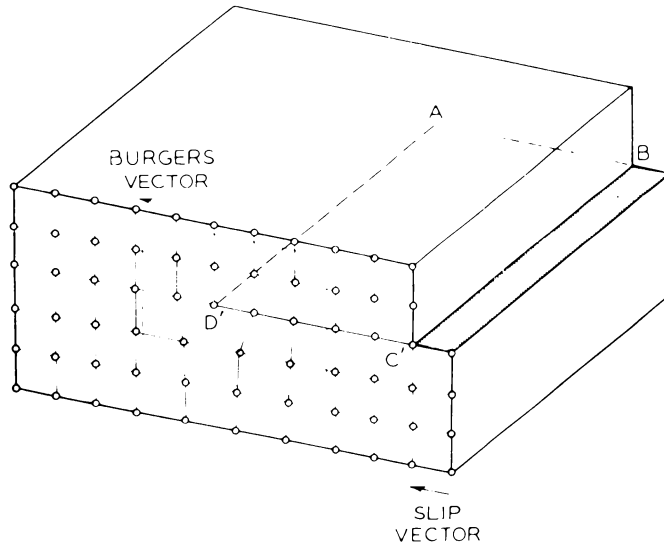


Fig.(3) Atomic arrangement around an edge dislocation.

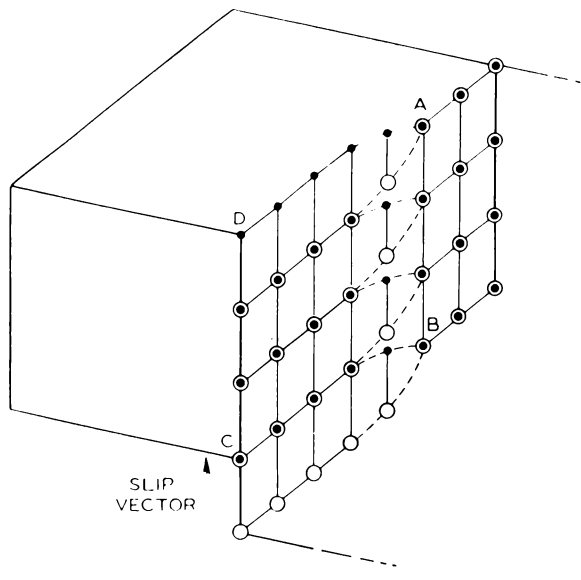


Fig.(4) Atomic arrangement around a screw dislocation.

For a screw dislocation, the helical arrangement of atoms suggest a deformation

$$u(r, \theta, z) = 0 \quad (69)$$

$$v(r, \theta, z) = 0 \quad (70)$$

and $w(r, \theta, z) = \frac{b}{2\pi} \theta \quad (71)$

where b is the magnitude of the Burgers vector and has a range of 2π . This deformation converts the xy -plane into a screw plane pointing in the z -direction. A similar treatment on an edge dislocation yields,

$$u(r, \theta, z) = b/2\pi \left[\theta + \frac{\sin(2\theta)}{4(1-\nu)} \right] \quad (72)$$

$$v(r, \theta, z) = -b/2\pi \left[\frac{1-2\nu}{2(1-\nu)} \log(r) + \frac{\cos(2\theta)}{4(1-\nu)} \right] \quad (73)$$

$$w(r, \theta, z) = 0 \quad (74)$$

The Burgers circuit can be expressed as

$$b = \oint \frac{\delta \bar{u}}{\delta s} ds \quad (75)$$

The evaluation of this integral for a screw dislocation with θ as variable gives

$$b_1 = b_2 = 0 \quad (76)$$

$$b_3 = b/2\pi \int_0^{2\pi} d\theta = b \quad (77)$$

and for an edge dislocation

$$\bar{b} = (b_1, 0, 0) \quad (78)$$

The stress field is coupled to the strain field. The strain field is a vector field and the stress field is a tensor field. The stress field can be best described by considering a cube with force components on the surfaces. In the cylindrical polar coordinates the edges are set parallel to the r , θ and z axes. In the orthogonal cartesian system if σ_1 , σ_2 and σ_3 are the stresses on the faces perpendicular to the x , y and z axes, the equilibrium of the cube will lead into six independent stresses forming a tensor,

$$\begin{pmatrix} \sigma_{11} & \sigma_{12} & \sigma_{13} \\ \sigma_{21} & \sigma_{22} & \sigma_{23} \\ \sigma_{31} & \sigma_{32} & \sigma_{33} \end{pmatrix} \quad (79)$$

In the case of a right handed screw dislocation described in cylindrical coordinates (79) reduces to

$$\begin{pmatrix} 0 & 0 & 0 \\ 0 & 0 & \sigma_{23} \\ 0 & \sigma_{32} & 0 \end{pmatrix} \quad (80)$$

with $\sigma_{23} = \sigma_{\theta z} = \frac{Gb}{2\pi r}$ (81)

where G is the shear modulus. Thus the shear stress

acts on the plane normal to the θ -direction. For an edge dislocation the stresses are

$$\sigma_{11} = \sigma_{22} = \sigma_{rr} = \sigma_{\theta\theta} = \frac{\tau_0 b}{r} \sin\theta \quad (82)$$

$$\sigma_{12} = \sigma_{r\theta} = + \frac{\tau_0 b}{r} \cos\theta \quad (83)$$

$$\sigma_{33} = \sigma_{zz} = - \frac{\tau_0 b}{r} 2\nu \sin\theta \quad (84)$$

where ν is the Poisson ratio and $\tau_0 = G/2\pi(1-\nu)$. A detailed derivation of the above equations is given by Hirth and Lothe [190].

A dislocation possesses a physical individuality and can be put into motion by the application of forces. If an edge dislocation of strength b , traverse through the whole crystal of length l and breadth a under a shear stress τ , one part will get displaced with respect to other by b . The work done by the total force on the crystal is then given by,

$$W = \tau(l a) b \quad (85)$$

This may be also considered as the work done by a force on the dislocation.

$$W = f l a \quad (86)$$

where f is the force per unit length of the dislocation, l is the length of the dislocation and a , the distance

moved by the dislocation. Comparing (85) and (86)

$$f = \tau \cdot b \quad (87)$$

In general, the force df on a dislocation is given by

$$df = b \quad [\sigma_b \times dl] \quad (88)$$

where b is the Burgers vector, dl is the vector element in the direction of the dislocation line and σ_b , the stress normal to b . The equation (88) is known as the Peach and Koehler formula [191]. It gives the force which act on a dislocation in a stress field. The stress field may arise from external forces or from the stress fields of other dislocations.

In the case of two parallel screw dislocations with one of them along the z -axis the stress is given by equation (81).

$$\sigma_b = \sigma_{\theta z} = \frac{Gb}{2\pi r} u_\theta \quad (89)$$

The force per unit length of the dislocation line is obtained by substituting this value of σ_b in equation (88)

$$f = |\bar{b}| \frac{Gb}{2\pi r} (u_\theta \times u_z) = \frac{Gb^2}{2\pi r} u_r \quad (90)$$

where u_r , u_θ and u_z are the unit vectors in the r , θ and z directions in cylindrical polar coordinates [192]. This force is repulsive and is $\propto 1/r$. For a right handed screw and a left handed screw the force becomes attractive.

A similar treatment for the edge dislocations gives

$$f_x = b \cdot \sigma_{xy} = \tau_0 b^2 \frac{x(x^2 - y^2)}{(x^2 + y^2)^2} \quad (91)$$

$$\text{with } \tau_0 = \frac{G}{2\pi(1-\nu)} \quad (92)$$

The equation shows the existence of four segments.

The segments are characterised by

1. $x > 0 \quad |x| > |y| \quad f_x > 0$
2. $x > 0 \quad |x| < |y| \quad f_x < 0$
3. $x < 0 \quad |x| < |y| \quad f_x > 0$
4. $x < 0 \quad |x| > |y| \quad f_x < 0$

It is seen that the stable configurations for two parallel edge dislocations exist at $x = 0$ and for two edge dislocations of opposite sign at $|x| = |y|$.

4.3. Dislocation Reactions

a) Coalescence of dislocations

A dislocation can interact with another to form a single dislocation. This unification need not take place along the whole length of the dislocation line but may result in nodes. The Frank's law of conservation of

Burgers vectors states that the sum of Burgers vectors flowing into the node is equal to the sum of Burgers vectors flowing out of the node. In mathematical form it may be written as

$$\sum_i \bar{b}_i(\text{in}) = \sum_j \bar{b}_j(\text{out}) \quad (93)$$

Though the above condition conserves the Burgers vector it does not indicate whether the reaction will take place or not, The probability of reaction depends on the change in the energy during the reaction. Taking an approximation that the energy per unit length of the dislocation line is directly proportional to the square of the Burgers vector, the criterion for combination of two dislocations may be written as,

$$b_1^2 + b_2^2 > b_3^2 \quad (94)$$

where b_1 and b_2 are the Burgers vectors of the two dislocations, combining to form a dislocation of strength b_3 . By the node condition

$$\bar{b}_1 + \bar{b}_2 = \bar{b}_3 \quad (95)$$

This indicate that the three vectors should form a triangle geometrically. The stability decreases as the triangle passes from an acute angled one to a right angled and then to an obtuse angled one.

b) Dislocation multiplication

The participation of a large number of dislocations in plastic deformation requires generation of fresh dislocations within the crystal. A dislocation may provide such a source for the production of infinite number of new dislocations under certain configurations. Frank and Read [193] have proposed a mechanism by which dislocation multiplication can occur. The different stages of dislocation production under this mechanism are shown in figure (5). The dislocation line ABCD with a Burgers vector b has a portion BC, on the slip plane. In this case only those parts on BC can move while AB and CD remains anchored at B and C. On applying a small stress, BC curves out and get unstable due to the imbalance of forces arising out of the curvature of the dislocation line. The line tension T , defined as the self energy per unit length of the dislocation is given by

$$T \sim \frac{Gb^2}{4\pi} \log (R/5b) \quad (96)$$

where R is the radius of curvature and G is the shear modulus. The line tension of a curved dislocation segment produces a force per unit length with a magnitude of

$$|F| = T/R \quad \frac{Gb^2}{R} \quad (97)$$

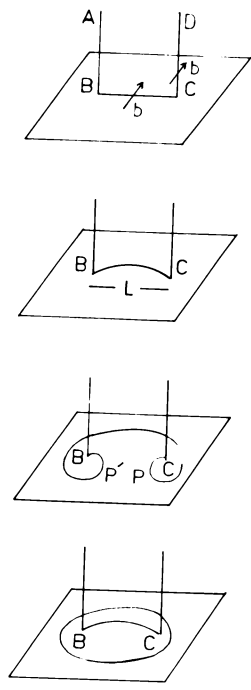


Fig.(5) Dislocation multiplication by the Frank-Read mechanism.

In the present configuration the curvature of the segment BC, under the applied stresses equals, $1/L$, the length of the segment. Thus the applied stress is given as

$$\sigma \sim 2Gb/L \quad (98)$$

When the points P and P' shown in the figure, which have opposite signs meet, they annihilate. A dislocation loop is thus pinched off and BC returns to the original position. By repeating this process infinite number of dislocations having the same Burgers vector, can be produced.

c) Grain boundaries

A grain boundary is the border line of two grains of the same material misoriented at an angle to each other. Bragg [194] and Burgers [195] suggested a dislocation model of the grain boundary taking into consideration the energy change associated with the spacial configuration of dislocations. They showed that the atomic misfit between two grains at small angles at the boundary result in an array of individual dislocations. The misfit can be produced by either a rotation of a grain relative to the other placed below; or by the relative orientation change in adjacent grains. The

former is called a twist boundary while the latter is a tilt boundary. The geometry of two misoriented grains automatically result in an array of edge dislocations. The spacings between the individual dislocations is a function of misorientation θ . The greater is the angle the closer is the spacings of the dislocations in the boundary. The relation between θ and the spacings D is

$$\theta = b/D \quad (99)$$

where b is the magnitude of the Burgers vector of the dislocations. The grain boundary possesses an energy and can move under stresses in special cases [196].

4.4. Cleavage

In brittle materials the application of large enough forces result in the breaking up of the crystal into two, along a closed packed plane. This process, called cleavage can be described satisfactorily in terms of dislocations. Since the cleavage is not an instantaneous process, it should start from an initial crack and should propagate from point to point to bring out cleavage. The process involves the production of two free surfaces and hence require large energies. Cleavage can be brought out by the diffusionless climb of dislocations. The crack front produces the dislocations

due to the applied stress and these 'cleavage dislocations' climb without diffusion in the cleavage plane. If a dislocation of strength b climbs normal to its glide plane to sweep out an area ds , an empty volume dV is left out given by

$$dV = ds \cdot b = ds \cdot b \cdot \sin \psi \quad (100)$$

where ψ is the angle made by the dislocation line with its Burgers vector b . If the atomic volume is taken as b^3 , then,

$$dN/v = \frac{dV}{v} = \frac{ds}{b^2} \sin \psi \quad (101)$$

gives the distribution of atomic defects, vacancies or interstitials. The force, F_m , per unit length of the line necessary for climb is given by [197],

$$\begin{aligned} F_m &= U_f \, dN/ds \\ &= (U_f/b^2) \sin \psi \end{aligned} \quad (102)$$

where U_f is the energy of formation of atomic defects.

Cleavage is confined to the closed packed crystallographic planes due to the low surface free energy. The cleavage process often produces river patterns on the newly created surfaces. The origin of these patterns have been traced due to the interaction

of the cleavage crack with the numerous dislocations piercing the cleavage plane. The visible steps have been found to be a combination of smaller steps and steps of opposite sign have been found to annihilate each other. In general the steps are curved except in ionic solids which has highly anisotropic surface tensions. In ionic solids the steps often have a zig-zagging shape running along the closed-packed crystallographic directions.

4.5. Plastic Deformation

The plastic deformation in a crystal occurs by the movement of lamellae of the crystal, one over the other. The displacement takes place along specific planes called slip planes and specific directions called slip directions. The slip planes and slip directions are usually closed-packed ones. The intersection of slip planes on the surface during slip produce lines and bands, on it. The slip traces are straight if only one set of planes is active in slip and are wavy if there exist more than one set of slip-planes. Clustering slip lines to form slip bands have been observed on several substances.

In the microscopic form the slip involves a movement of a periodic atomic layer over another. Equilibrium positions with minimum energy are separated

by intermediate positions of maximum energy. Thus the stress required to overcome the maximum energy points during slip has a sinusoidal nature expressed as

$$\sigma = \frac{Gb}{2\pi a} \sin\left(\frac{2\pi x}{b}\right) \quad (103)$$

where b is the period of the lattice and a is the inter atomic distance. σ gives the stress required for a displacement of x . The theoretical elastic limit is thus given by

$$\sigma_0 = Gb/2\pi a \quad (104)$$

Actual observations showed that the theoretical value is far greater than the stresses required to bring out slip.

The introduction of the idea of dislocations solved this problem. The edge dislocations and screw dislocations present in the crystal can move under low stresses and will cause slip resulting in traces with a step height equal to the Burgers vector.

Peierls [198] and Nabarro et al [199] calculated the energy required to move a dislocation over a barrier of sinusoidal nature, and obtained an expression of the form given in equation (103). The activation energy ΔW per unit length under a critical stress σ_c is given as

$$\Delta W \sim \frac{Gb^2}{2\pi K} \exp(-2\pi a/Kb) \quad (105)$$

The critical stress is given by

$$\sigma_c = (2G/K) \exp(-2\pi a/Kb) \quad (106)$$

where $K = 1$ or $(1-\nu)$ depending on the nature of dislocation involved namely whether edge or screw.

The minimum energy, W_0 is given by

$$W_0 \sim (Gb/4\pi K) \log\left(\frac{Kr_1}{a}\right) \quad (107)$$

The critical shear σ_c calculated from equation (107) is much lower than that obtained from equation (104) and approaches the experimental values. This theory is capable of giving only the order of magnitude which varies from a large value for metallic crystals to a low value for covalent or ionic crystals.

4.6. Direct Observation of Dislocations

For the direct observation of dislocations a variety of techniques have been developed, all of which utilises either the atomic disorder or the increased strain energy at dislocations. The different techniques described here are rather supplementary to each other than individually sufficient in completely characterising the dislocations.

a) Etching

The treatments on the etching process and formation of etchpits at dislocation sites are focussed

around the strain energy or core energy of dislocations. Though the elastic strain is known to promote localised etching [200], the role of it in the formation of etch pits at dislocation sites is questionable. The screw dislocation possesses pure shear stress fields which vanishes at the surface except at the core, whereas strain energy associated with an edge dislocation is retained at the surface and extends to a considerable distances beyond the core. This difference in energies are not reflected in the etch rates in many crystals [201]. Both screw and edge dislocations have been revealed by etching. It has been proposed that the deciding factor is the dislocation core energy rather than the elastic energy [202]. Some arguments against the role of elastic strain energy in dissolution and in favour of the role of core energy are given below.

1) In metals, where the core energy of dislocations is less than other materials it is difficult to reveal dislocations. In covalent and ionic materials the preferential etching is produced easily which has greater core energy. Metals, covalent and ionic materials have the same strain energy associated with dislocations.

2) In a tilt boundary where the dislocations are close to each other the stress fields should cancel and hence should not be as easily revealed as individual

dislocations. But different dislocations have been known to etch at approximately equal rate in a specific crystal. The necessity of impurity segregation for the nucleation of etch pits have also been questioned. Thus, though there is conclusive proof that the dislocations are revealed by etch pits, the etching process is not clearly understood.

1) Chemical, solvent and thermal etching

The chemical etching involves the utilisation of enhanced chemical reactivity at the dislocation. In this technique the crystal is immersed in a chemical reagent which will react with the crystal material to form products, soluble in the reagent itself or in any other non-reactive solvent. The difference in chemical reactivity along different crystallographic directions result in the symmetrical development of etch pits. For a crystal, the dissolution rates on various faces differ widely to such an extent that an etchant is capable of revealing dislocations only on certain faces.

The solvent etching, where the crystal is immersed in the solvent or in an undersaturated solution of the material, is also effective in bringing out dislocations. The process involves no chemical reaction but depends on the increased solubility at the dislocation

sites. Several authors have listed etchants suitable for revealing dislocations in various crystals [203,204].

To ascertain that the etch pits are produced at sites of dislocations the following observations are usually made. If the crystal exhibits a cleavage the etch patterns on the matched cleavage faces obtained should show a 1 : 1 correspondence. The successive etching of the same surface should not result in the spurious development of new pits, but should deepen and widen the existing pits. Etching both sides of a thin flake should exhibit similar etch patterns.

Some etchants are capable of distinguishing between edge and screw dislocations [205]. The delineation of dislocations at grain boundaries and the ability to reveal fresh dislocations produced by scratching [206] or indentation [207] can also be taken as evidence that the etchant is capable of delineating the dislocations.

Thermal etching has also proved to be useful in revealing dislocations. In this technique the crystal is kept at a high temperature, often assisted by a hot stream of inert gas or air. In thermal etching, pits are produced by the easy sublimation of atoms or molecules loosely bound at the dislocation.

ii) Morphology of etch pits

Several factors influence the morphology of etch pits. The importance of crystal structure in determining the etch pit shape have been shown by Wooster [208]. He has shown that the etch pits on various faces of cuprite, quartz and tourmaline crystals have shapes related to the atomic arrangements on these faces, and exhibit often the symmetry of the faces. In tellurium crystals, the etch pits have been shown to depend strongly upon the crystal structure [209]. The morphology of etch pits also depends on the characteristics of the etchants used [210]. Somaiah et al [211] have studied the effect of chemical reagents used for dislocation etching on the morphology of etch pits. In BaFBr crystals the orientation of etch pit edges have been reported by them to change from $\langle 100 \rangle$ direction to $\langle 110 \rangle$ direction with change of etchants. On the cleavage faces of $K_2O-SrO-Nb_2O_5$ crystals a change of etchant have been found to produce a striking difference in the shape of etch pits [212]. Impurities present in the crystal as well as intentionally added to the etchant, have been reported to change the morphology of etch pits. The addition of CdI_2 in the formic acid-water etchant for BaFBr crystal have been reported to produce a change in the shape of pits from pyramidal to

octagonal [211]. The presence of excess potassium ions, preferentially segregated at dislocations in $K_2O-SrO-Nb_2O_5$ system, have been suggested to explain the appearance of etch hillocks [213]. The morphology is also influenced by the nature of dislocations and their relative orientation with the surface. Livingston [214] have found that in copper crystals, the pits at edge dislocations differ markedly in depths according to the sign. Gilman et al [215] have reported an etchant for LiF to distinguish between edge and screw dislocations. The relative orientation of the dislocation with the surface affects the symmetry of pits. The dislocation if perpendicular to the surface will produce symmetrical pits while any deviation from it produce asymmetry [203]. If the dislocations are parallel or almost parallel to the surface, etch grooves or pits elongated in the direction of dislocations will result [216]. The etch pit shapes have been utilised by Ito et al [217] in $Sr_xBa_{1-x}Nb_2O_6$ crystals to distinguish helical dislocations.

The movement of dislocations have been known to produce flat bottomed pits in several crystals [218]. Flat bottomed pits have been observed also due to abrupt bending away of dislocations at cleavages and at points of surface irregularities. The successful formation of

an etch pit is also influenced by the etching rates along the dislocation line (R_D), parallel to the surface (R_L) and perpendicular to the surface (R_V) [201].

Depending upon the relative values of the etching rate the morphology of pits will change. For $R_D > R_L$, conical etch pits with curved faces will result. If $R_D > R_V > R_L$ then the pits will exhibit a terraced structure. In cases where $R_D > R_A > R_V$, well defined etch pits have been found to result, where R_A is the etching rate perpendicular to the faces that bind the pit.

b) Decoration

The decoration technique involves the preferential deposition of impurity atoms along the dislocation line. The dislocations get decorated by foreign atoms due to the following reasons.

1. The dislocation stress field, in the presence of an edge component will attract foreign atoms.
2. Along the dislocation line, an enhanced diffusion mobility helps to feed the impurity atoms, to nucleate and to precipitate.
3. A dislocation can act as a source of vacancies by 'climb'. This further promotes the growth of the precipitate.

The introduction of a material as an impurity can be effected by a variety of techniques. The photolytic silver has been used to decorate AgCl and AgBr crystals by Hedges et al [219]. Amelinckx et al [220] have used the enhanced diffusion of impurity material during high temperature annealing. The three dimensional dislocation configuration can be conveniently examined by optical microscopy or ultramicroscopy if the sample is transparent. The main disadvantages of the technique are that 1) the method is destructive and 2) the method requires specific impurities for decorating specific materials.

Many of the dislocation configurations like helical dislocations and Frank-Read sources have been observed with this technique. The alkali halides have been decorated by gold particles to reveal spiral steps and the dissolution phenomena [221,222]. The occurrence of axial dislocations in whiskers, as predicted by Sears [130], have been observed in whiskers by decoration. Good reviews on the decoration techniques are given by several authors [203,223].

c) X-ray topographic technique

Line broadening in X-ray diffraction due to the structural deformation has been known as early as 1931 [224]. A double crystal spectrometer has been

used to detect the imperfections of crystals which has a high density of dislocations. The line broadening technique is limited to crystals having dislocation densities greater than 10^5 per cm^2 . In crystals with lesser dislocation densities the line broadening is negligible and methods suitable for mapping individual dislocations are to be used.

Various configurations of X-ray beam, crystal orientation and photographic film, to reveal individual dislocations have been developed by several authors. Borrmann et al [225] used the anomalous transmission of X-rays in crystals. The regions of disorder was marked by regions of reduced intensity in the photographic plate kept in contact with the crystals. Barrett [226] oriented the crystal and film to collect only the Bragg reflected rays. The dislocations were seen to be marked by regions of higher intensity, in contrast to the Borrmann's technique. The various other configurations have been described by Webb [227].

The most frequently used topographic technique is that of Lang [228]. In his technique a well collimated X-ray beam is allowed to fall on the specimen, set at the Bragg angle, for reflection. The direct beam transmitted by the crystal is stopped by a shield while the diffracted beam is allowed to fall on a photographic film through a

slit. The film and crystal is moved together to scan the whole sample. In this method the strain field around a dislocation reduces the primary extinction to result in areas of greater intensity. Large crystals upto 1" x 1" can be easily scanned and photographs can be obtained which shows the dislocations as areas of increased intensity.

The general condition for the visibility of a defect is that it produces a sufficiently large disturbance of the set of reflecting planes used. For dislocations, in terms of the Burger vectors \bar{b} and diffraction vector \bar{g} , this means a minimum contrast for $\bar{g} \cdot \bar{b} = 0$ and a maximum for $\bar{g} \parallel \bar{b}$.

The topographic techniques have been reviewed by several authors [223,229,230,231]. The method have been successfully used to characterise various crystals [231,233,234]. The disadvantages of this method are the long exposures required and the limitation of magnification to photographic enlargement. Higher speeds and resolution have been attained by the use of synchrotron radiation, in the X-ray range [235,236].

d) Electron microscopy

Electron microscopy has been successfully used to study dislocations by Hirsch et al [237]. Electron microscopy may be used either in transmission or reflection modes.

In the transmittive mode the electron beam is allowed to fall on the crystal specimen, suitably thinned by chemical methods or otherwise. The Bragg reflection from the various $\{hkl\}$ planes forms different diffracted beams. Beams that make equal inclination to the vertical axis of the microscope are focussed in the back focal plane to form the diffraction pattern.

The theory of this highly useful technique has been extensively developed by Hirsch et al [238]. The visibility of defects in thin samples arises out of the elastic stress field existing around any defect. This causes bending of the Bragg reflecting planes $\{hkl\}$. The planes either stack together towards or away from the normal position to decrease or increase the scattering amplitude. The dislocation thus appears as a line of changed brightness. The contrast become zero for $\bar{g} \cdot \bar{b} = 0$, where \bar{g} is the reciprocal lattice vector normal to $\{hkl\}$ planes and \bar{b} is the Burgers vector. The technique has been described in detail by Amelinckx [220].

In the reflection mode, the back scattered electrons from the surface is used to observe the dislocations. The method, developed by Clarke [239] and Morin et al [240], utilises either electron emission

or cathodoluminescence of the solid upon bombardment with electrons. The crystal defect pattern and the cathodoluminescent pattern has been shown to have one-to-one correspondence by Tajima et al [241].

CHAPTER FIVE

ELECTRICAL CONDUCTIVITY OF ORGANIC CRYSTALS

5.1. Introduction

The conduction phenomena in organic crystals is complicated by the molecular nature of bonding and large relaxation times involved. The extended band model, successfully used to explain the semiconduction of inorganic materials like Si and Ge, cannot be applied as such to the organic materials. In molecular crystals the crystal interaction perturb the molecular levels only slightly, as evidenced by the similarity of photo conduction and absorption spectra in vapour, solution and crystalline materials and hence the mechanism of conduction should be predominantly molecular. The involvement of metastable triplet state in the conduction mechanism has been reported by Rosenberg [242] and Northrop et al [243]. According to the triplet state theory the triplet states of the individual molecules combines to form a Bloch orbital which serves as a conduction band. Optical excitation [242] or thermal activation [244] would put the molecules in their first excited singlet state, from which they would then thermally degenerate into the triplet conduction band. A similar

approach by Eley [245] takes into consideration the tunnelling probability of an electron from some excited state to the excited states of neighbouring molecules.

These and other models have been described in detail by several authors [246,247].

On the experimental part, the electrical measurements on organic crystals are beset with difficulties not encountered in inorganic crystals. Intensive purifications are often required to remove the various impurities inherently present in commercially available material. The difficulty of growing large and perfect single crystals of many organic materials have forced many workers to use either compact powders or other polycrystalline samples. Finally, the large impedance of organic materials and the low mechanical stability of crystals imposes restrictions on the measuring instruments and sample holders. The input impedance of the instrument should be preferably above 10^{19} ohms. At these high resistance values the necessity of proper shielding and removal of water vapour becomes acute.

The specimen for electrical measurements can be prepared in the form of thin films, compacted powders cast slabs, or single crystals. Since the anisotropy of conduction is of interest in elucidating the mechanism involved a single crystal is preferred whenever possible.

The electrical contacts can be made by painting, evaporation or by melting. Of the different contacts, the evaporated ones seems to be widely accepted. To form an ohmic contact, electron or hole injecting electrolytic contacts have been used by Kallmann et al [247]. Holders, suitable for the various specimens have been described by several authors [248,249,250].

5.2. Observable Parameters

The mechanism of conduction in organic solids can only be investigated by measuring a series of parameters. The dark conductivity and its variation with a variable function is often measured by dc or ac methods. The electrical conductivity in the various directions in a single crystal is to be measured to study the anisotropy of conduction. The dimensions of the sample also influences the conduction. The current I flowing through a crystal for a given voltage V is inversely proportional to the length of the sample and directly proportional to the cross-sectional area a . The measurement of the variation of dark conductance with the magnitude of applied voltage often helps to distinguish between ohmic and space charge limited currents.

The conductivity of organic crystals very often follows a relation of the form

$$\sigma = \sigma_0 \exp(-E/2KT) \quad (108)$$

If a plot of the logarithm of the conductivity against $1/T$ is drawn, the activation energy E can be calculated.

The conductivity depends on the drift mobility and density of carriers and hence their measurements are desired wherever possible. Drift mobility is defined as the distance travelled in the field direction by a carrier in unit time in a unit field. The drift mobility is differentiated from macroscopic mobility by the fact that while the former is dependent on the extent of trapping the latter is dependent on the motion between traps. The drift mobility is inversely proportional to the number of traps and their depth. Many et al [251] used the relation,

$$\sigma = e \mu N_0 \exp(-E/KT) \quad (109)$$

to measure the mobility, where e is the electronic charge, μ is the mobility and N_0 the number of charge carriers. Kallmann [252] modified this simple equation as

$$\sigma = (N_0 n_0)^{-1/2} \mu \exp(-E_0/2KT) \quad (110)$$

where N_0 is the density of donor states and n_0 is the density of states in a band, μ is the mobility and E_0 the difference in the energy between the donor level and conduction band.

The sign of the majority carriers involved in the conduction can be determined by measuring the Hall coefficient. To measure the Hall coefficient the crystal is to be prepared in the form of a rectangular bar. A magnetic field H is applied perpendicular to a flat surface while a current I is passed through a direction perpendicular to the magnetic field. The voltage V_H which appears on the remaining faces perpendicular to both the magnetic field and current direction is measured. The Hall coefficient R_H defined as

$$R_H = V_H/IH \quad (111)$$

and the sign of V_H determines the sign of the charge carriers. If the conduction is brought out by only one kind of carriers,

$$R_H = 1/\rho ec \quad (112)$$

where ρ is the concentration of carriers, e the electronic charge and c , the velocity of light. If both carriers are present and if P and n denote their concentration and b denotes the ratio of the mobilities of negative to positive carriers, then,

$$R = (P-nb^2)/(p+nb)^2 ec \quad (113)$$

The measurement of Hall voltages in organic crystals and the theoretical validity of the conventional formulae in organics have been well documented [253,254,255].

The study of photoconduction along with the absorption, fluorescence and phosphorescence spectra often helps to elucidate the different energy levels involved in the electrical conduction mechanism. In the pulsed photoconductivity method developed by Kepler [256] and LeBlanc [257], a crystal is placed in between two electrodes of which, one is a conducting semitransparent electrode. A light pulse of 1μ sec. duration from a flash tube is allowed to fall on the crystal through the semi-transparent electrode. The carriers produced by the external excitation move in the electric field applied to the electrodes and they produce a potential drop in the external circuit which is detected by a cathode ray oscilloscope. The obtained trace can be used to calculate the mobility of the carriers.

5.3. Conductivity Measurements

a) D.C. Methods

The direct current measurements in organic crystals may be made under a two-probe or four-probe configuration. In the two-probe method a voltage V is applied to the specimen by means of two electrical contacts, and the current flowing through the external

circuit is measured [258]. If a is the cross-sectional area and l is the length of the sample, the d.c. conductivity σ can be calculated as

$$\sigma = Il/Va \quad (114)$$

The inherent disadvantages of this method are

1) there may exist a high resistance at the crystal-contact interface and 2) contacts, either carrier injecting type or barrier type may influence the conduction process.

The measuring instrument can be either a galvanometer or d.c. amplifier [259]. Bridge methods can be profitably used to measure resistances upto 10^{14} ohms. For still higher resistances vibrating-reed electrometers having input impedences of 10^{19} ohms, should be used. Of the different methods the pulse method is the most satisfactory [260]. In this method a high voltage pulse is applied across the sample for a fraction of a second and the current or voltage appearing across a resistor is measured.

The inefficiency of electrical contacts in two-probe methods can be overcome with the use of four electrodes. The four electrodes may be used in different configurations. Two probes can make contacts with one face of the sample having the form of a parallelepiped,

two opposite faces of which meet two electrodes. A current is passed through the two electrodes, and the voltage drop between the two probes can be measured.

Instead of two extended electrodes and two measuring probes, all the four electrodes can be used as probes [259]. The four probes, kept in a line and separated by equal distances, are made to make contacts on the crystal surface. A current I is passed through the outermost probes while the voltage V , developed between the inner probes is measured. If S is the inter-electrode spacing, σ is given by

$$\sigma = I/2\pi VS \quad (115)$$

The contacts to the crystal should be made clear of boundaries and the smallest dimension of the crystal should be very large compared to the electrode spacing [260,261].

b) A.C. Methods

In the a.c. method an alternating voltage is applied to the specimen. The resultant current depends both on the capacitance and resistance of the specimen. For an organic material placed between two electrodes, the system can be treated as a capacitance and a resistance connected in parallel. The a.c. conductivity

$$\sigma_{ac} = \omega \epsilon'' \epsilon_0 \quad (116)$$

where ϵ'' is the imaginary part of the permittivity in,

$$\epsilon = \epsilon' + i\epsilon'' \quad (117)$$

and ω is the frequency of the a.c. voltage. σ_{ac} is thus not a constant of the material but varies with frequency. The a.c. resistance cannot be taken as a bulk property since the motion of charge carriers over large distances give rise to a loss. The rotation of the dipoles associated with groups of atoms in a molecule in the solid also result in loss.

5.4. Charge-transfer Complexes

Several organic and semiorganic systems have been found to possess high electronic conductivities in contrast to the high resistances generally offered by organic crystals [262,263]. These systems contain two species of molecules which are stacked alternatively with one species acting as electron donors and the other as electron acceptors. The ratio of the individual components in the complex may vary from 1 : 1 to 57 : 1 [264,265]. The typical resistivities also vary from 0.5 ohm-cm [266] to 10^8 ohm-cm [267].

The majority of these charge-transfer complexes exhibit an exponential temperature dependence of

resistivity,

$$\rho = \rho_0 \exp (E/2KT) \quad (118)$$

In the band model E stands for the activation energy which is the energy difference between the highest level in the valence band and the lowest level in the conduction band.

The study of single crystals of several complexes have shown the high anisotropy of conduction in them. This is due to the peculiar crystal structure and molecular stacking. The easy direction of conduction is often found to be the direction along which the molecules are strongly bonded. In the case of TCNQ/TEA [268], crystal the conductivity have a value of $4 \text{ ohm}^{-1} \text{ cm}^{-1}$ in the easy direction, which is normal to the TCNQ molecules. The effect of structure is more evident in the case of TTF-TCNQ complex [269]. In this, the crystal structure consists of parallel conducting stacks. The neighbouring stacks composed of flat molecules, are tilted with respect to each other. Within a stack both TTF and TCNQ molecular orbitals overlap making conduction of electrons easy while due to the lack of interaction between the stacks the charge transport perpendicular to them is poor.

Reliable measurements requires a perfect single crystal specimen and the growth of single crystals have

been found to be very difficult. Almost all crystals of charge-transfer complexes are very fragile and needle like. The size of crystals are very small, only several millimeters long and hundredths of a millimeter thick. The method of growth of these crystals utilizes the diffusion of the components in a solvent. Several authors have reported the growth of charge-transfer crystals in different apparatus [270,271,272,273]. The crystals usually exhibit a golden metallic lustre except TTF/TCNQ and some others which are black. The specimen preparation and measurement of electrical conduction have been described in several articles [274,275].

CHAPTER SIX

EXPERIMENTAL TECHNIQUES

6.1. Introduction

The present chapter describes the various experimental techniques used in the study of the growth, defect structure and electrical properties of phthalic anhydride and potassium acid phthalate crystals.

6.2. Material Preparation

In the case of phthalic anhydride the material was purified first by recrystallisation from benzene (BDH, Analar) and then by chromatography. For chromatography, the apparatus used was essentially the same as described by Sangster et al [274]. Two columns of approximately 50 cms length filled with either Al_2O_3 or silica gel were used to remove the impurities. The solution, kept above these columns filtered through the columns and pure material was collected at the round bottomed flask kept on a heating mantle. The temperature of the bottom flask was kept above the boiling point of the solvent. The vapours of the solvent were transferred back to the upper flask, through a water cooled condenser

by passing nitrogen gas. The process was repeated and the material crystallised out at the bottom flask. This material was further purified by sublimation in vacuum.

Potassium acid phthalate (BDH Analar) was used, without any further purification.

6.3. Growth of Crystals and Specimen Preparation

a) Growth from solution

Phthalic anhydride crystals were grown from benzene or acetone (BDH, Analar) solutions while potassium acid phthalate crystals were grown from aqueous solutions.

For growth by slow evaporation, saturated solutions of phthalic anhydride in benzene or acetone were prepared at room temperature. The solutions were filtered and kept in a 500 ml beaker for one day after which crystallisation was found to occur. The solution was then again filtered into another beaker of the same capacity and covered with a filter paper. Good quality seeds were introduced into it through holes made in the filter paper. The beaker was then kept in a desiccator provided with stop-cocks. The evaporation rate was controlled by partially opening the stop-cocks. In the

case of acetone solutions the beaker was placed in a desiccator on a wire gauze kept above a petri dish containing water. The desiccators were placed on a bed of thermocole sheets to avoid shocks.

Potassium acid phthalate crystals were grown by the slow cooling method in a Holden crystalliser [275], constructed in this laboratory. The crystalliser is shown in figure (6). It consisted of an air tight container (C) of 1 litre capacity, placed on the platform (P). The heating of the solution in the container was effected by an Infraphil bubb (L), kept below the platform. The lid of the container had provisions for introducing a seed holder (S) and thermometer (T). The seed holder was rotated alternatively in the clockwise and anticlockwise directions by means of a motor (M) and coupling discs (C) [276]. In the actual run a concentrated solution was prepared at 50°C and the seed, properly fixed on the holder by epoxy resin, was introduced into the container. The temperature was then slowly reduced by reducing the voltage applied to the bulb by means of a auto-transformer coupled to a geared motor.

b) Growth from vapour

The experimental set up used for the growth of crystals from vapour is shown in figure (7a,b).

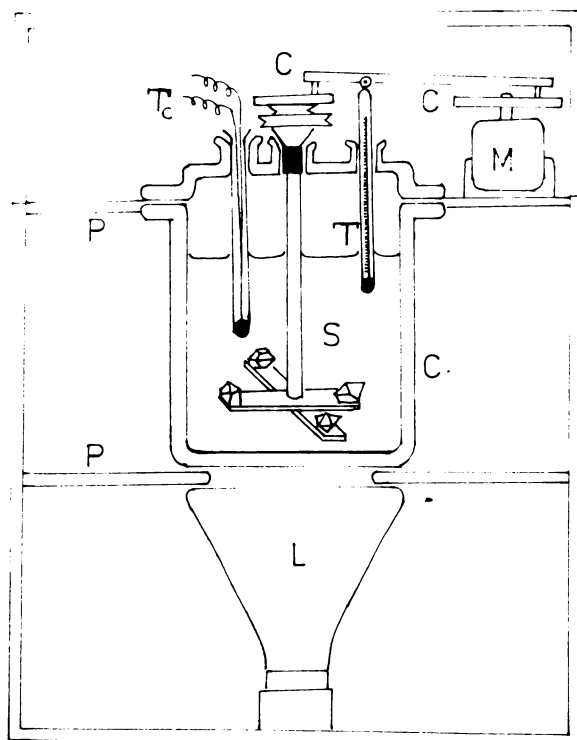


Fig.(6) Apparatus for the growth of crystals by slow cooling.

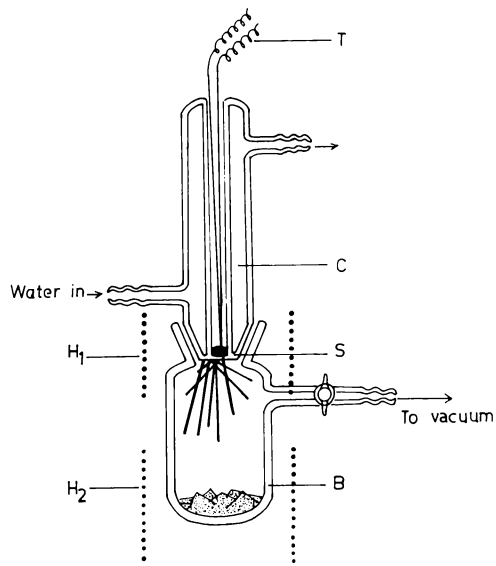


Fig. (7a)

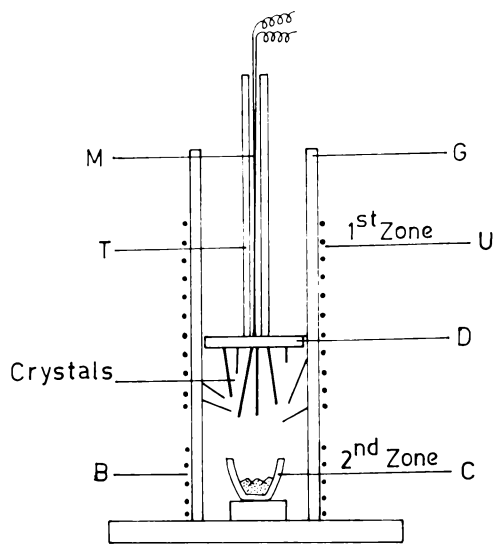


Fig. (7b)

Fig. (7a,b) Experimental set up for the growth of crystals from vapour.

In the set up shown in figure (7a), the material was kept in the bottom flask (B). The flask had an outlet and stop-cock. The substrate (S), on which the crystals are to be grown, was the bottom of a condenser (C) which was joined to the flask by grease-less joints. The condenser had a central hole into which thermocouples (T) were introduced to measure the temperature of the substrate. The temperatures of the source and substrate were controlled by heaters H_1 and H_2 and by the rate of flow of water through the condenser. For growth, the lower flask containing the material was evacuated by a rotary pump and was then isolated by closing the valve. The material and substrate were kept at different constant temperatures. Whisker crystals, growing on the substrate were investigated for the change in morphology with growth temperatures.

In the above set up the distance between the source and substrate could not be varied. The effect of this distance was studied by the apparatus shown in figure (7b). It consisted of a glass tube furnace (G) with two separate zones. The furnace was kept vertical and the source material in a crucible (C) was introduced in the bottom zone (B). The substrate was a glass disc (D) with a diameter equal to that of the inner

diameter of the tube. A glass tube (T) was fixed at the centre of the disc and was placed in the upper zone (U). A thermocouple (M) was introduced through the tube to measure the temperature of the substrate. In this assembly the distance between the source and substrate and the temperature can be varied independently.

The basal plane growth of phthalic anhydride whiskers were studied by a closed vapour-crystal cell [277]. The cell is shown in figure (8). It consists of two glass slides (A) separated by a thin mica sheet (B) of thickness approximately 0.03 cm and having the same size of the slide but cut so as to form a cavity. One side of the cell was left open. The whole assembly was pressed together by copper blocks (C) with a nichrome strip heater (H) at the open end in contact with the bottom slide, forming the hot zone. Chromel/alumel thermocouples (T_c) were used to control the temperature of the hot zone and to plot the temperature profile of the upper and lower slides. During the experiments, the hot zone was kept at different temperatures at or above the melting point. Whiskers obtained by the sublimation of recrystallised material were introduced into the cavity so that it melted and filled

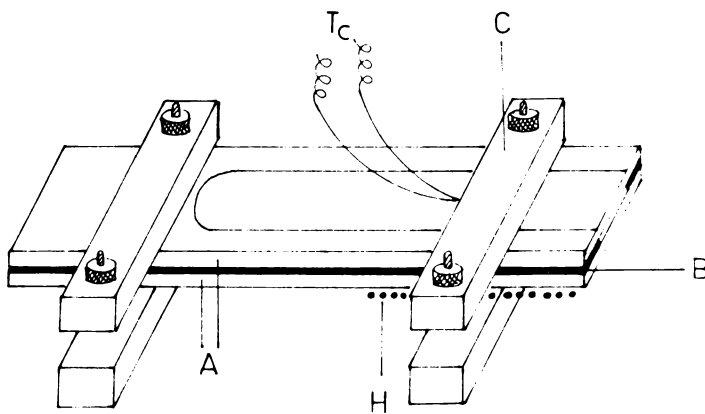


Fig.(8) The closed crystal-vapour system.

the open end upto 0.5 to 1 cm. After two to three minutes after the charge was melted the heater was switched off and allowed to cool to room temperature. The experiments were repeated by changing the temperature of the hot zone and the thickness of the cavity.

c) Growth from melt

Phthalic anhydride was grown from melt by the Bridgman method in a specially built furnace and ampoule.

(i) Furnace

The furnace, used for the growth of phthalic anhydride crystals is shown in figure (9). The design of the furnace suitable for growing organic crystals was made taking into account the low melting points and super cooling tendencies of organic materials. A glass tube (G) of inner diameter 4 cms, thickness 0.4 cm and having a length of 40 cms was wound with nichrome wire. The winding was done mechanically with 4 turns per cm. The furnace had two zones separated by 2 cms. The glass tube was kept in a rectangular enclosure formed by asbestos sheets (S). In the front sheet a rectangular slit (R) was made and a glass window (W) was fixed on it. The length of the window was so made that the lower half of the upper zone and upper half of the lower zone were

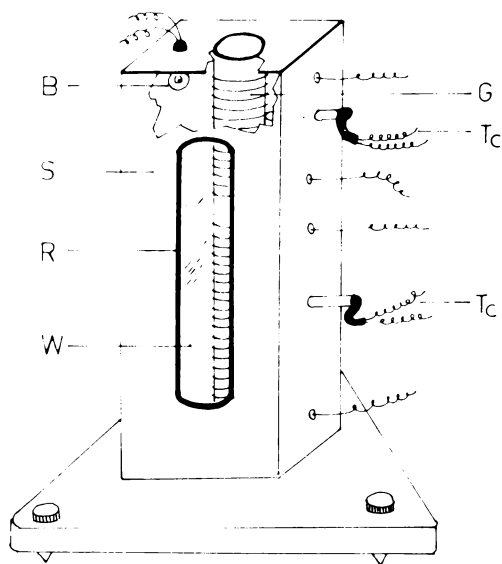


Fig.(9) Furnace suitable for the growth of crystals of low melting point materials by the Bridgman's method.

visible. On the other side holes for introducing of thermocouples (T_c) and the bulb (B) were made. The thermocouples were insulated electrically by means of thin walled glass tubings and were kept in contact with the glass tube furnace at the center of the zones. The whole assembly was placed over a triangular base plate with levelling screws. The top of the furnace was kept closed except for a small hole for the introduction of the growth ampoule. The temperatures of the zones were controlled by means of an Aplab temperature indicator/controller using iron/constantan thermocouple sensors.

(ii) The shape of ampoules

Glass tubes of various diameters were used for the construction of Bridgman tubes. The tubes, properly washed in cleaning solutions and analar grade acetone, were dried in an oven. The tubes were drawn into the shape shown in figure (10). Various tip shapes ranging from simply tapered end to capillary tips with a constriction above were prepared. The purified material was transferred to the ampoule and melted in air to drive out the air bubbles. The melt was then allowed to solidify. The tube containing the material was then fused under vacuum providing a hook for suspending the ampoule. The vortex angle from the constriction was varied over a wide range to study its effect



Fig.(10) A typical Bridgman tube. θ was varied and for $\theta = 15^\circ$ good quality crystals were consistently obtained.

on the formation of single crystals. The ampoule was suspended by a thin copper wire from a geared motor. The ampoule can be either raised or lowered at different speeds from 12.42 cm/mt to 0.06 cm/hr.

d) Specimen preparation

Phthalic anhydride crystals grown by the Bridgman method were cleaved along the $\{110\}$ planes and cut perpendicular to the C-axis using a solvent-string method. The potassium acid phthalate crystals were cleaved along the $\{001\}$ planes and cut into slabs having $\{010\}$ and $\{100\}$ faces. The solvent-string cutter used to cut crystal slices along the desired directions is shown in figure (11). The movable arms of a spectrometer (A) were fixed with pulleys with multiple grooves (P). The prism table (T) formed the specimen holder. The string (S) was attached to the rim of a cam, rotated by a slow motor (M). The string was passed over the pulleys and a weight was attached to the other end of the string. The solvent (Benzene in the case of phthalic anhydride and undersaturated aqueous solutions in the case of potassium acid phthalate) kept in a burette (B) was allowed to drip at a constant rate on the string. As the motor rotated, the string

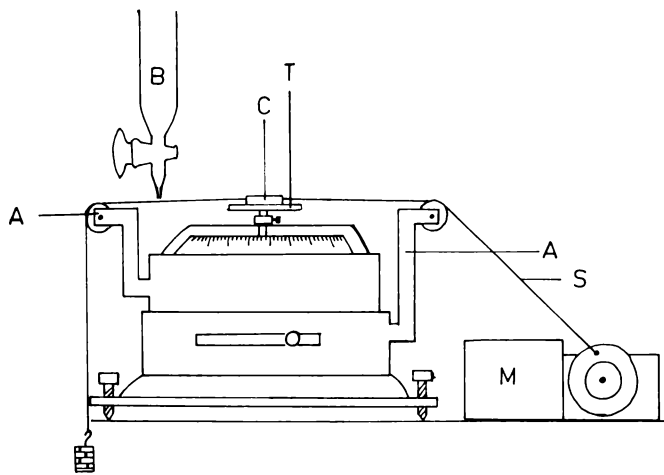


Fig.(11) The solvent-string crystal cutter.

wet with the solvent, made to and fro motion over the crystal (C), oriented suitably. The perfection of the cut depends on the speed with which the string moves over the crystal, the rate at which the solvent wets the string and the pressure exerted on the crystal by the string. At high pressures and speeds the cut gets slanted and at low pressure and low speeds the groove of the cut widens and becomes irregular. The optimum conditions for a perfect cut are to be found out by trial and error.

The chief advantages of the cutter described here are that 1) it allows fine adjustments of pressure exerted by the string by raising or lowering the platform, 2) the rotating arms can be adjusted with accuracy to effect parallel cuts on a crystal without dismantling the crystal and 3) the fine adjustment knobs of the spectrometer can be conveniently used to cut slices whose thickness is limited only by the width of the groove made by the string.

The cut crystals were first polished using a 4/0 emery paper or ground glass and then on a filter paper/lens cleaning paper soaked with suitable solvents. The phthalic anhydride crystals were polished very carefully giving the minimum pressure possible to avoid mechanical deformations.

6.4. Defect Structure

The topographical investigations on the different faces of the crystals were done with a Carl-Zeiss metallurgical microscope. The dislocation configurations and density were determined by chemical and thermal etching.

The crystals were immersed in various chemical reagents for different periods and washed in suitable solvents. The samples were then dried by passing a jet of hot air and then examined for etch-pits. Correspondence of etch pits on the matched cleavage faces of the crystals was taken as evidence that the pits are formed at the emergence points of dislocations on the surface. Successive etching and etching of thin slices of the crystals were also performed. An alternate cleaving and etching procedure was used to study the dislocation configurations.

The effect of annealing on the dislocation content was studied by comparing the etch pit density on the as grown and annealed crystals. The annealing of crystals were done by keeping the crystal at an elevated temperature for long periods.

6.5. Surface topography of crystal cleavages

The technique of Multiple-Beam Interferometry [278,279,280,281] was used to observe the topographical features on the cleavage surfaces of the potassium acid phthalate crystals.

(1) Preparation of specimens

Since the crystals were transparent, vacuum evaporation was used to prepare reflecting films, on the surfaces. The evaporation was done in a vacuum coating unit supplied by Hind-High Vacuum Co. Pvt. Ltd. capable of producing a vacuum of better than 10^{-5} torr. The freshly cleaved crystals were kept in the bell jar of the unit and silver of 99.999 % purity was evaporated from a molybdenum boat on to it at 10^{-5} torr. Semitransparent films were likewise prepared on microscope slides or cover slips.

The conventional jig was modified to suit the Carl-Zeiss microscope. The modified jig is shown in figure (12). It consisted of three stainless steel discs (D). The upper disc was made so as to fit the mechanical stage of the microscope. The lower disc, was fixed to the upper by means of three rods (R), and had a circular hole in it. The central disc was capable

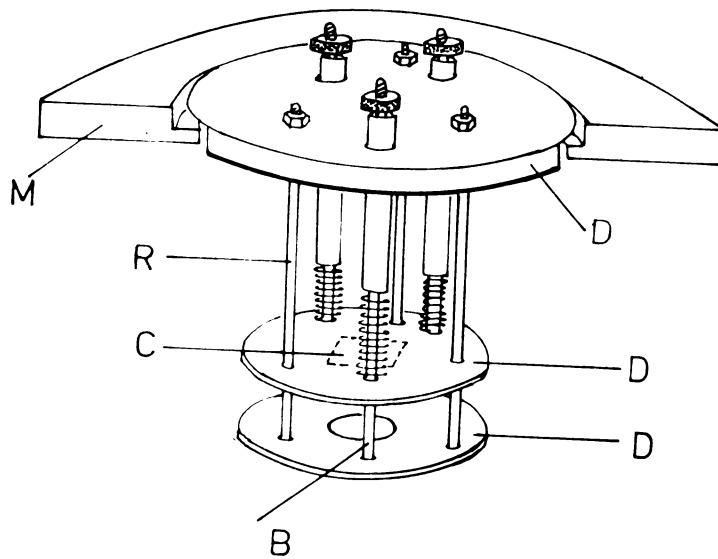
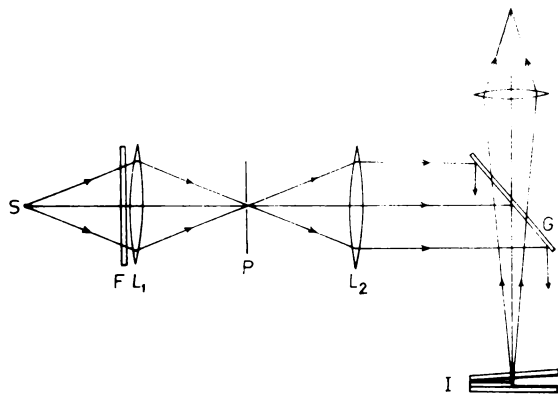


Fig.(12) The modified jig for multiple-beam interferometry.

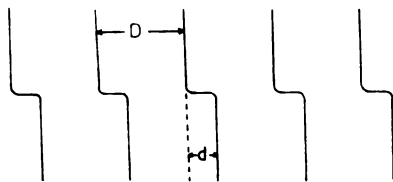
of free movement over these rods. Another set of three rods (B) carrying brass tubings and springs were used to adjust the wedge angle. The crystal (C) was fixed on the bottom side of the central disc and the semi-transparent glass plate was placed over the hole of the lower disc. The illumination was effected, by a 12V, 100 watt bulb with tungsten filament for the observation of fringes of equal chromatic order. The bulb was replaced by a suitably collimated mercury green light to observe the Fizeau fringes.

(ii) Fizeau fringes

Multiple-beam interferometry utilises the interference of light waves formed at the wedge between a highly reflecting surface of the object and a semi-transparent glass plate. The Fizeau fringes are formed when the illumination is by monochromatic light. The experimental arrangement is shown in figure (13a). Light from the source (S) is made monochromatic by means of a filter (F) and is focussed on a slit (P) by means of a lens (L_1). The light rays from the slit is then focussed on the wedge by another lens (L_2). The wedge (I) is formed by a semisilvered glass plate and reflecting surface under observation. A typical fringe system observed in the case of an abrupt step is shown



(a)



(b)

Fig.(13a) Interferometer arrangement for Fizeau fringes.

(13b) Fringes produced by the interferometer at an abrupt step.

in figure (13b). The separation of two adjacent fringes corresponds to $\lambda/2$ where λ is the wave-length of the monochromatic light used. The step height is thus given as

$$t = (d/D)(\lambda/2) \quad (119)$$

where d is the relative shift in the upper and lower fringe systems and D is the spacing between adjacent fringes.

(iii) Fringes of equal chromatic order

To obtain the fringes of equal chromatic order, the monochromatic light is to be replaced by a white light source. The arrangement for obtaining FECO is shown in figure (14a,b) along with the fringe system. White light emitted by the source (S) is focussed on to a wedge (I) by means of lens (L_1) and a beam splitter (G). The reflected rays from the wedge (I) is collected by another lens (L_2) and focussed on the slit of a constant deviation spectrograph (P). In the spectrogram the fringes appear at different wavelength regions--from red to violet. The fringe system shown in figure (14b) is typical of an abrupt step. Considering two fringes corresponding to λ_1 and λ_2 , having a fringe shift $\Delta\lambda$ the step height is given by,

$$t = \frac{\lambda_2}{2} \frac{\Delta\lambda}{\lambda_1 - \lambda_2} \quad (120)$$

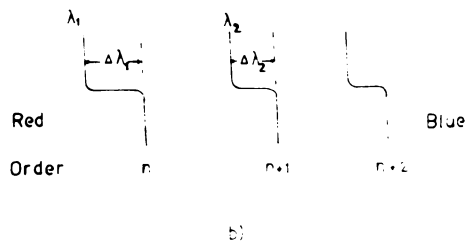
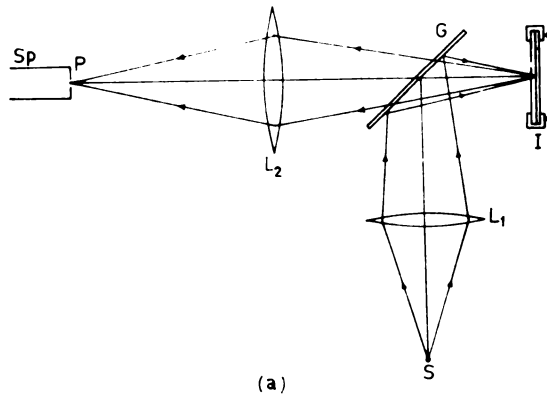


Fig.(14a) Interferometer arrangement for fringes of equal chromatic order.

(14b) Typical fringes of equal chromatic order.

6.6. Investigations on Slip Systems

The crystal specimens were indented by a Hanemann microhardness indenter supplied along with the Carl-Zeiss microscope.

The Hanemann hardness tester consisted of a diamond, polished in the shape of a quadrangular pyramid, whose sides have a slope of $\beta = 22^\circ$. The bottom of the diamond, shaped in the form of a short bar, is mounted on a small hole drilled into the front lens. Large annular portions are left free in the front lens for illumination and observation of the object. It also had an optical device to indicate the testing load. The objective, with the diamond is suspended from two disc springs. Any load applied to the diamond caused the suspension to activate the optical system which indicated the load through the eye-piece.

The eye-piece had two reticles (one stationary and other free to move), each of which is a right angle. The two markings can be used to measure the diagonal length or the area of the indentation mark. By proper calibration of eye-piece and load scales, loads as small as 0.2 grams and as great as 200 grams can be applied to the specimen surface.

Indentations were made on the {001} faces and {110} faces of phthalic anhydride crystals. On potassium acid phthalate the {001}, {100} and {010} faces were indented. The slip traces around the indentation marks on the different faces were recorded photographically, and were used to identify the slip system.

6.7. Conductivity Measurements

The crystal holder and enclosure used to study the conductivity is shown in figure (15). The holder consisted of two copper electrodes (E) isolated from the rest of the holder by teflon discs (F). The spring loaded cell had a base plate on which a glass heater wound with nichrome tape, was placed. The holder was suspended on a glass supporting rod (G). The cell (C) had provisions for evacuation (V) or for the flow of an inert gas (I). The electrical connections were taken out through the top lid, insulated by teflon spacers. The spacers were fixed on the holes of the lid by means of araldite. Chromel/Alumel thermocouples were used to measure and control the temperature. Activated silica gel was kept at the bottom of the cell to absorb any water vapour present.

The crystal specimen properly cut and polished had either the shape of a circular disc or rectangular

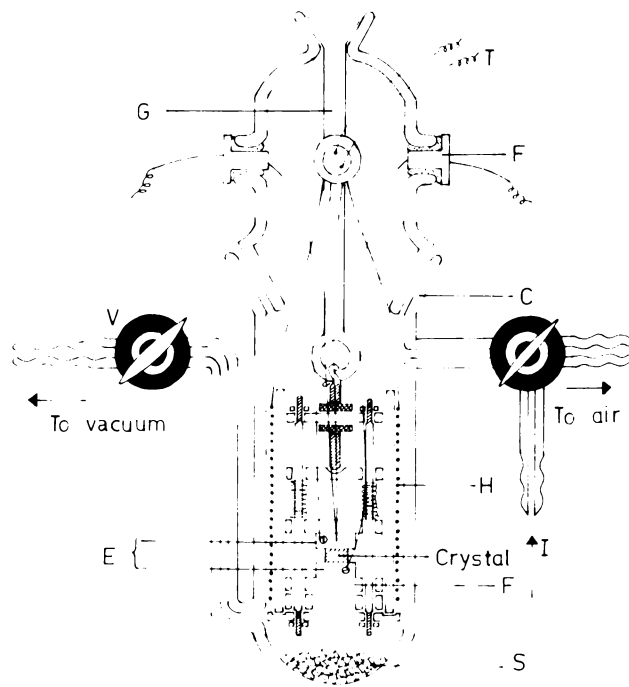


Fig.(15) The crystal holder and cell for d.c. conductivity studies.

slabs. The crystal faces were painted with air drying silver paint and kept between the copper electrodes pressed by the light springs. The conductivity at different temperatures was measured with a ECIL electrometer or British Physical Laboratory million-meg-ohm meter. A d.c. voltage was applied to the crystal and the current flowing through the external circuit was measured. The temperature dependence of conductivity was investigated by heating/cooling the crystal. In the case of phthalic anhydride the resistance variation with temperature was investigated in the $\langle 001 \rangle$ direction and in a direction perpendicular to it. In potassium acid phthalate the measurements were made in the $\langle 001 \rangle$, $\langle 010 \rangle$ and $\langle 100 \rangle$ directions.

The problem of stray charge accumulation was avoided by keeping the whole cell in a rectangular copper enclosure, connected to the earth, and by using shielded wires of short length, for electrical connections.

CHAPTER SEVEN
RESULTS AND DISCUSSION

7.1. Introduction

Phthalic anhydride [$C_6H_4(CO)_2O$] is a member of the carboxylic acid anhydrides. The material was studied by Groth [282] in the crystalline form and was classified as orthorhombic. The lattice parameters were determined by X-ray diffraction by Williams et al [283], to be $a = 7.90\overset{\circ}{\text{Å}}$, $b = 14.16\overset{\circ}{\text{Å}}$ and $c = 5.94\overset{\circ}{\text{Å}}$. By single crystal rotation techniques, Pandey [284] modified these values as $a = 7.86\overset{\circ}{\text{Å}}$, $b = 14.18\overset{\circ}{\text{Å}}$ and $c = 5.904\overset{\circ}{\text{Å}}$. The crystal was shown to belong either to C_{2v}^9 or D_{2h}^{16} space group. Banerji [285] removed this ambiguity in the space group and assigned the non-centrosymmetric space group C_{2v}^9 , for the crystal.

Though it has been reported [283] that the crystals of this material can be grown from alcohol, acetone or chloroform, the crystals obtained were of small sizes suitable, perhaps, only for X-ray work. Bradley [286] has grown long whisker crystals from vapour and has measured the Youngs and Shear moduli. Buckley [287] has also mentioned the growth of whiskers

of this material by the chemical decomposition of phthalic acid.

Potassium acid phthalate [$\text{COOKC}_6\text{H}_4\text{COOH}$] is an ortho-substituted benzo acid derivative. Potassium acid phthalate, has been shown to belong to the orthorhombic system by Groth [288]. Okaya et al extended the study of the crystal structure of ammonium acid phthalate to the potassium salt and assigned a space group of $P2_12_12$ [289]. Later Okaya [290], by more refined experimental techniques, corrected the space group as $P2_1ab(C_{2v}^5)$. The lattice parameters were determined to be $a = 6.46\text{\AA}$, $b = 9.60\text{\AA}$ and $c = 13.85\text{\AA}$.

Bohm et al [291] have reported the growth of large single crystals of this material. The crystals were grown by the slow cooling of aqueous solutions from 50°C to 30°C . Though the crystal finds applications in the fields of soft X-ray spectroscopy [28] and piezoelectricity [26], no attempt hitherto has been made either to study the morphology or the perfection of these crystals.

7.2. Growth of Crystals

a) Phthalic anhydride

Phthalic anhydride was extensively purified, as described earlier, by recrystallisation, column

chromatography and sublimation. The purified material was used for the crystal growth from solution, vapour and melt.

(i) Solution growth

Phthalic anhydride is only sparingly soluble in many solvents. Table (1) gives the solubility data in water, carbon di-sulphide, formic acid and pyridine. Of these solvents only water and pyridine have solubilities suitable for crystal growth. But the possible reaction between water and phthalic anhydride and the high viscosity of pyridine prohibit the use of both these solvents. The organic solvents, such as, acetone, benzene and chloroform, suggested by Williams [283] were more suitable. But, the high volatility of these solvents prevented the growth of large single crystals. These solvents produced rapid evaporation and 'creeping' on the sides of the container. The acetone solutions were found to be relatively more suitable compared to others. The solution grown crystals were small and exhibited prism $\{110\}$, brachydome $\{011\}$ and pyramid $\{111\}$. Orthographic projection of a typical crystal of phthalic anhydride is shown in figure (16).

(ii) Whiskers and hollow crystals - Vapour growth

Phthalic anhydride, due to its high vapour pressure, can be conveniently grown from vapour. Table (2)

Table (1)

Solubility of Phthalic Anhydride in Various Solvents

Solvent	Temperature in °C	Solubility gm/gm of solvent
Water	25	0.62
Water	135	95.00
Carbon di-sulphide	20	0.70
Formic Acid	20	4.70
Pyridine	20	80.00

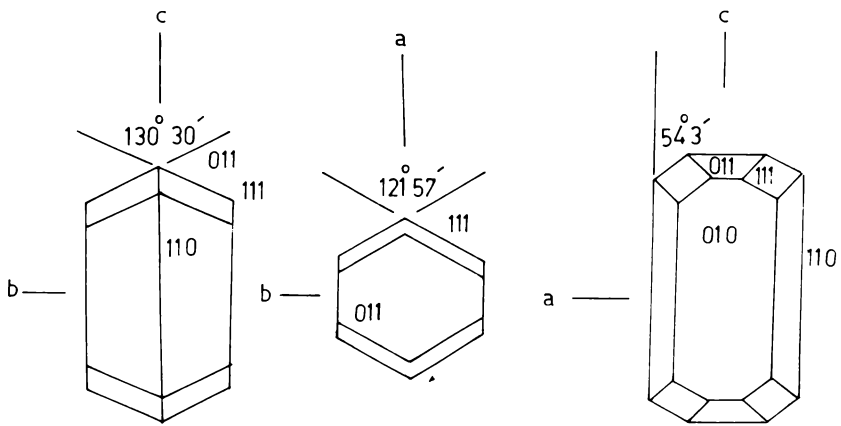


Fig.(16) Orthographic projection of a typical crystal of phthalic anhydride.

Table (2)

Vapour pressure of Phthalic Anhydride at various temperatures

Temperature in °C	Vapour pressure in mm of Hg
96.5	1.0
132.0	6.0
135.0	7.0
140.0	8.7
160.0	20.5
180.0	41.0
197.0	75.0
200.0	80.5
284.5	760.0

gives the vapour pressure of phthalic anhydride at various temperatures.

Crystals were grown by the methods already described [figure (7a) and figure (7b)]. A typical whisker crystal grown by the set up [figure (7a)] is shown in figure (17). Such whiskers were formed on the glass substrate. The whiskers were uniform throughout their length and had parallelogram cross-sections. The parallelogram had angles 58° and 122° . As observed by Bradley [286] these whiskers were bound by $\{110\}$ faces which are the cleavage planes of the crystal. The temperature difference between the source material and substrate ($\Delta T^\circ\text{C}$) was found to have a strong effect on the morphology of the crystals. At low values of ΔT the growth was slow and resulted in whiskers. At large values of ΔT the whisker crystals were found to develop with a slightly modified morphology at the tip. The crystals grown by the experimental set up, shown in figure (7b), also exhibited similar tendency. Whiskers were formed on the side walls of the furnace tube as well as on the glass disc. The crystals on the glass disc were oriented perpendicular or nearly perpendicular to it

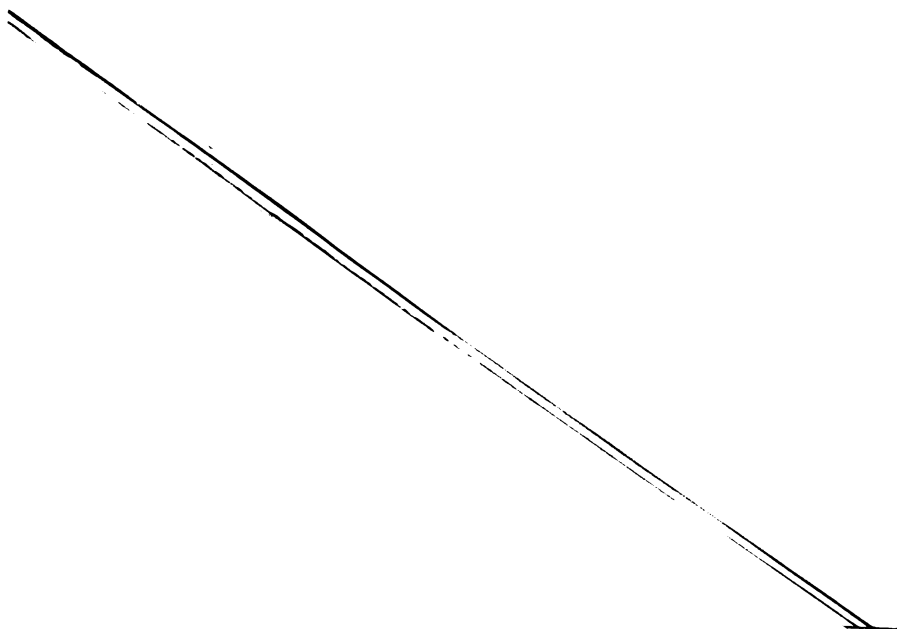


Fig.(17) A typical whisker crystal of phthalic anhydride (x 36).

while crystals formed on the furnace tube were randomly oriented. At low temperature differences of charge and substrate, uniform transparent hollow crystals with cross sections ranging from wedge to parallelograms were observed. Openings were left in the prismatic walls as shown in figure (18). At high temperature differences of charge and substrate hollow crystals with a bead at top were observed.(figure 19). Beaded crystals were also observed at low temperature differences after long intervals of time. In general the growth process seemed to be the same except for the slow growth rates at low $\Delta T^{\circ}\text{C}$.

Hollow crystals with an opening left in their prismatic faces have been observed in several materials. Iwanaga et al [154] have observed similar morphology in ZnO and ZnSe crystals. They have observed a large number of striations parallel to the whisker axis and have suggested a mechanism which essentially consisted of space filling between the spaces of an array of whiskers growing parallel to each other. But the formation of a hollow crystal with well defined planes requires a regular formation of whisker array even in the nucleation stage. Later the same authors extended their study of these hollow crystals by

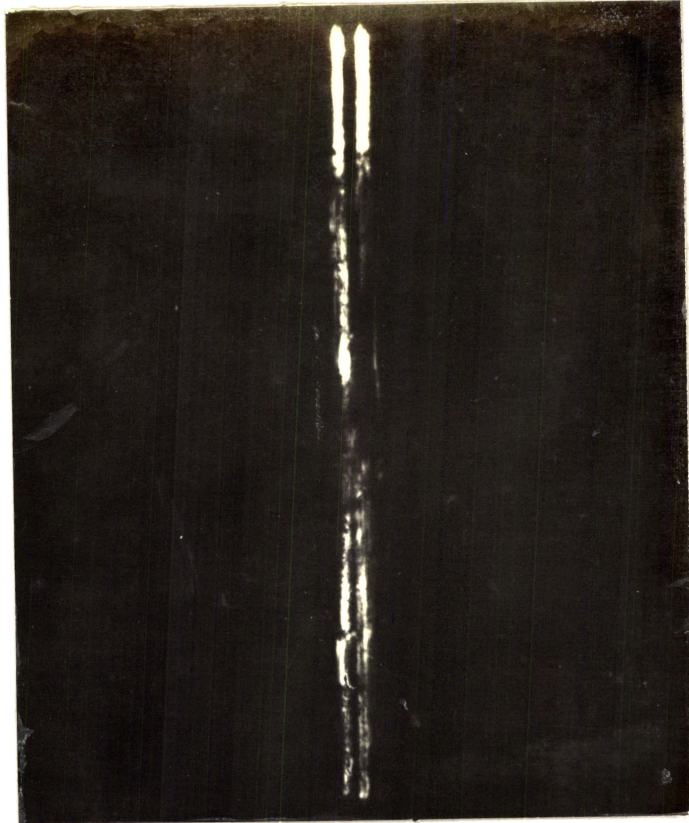


Fig.(18) A uniform hollow crystal with an opening in the prismatic wall (x 40).



Fig.(19) A beaded crystal with the side channel (x 100).

electron microscopic observations and have shown that dendritic growth preceded the formation of hopper crystals. In phthalic anhydride striations parallel to the whisker axis were not observed. The growth of phthalic anhydride hollow crystals was seen to begin with the development of one or two of the $\{110\}$ planes that bound the crystal. Figure (20) shows the wedge shaped crystal tip with $(1\bar{1}0)$ and $(\bar{1}\bar{1}0)$ faces. Observations on the $\{110\}$ faces of the initially grown whisker showed profusely growing short side whiskers. These side whiskers apparently grow in the $\langle 110 \rangle$ directions and the faces of hollow whiskers were produced by the filling of space between these side whiskers. Figure (21) shows the side whiskers growing on an $\{110\}$ face of a whisker. The $(1\bar{1}0)$ and $(\bar{1}\bar{1}0)$ faces after growing approximately to the same extent were found to wind round to form the (110) and $(\bar{1}10)$ faces. The tip of a hollow crystal which has the four faces is shown in figure (22). In the figure the fourth face has not completed growth. As the last face surrounding the cavity has started to grow, this face exhibited a tendency to grow in the $\langle 001 \rangle$ direction rather than in the $\langle 110 \rangle$ direction. Thus the crystal grew in the $\langle 001 \rangle$ direction leaving an opening in their prismatic face. The formation of the narrow



Fig.(20) A wedge shaped crystal tip (x 480).



Fig.(21) side whiskers growing from an $\{110\}$ face of a whisker crystal (x 400).

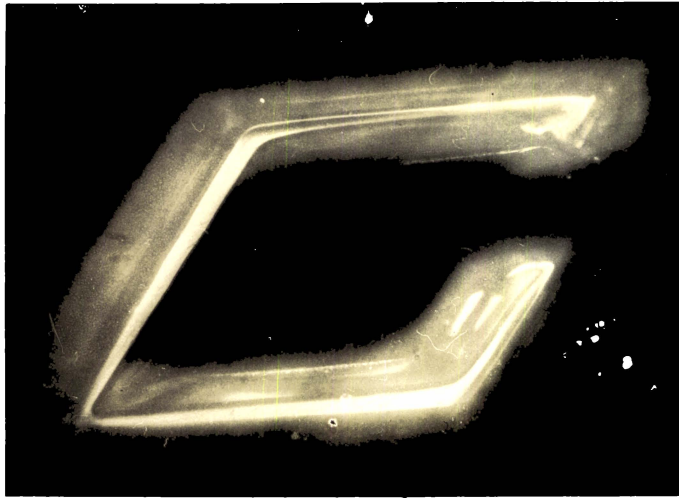


Fig.(22) Growing tip of a hollow crystal with an opening in the prismatic wall (x 120)



Fig.(23) Longitudinal view of a hollow crystal showing steps along the groove (x 150).

opening was also facilitated by the increasingly difficult nucleation inside the gap as the faces closed up. The whiskers or hollow crystals were found to cease growth after a certain length along the $\langle 001 \rangle$ direction, probably due to the change in temperature as the crystals grow towards the source. Further growth occurred at the tip only. The vapours now condensed at the tip to close the opening and started to fill the cavity at the tip. This occasionally resulted in the formation of steps inside the channel at the tip as shown in figure (23). Further growth took place at the tip forming the $\{010\}$ planes and thus converting the parallelogram cross section, to hexagonal cross section. A partially filled and completely filled hexagonal tips of hollow crystals are shown in figure (24) and (25). After the formation of hexagonal tips the growth proceeded in the $\langle 110 \rangle$ directions in which the wedge was first formed. These faces slowly wind round at the tip as shown in figure (26).

The growth process is shown schematically in figure (27).

To study the basal plane growth of these whiskers, the closed crystal-vapour system already described in 6.3(b), was used. The entire length of

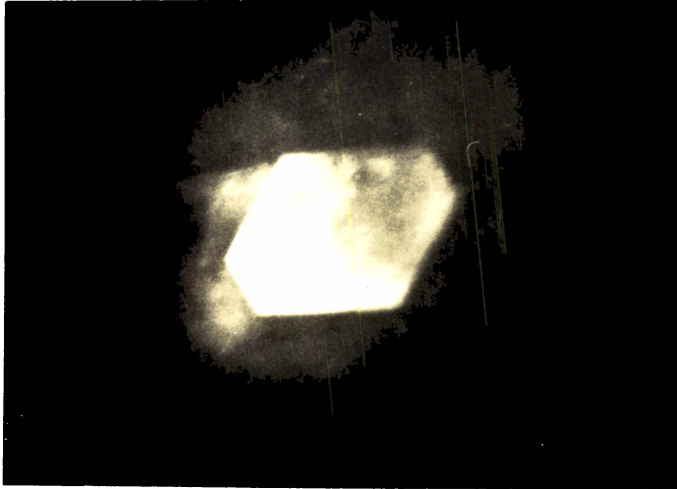


Fig.(24) Partially filled hexagonal tip of a whisker crystal (x 200).

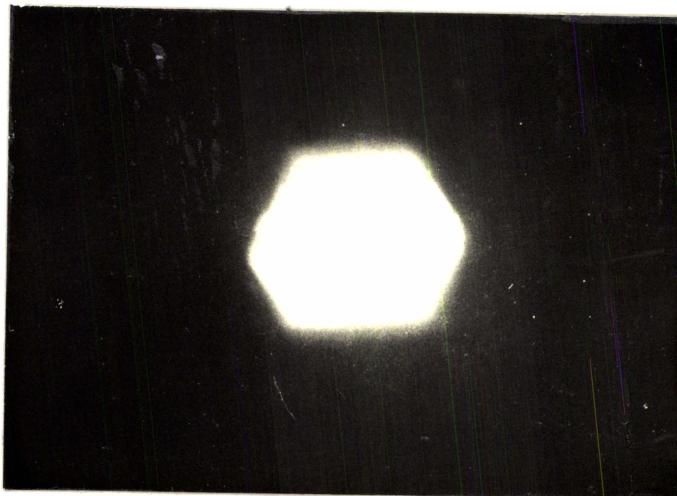
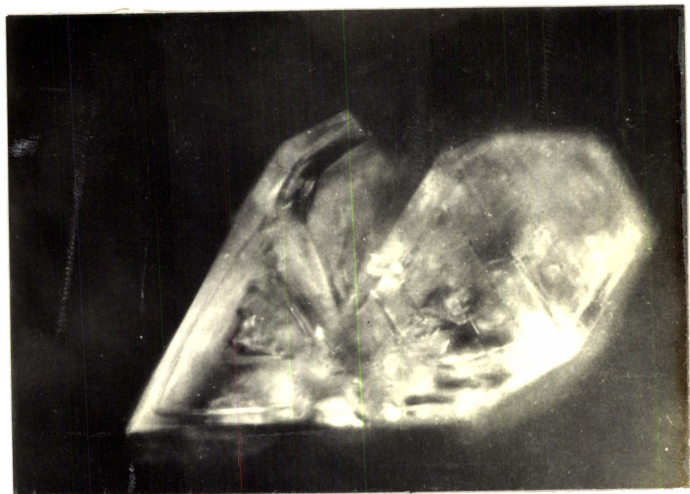


Fig.(25) Completely filled tip of a hollow crystal (x 200).



**Fig.(26) A hollow crystal with hexagonal tip
with a wedge (x 80).**

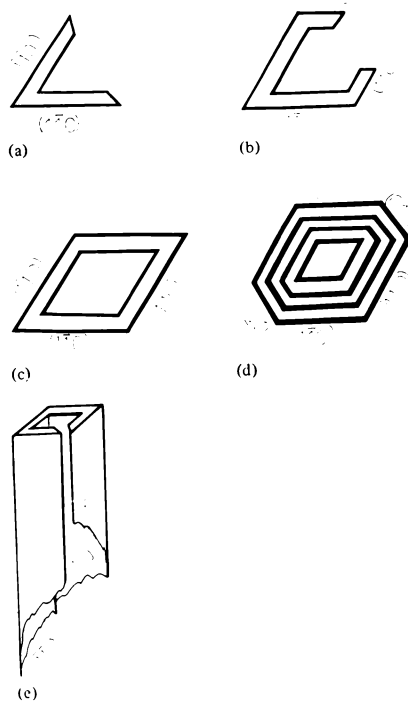


Fig.(27) Schematic diagram showing different stages of growth: (a) to (c) formation of parallelogram tip from wedge shaped tip; (d) transition from parallelogram to hexagon; (e) longitudinal view of the crystal with an opening in the prismatic wall.

the cell could be divided into three regions. The first region, that is the hot zone, contained the material and the heater. The second zone was close to the hot zone and was about 1 to 1.5 cm long. This zone was free of any crystals. In the third zone beyond the second, clusters of crystals were observed. The temperature profile along the cell, at a particular temperature of the hot zone is shown in figure (28).

According to Sears [292], the whisker crystals probably nucleate at the imperfections of the glass substrate. In the present cell, the growth along the whisker axis was suppressed by the upper slide and the growth in the basal plane alone was allowed. The third zone contained crystals in the various stages of growth. The sequential development of the crystals nucleated are shown in figure (29a,b,c). The nuclei, after attaining a critical size was observed to develop side branches in $\langle 110 \rangle$ directions as shown in figure (29a). These branches were observed to wind round in the other $\langle 110 \rangle$ directions [figure (29b)]. The process was seen to be followed by space-filling, to result in the perfect parallelogram platelet crystals as shown in figure (29c). This growth sequence supported the mechanism suggested for the hollow crystals.

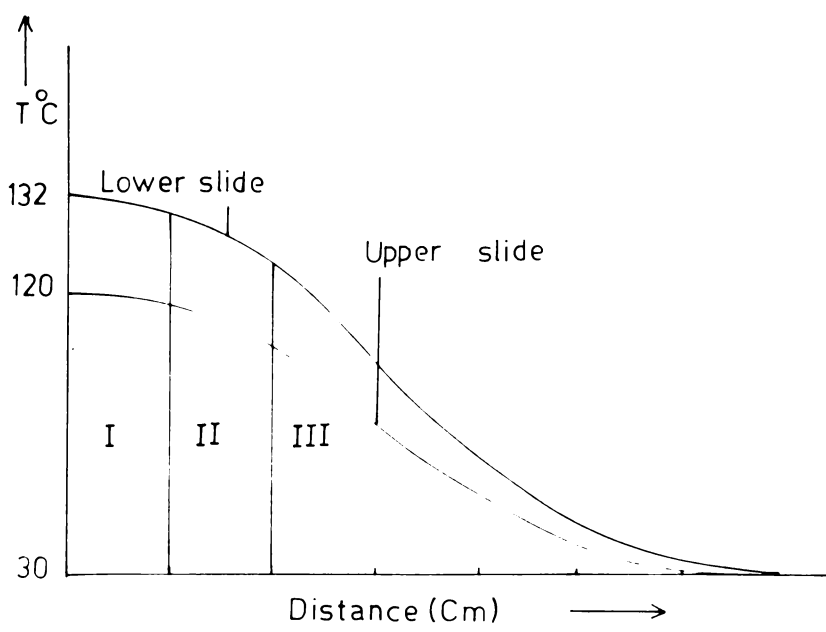


Fig.(28) Temperature profile along the cell.



Fig.(29a)

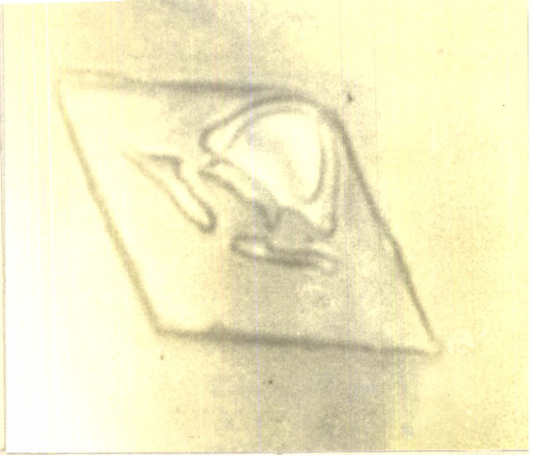


Fig.(29b)

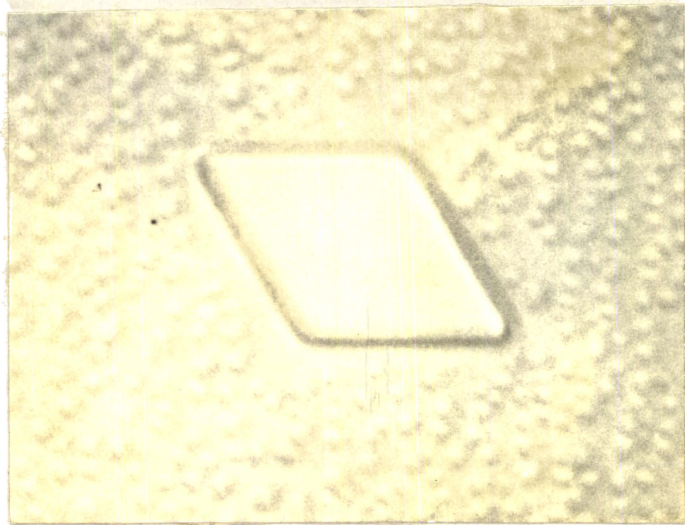


Fig.(29c)

Fig.(29a, b & c) Sequential development of platelet crystals growing in the (001) plane (X 400)

(iii) Dendritic growth

Due to the active role played by the dendritic branching in the hollow crystal formation and basal plane growth, it was thought useful to study the dendritic growth of this material in detail. Phthalic anhydride dendrites were obtained from solution and melt. Solutions were prepared with different concentrations, in benzene (Analar BDH) and were decanted on microscope slides by a graduated syringe. The slides were kept in an enclosure and were allowed to evaporate. The solutions, on evaporation produced crystals of various morphology. Table (3) gives the relative abundance of each type of habit at various concentrations of the solution. It was seen that dendrites predominated at a concentration of $1/500 \text{ gm/cm}^3$.

To grow dendrites from melt, the material was sandwiched between two glass slides and melted by placing it over a wire wound strip-heater controlled by a thermostat. The melt after attaining the desired temperatures was transferred quickly to a metal block, kept at different constant temperatures below the melting point of the material. The melt exhibited a tendency to remain supercooled. The habit of crystals showed a strong dependence on the temperature difference

Table (3)

The habit variation of Phthalic Anhydride with concentration

Concentration in gm/cm ³	Habit of Crystals		
	Dendrites	Fibrils	Platelets
1/1200	Nil	Nil	Nil
1/800	Nil	Nil	Nil
1/700	+	+	Nil
1/600	+	+	+
1/500	+++	++	++
1/400	++	+++	++
1/300	+	++++	+++

The number of + sign indicates the relative abundance of each habit.

between the metal block and the melt ($\Delta T^{\circ}\text{C}$). At low values of ΔT the habit was that of needles whose thickness decreased with increase of ΔT and at about $\Delta T = 30^{\circ}\text{C}$ to 40°C , dendritic growth was found to set in.

Irrespective of the method of growth, the dendrites exhibited the same morphology. It was possible to classify the dendrites into the following categories:

- 1) Six-armed dendrites
- 2) Inclined dendrites
- 3) Perpendicular dendrites

A six-armed dendrite is shown in figure (30). The different primary branches were inclined to each other by $\sim 60^{\circ}$. The secondary branches were likewise oriented to the primary branches. This type of dendrites may be formed by twinning about $\langle 110 \rangle$ directions. Arbitrarily selecting $\langle \bar{1}10 \rangle$ and $\langle 1\bar{1}0 \rangle$ as the directions in which the primary branches developed the other primary branches inclined at 60° to them grow on either side in $\langle 110 \rangle$ and $\langle \bar{1}\bar{1}0 \rangle$ directions. Because of the symmetry of these directions any direction can be taken as the twin axis.



Fig.(30) A six armed dendrite (x 1000).

The inclined dendrites shown in figure (31) had two $\langle 110 \rangle$ primary branches inclined at $\sim 60^\circ$ to each other. The secondary and tertiary branches developed in the space enclosed by these primary branches. The formation of inclined dendrites may be considered as a special case of six armed dendrites where only two neighbouring $\langle 110 \rangle$ branches are active.

A typical dendrite with perpendicular branches is shown in figure (32). It was seen that the tips of these perpendicular branches contained crystals of parallelogram shape. Figure (33) and (34) shows the dendritic tips with the parallelogram crystals. The crystals were exactly same as those obtained from the closed crystal-vapour system. From the crystal morphology, the dendritic branches of the perpendicular dendrites were seen to develop in $\langle 010 \rangle$ and $\langle 100 \rangle$ directions. The branch growing in $\langle 010 \rangle$ directions usually had the secondary branches in $\langle 100 \rangle$ directions. In some cases secondary branchings in the $\langle 110 \rangle$ directions were also observed, on either side of a primary branch developed in $\langle 010 \rangle$ or $\langle 100 \rangle$ directions. These branches were seen to wind round in the other $\langle 110 \rangle$ directions to form parallelogram crystals. This process was often found to result in the formation of linear crystal



Fig.(31) A portion of the inclined dendrites showing secondary and tertiary branching (x 400).

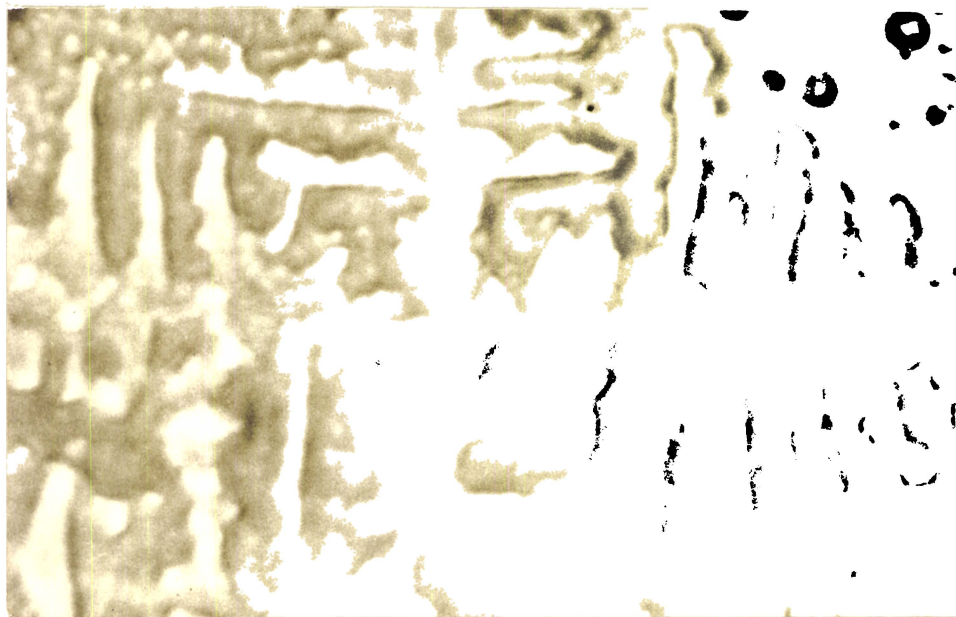


Fig.(32) A dendrite with perpendicular branches (x 500).



Fig.(33) The tip of a dendritic branch growing in $\langle 010 \rangle$ direction (x 900).

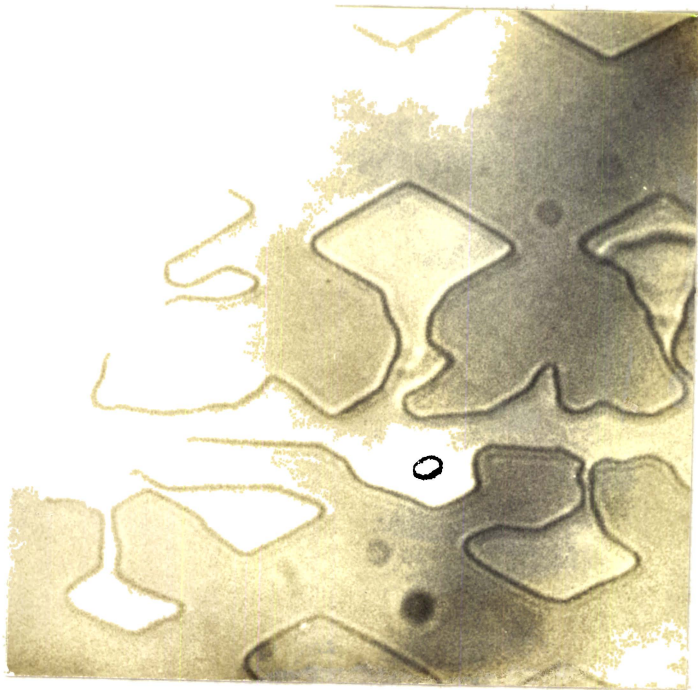


Fig.(34) The tip of a dendritic branch growing in $\langle 100 \rangle$ direction (x 500).

chains. The mechanism of growth of these crystals were found to be very similar to the mechanism suggested for hollow crystal formation.

In the case of $\langle 010 \rangle$ primary branches the $\langle 110 \rangle$ secondary branches were found to make an angle of $\sim 60^\circ$ to each other and in the case of a $\langle 100 \rangle$ primary branches they made an angle $\sim 120^\circ$ to each other. As growth proceeded the $\langle 110 \rangle$ branch tips were found to change their direction in the other equivalent $\langle 110 \rangle$ directions. Before completing the parallelogram these branches diverged again in the $\langle 110 \rangle$ directions. This process followed by space-filling resulted in linear chain crystals. The linear crystal chains growing in $\langle 010 \rangle$ and $\langle 100 \rangle$ directions are shown in figure (35) and (36). The process is schematically shown in figure (37). It was seen that the ratio of the maximum width [AB in figure (37)] to the width at which the next platelet started to grow [CD in figure (37)] remained as 4 : 1 for $\langle 010 \rangle$ chain axis and 2 : 1 for the $\langle 100 \rangle$ chain axis. The dendritic growth, followed by spacefilling, to result in hexagonal platelets is shown in figure (38).

The observations on the phthalic anhydride dendrites showed that the active growth directions in

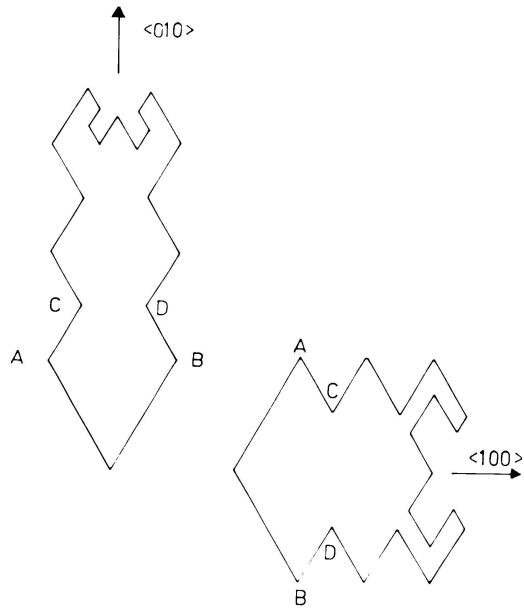


Fig.(37) Schematic diagram showing the formation of crystal chains.



Fig.(38) An hexagonal crystal growing from solution by the filling-in process (x 600).

whiskers, hollow crystals and dendrites were essentially limited to $\langle 001 \rangle$, $\langle 110 \rangle$, $\langle 010 \rangle$ and $\langle 100 \rangle$ directions.

(iv) Spherulitic growth

During the study of dendritic growth from melt, it was seen that the melt exhibited a tendency to supercool in the absence of any external interference. As mentioned in section 7.2(a)iii, the crystallisation started with the development of needles whose width decreased with ΔT . As such, it was thought interesting to examine in detail the crystallisation behaviour in the region of supercooling, by artificial nucleation. The molten material was prepared by heating the material between a glass slide and microscope coverslips. The molten charge was transferred to a metal block maintained at different constant temperatures below the melting point of the material and allowed to cool. Nucleation was artificially induced in these supercooled melts, by cooling the center momentarily. The cooling was effected either by placing a sharp metallic needle tip, or by blowing a jet of air through a fine nozzle at the center of the melt. The nuclei so generated were seen to develop as fibrils growing in all directions. The resultant morphology was similar to spherulites, observed

during the crystallisation of polymers [293,294] and inorganic materials [295]. A spherulite of phthalic anhydride grown from melt viewed under crossed polaroids is shown in figure (39). The simple maltese cross observed, was typical of spherulitic systems. The substructure of these spherulites were fibers whose thickness showed a strong dependence on the supercooling $\Delta T^{\circ}\text{C}$. Figures (40) and (41) show the spherulites grown at $\Delta T = 30^{\circ}\text{C}$ and $\Delta T = 10^{\circ}\text{C}$ respectively. The characteristic periodic splitting [296] was found to become less prominent as the supercooling was reduced and finally disappeared at very small ΔT .

According to Keith and Padden [296] the spherulitic growth is initiated by the impurities inherently present in organic materials. In phthalic anhydride the impurities even if present, does not produce point cooling initiating spherulitic growth. External cooling was found necessary without which no spherulitic growth started. The natural habit of phthalic anhydride crystals are needles or whiskers, as it should be expected according to the unit cell dimensions [297]. This habit was maintained in the artificially initiated spherulitic growth also. The

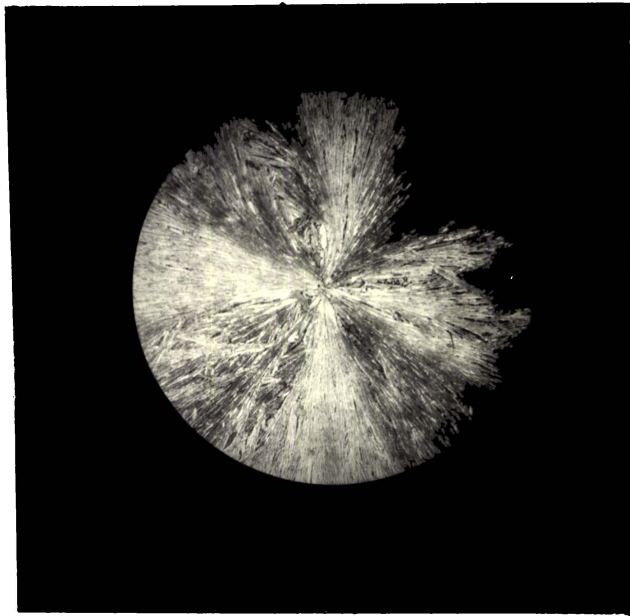


Fig.(39) A spherulite viewed under crossed polaroids (x 5).

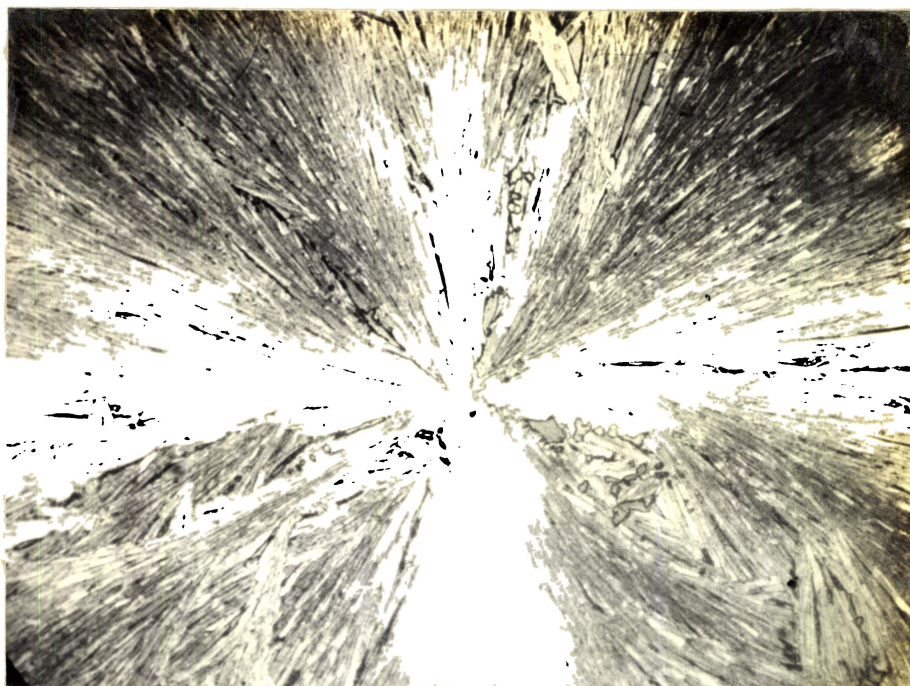


Fig.(40) A spherulite grown at $\Delta T = 30^{\circ}\text{C}$ (x 36).

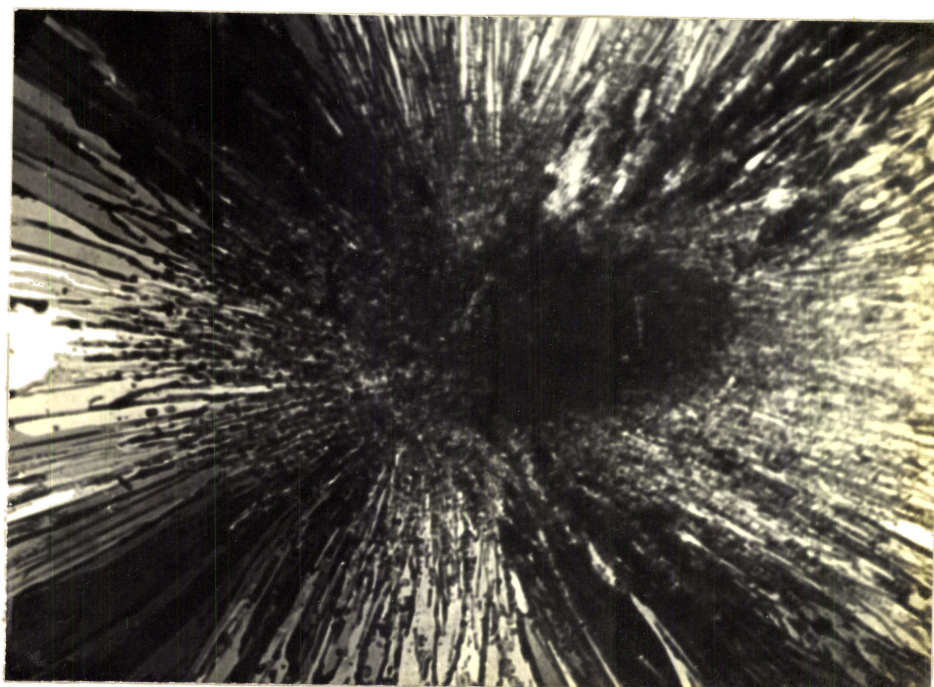


Fig.(41) A spherulite grown at $\Delta T = 10^{\circ}\text{C}$ (x 36).

substructure of these spherulites were found to be fibres growing in C-direction. The melt in between the initial fibres, crystallised slowly to thicken them. The fibre tips were faceted [Figure (42)]. Jackson and Hunt [298] on the basis of studies on organic materials and metals have shown that the freezing pattern depended on the value of α defined as equal to $\Delta S_f/R$, where ΔS_f is the entropy of fusion and R, the gas constant. They have shown that materials having high α values exhibit faceted growth while those with low α values freeze like metals. For phthalic anhydride $\alpha \sim 7$, and the observed faceted growth was thus in accordance with the theory. During spherulitic growth the initial fibre tip developed perturbations and grew out as branches. The branches were developed in non-crystallographic directions. The angle made by these branches with the initial fibre decreased with decrease of ΔT and at very low values of ΔT the non-crystallographic periodic splitting was completely absent. At these super-cooling the spherulitic substructure was well defined ribbons. These spherulites were examined by chemical etching. An etchant, composed by NH_4OH and H_2O in the ratio 1 : 3 by volume, found suitable for delineating

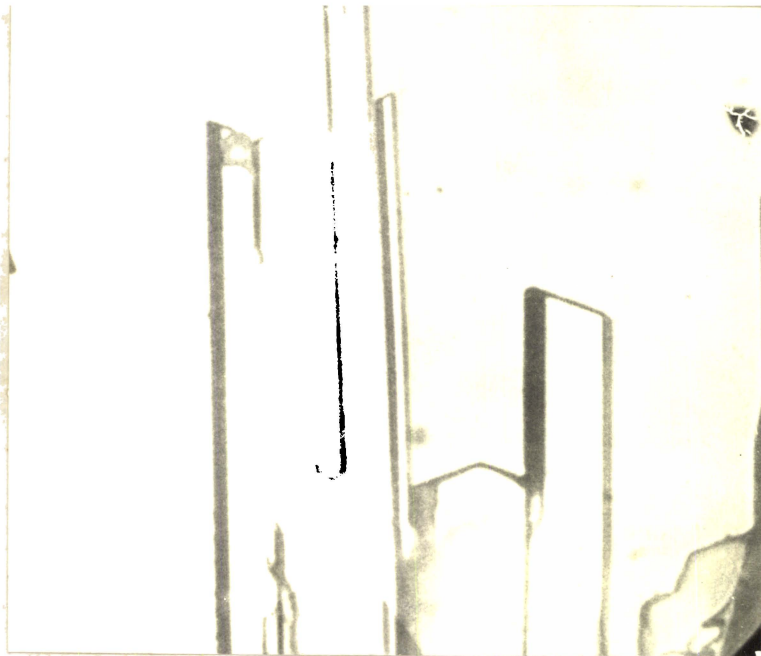


Fig.(42) Faceted tips of spherulitic fibers (x 200).

dislocations on $\{110\}$ and $\{001\}$ faces of phthalic anhydride single crystals [299], produced etch pits on the ribbon surfaces. The pits were characteristic of $\{110\}$ surfaces. The ribbons exhibited large number of grain boundaries running approximately along the radial direction. Examination of a large number of spherulites showed that the spherulitic film had always their $\{110\}$ faces aligned parallel to glass surfaces. This type of auto alignment under non-epitaxial, non-seeded conditions have been observed on several compounds [300]. The formation of large number of grain boundaries suggested a slight lattice mismatch during the crystallisation of the fibres. As stated earlier the angle made by the branches with the initial whisker decreased with decrease of ΔT . The circular volume requires a uniform fibril flux, which is met by the periodic splitting at large values of ΔT . At low values of ΔT the space filling between diverging fibres result in small angle grain boundaries. The formation of grain boundaries in these spherulitic ribbons were found to be very similar to the formation of such boundaries in dendrites with displaced secondary branches [301]. Figure (43) shows schematically the fibre coarsening and subsequent development of grain boundaries.

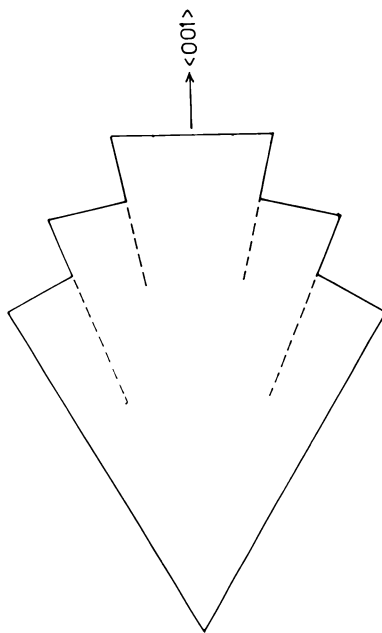


Fig.(43) Fibre coarsening and development of grain boundaries. Dotted lines are grain boundaries.

The spherulitic ribbons, when cooled quickly from the growth temperature exhibited parallel striations. These striations were always parallel to the fibre axis. Figure (44) shows such striations parallel to the $\langle 001 \rangle$ directions. On phthalic anhydride single crystals, such striations on $\{110\}$ faces have been observed [299]. By comparison, the parallel striations were identified as slip lines produced by the thermal strain. The upper and lower faces in contact with the glass slides were $\{110\}$ faces as evidenced by chemical etching. The slip planes active in this crystal had been identified as $\{110\}$ planes [299]. The slip lines on any $\{110\}$ plane should appear as parallel lines. The schematic diagram figure (45) shows the slip process.

Phthalic anhydride spherulites were also grown from solution. Concentrated solutions prepared at 30°C were cooled to $\sim 19^{\circ}\text{C}$. A seed was introduced to the solution and the solution was left for evaporation. After a few days spontaneous nucleation was found to occur on the seed crystal and three-dimensional spherulites developed within one or two weeks. The spherulite was seen to have needle substructure. The

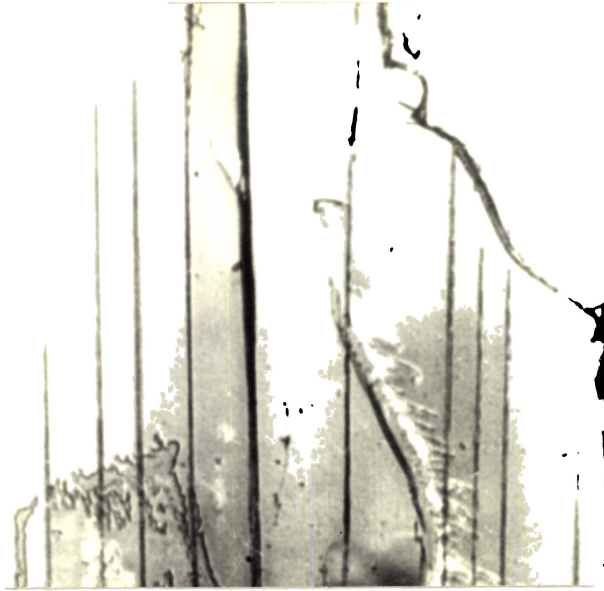


Fig.(44) Parallel striations on spherulitic ribbons (x 250).

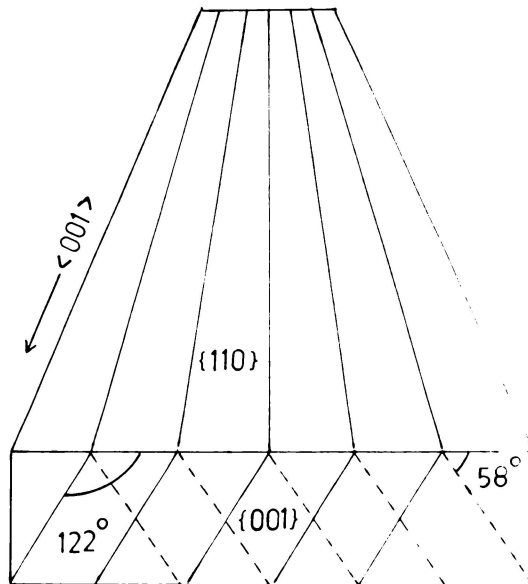


Fig.(45) Schematic diagram of the slip process in ribbons.

needles had hexagonal cross sections and were bounded by $\{110\}$, $\{010\}$ or $\{100\}$ faces. The needle axis was always the $\langle 001 \rangle$ direction. A typical spherulite is shown in figure (46). The characteristic periodic splitting is clearly shown in figure (47). The needles had fairly uniform cross sections, except at the splitting portion and exhibited essentially the same interfacial angles as observed on vapour grown hexagonal whiskers.

(v) Single crystals--Melt growth

The melting point of phthalic anhydride is at $131.1 \pm 0.01^\circ\text{C}$ and is much lower than the boiling point (284.5°C). The material exhibit a 23 % volume reduction on solidification [302]. As such, the Bridgman method was thought fit for the production of large single crystals. Since the melt exhibited supercooling tendencies it was essential to observe the growth, continuously. The furnace described in 6.3(c)i was fabricated for this purpose. The upper zone alone was found sufficient for growing single crystals. The temperature of this zone was maintained at 200°C . The ampoule containing the material, prepared as described earlier in 6.3(c)ii, was kept in the hot

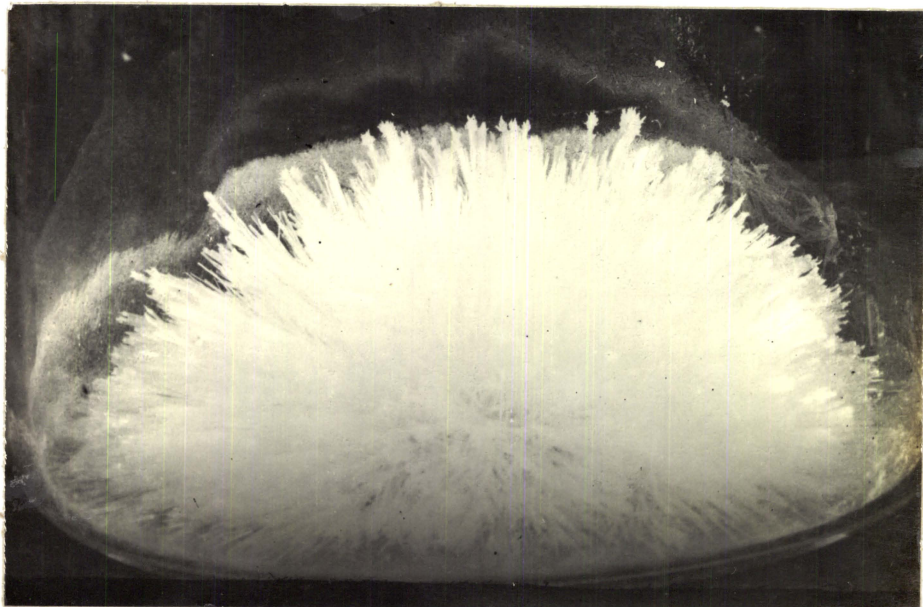


Fig.(46) A typical solution grown spherulite (x 2).

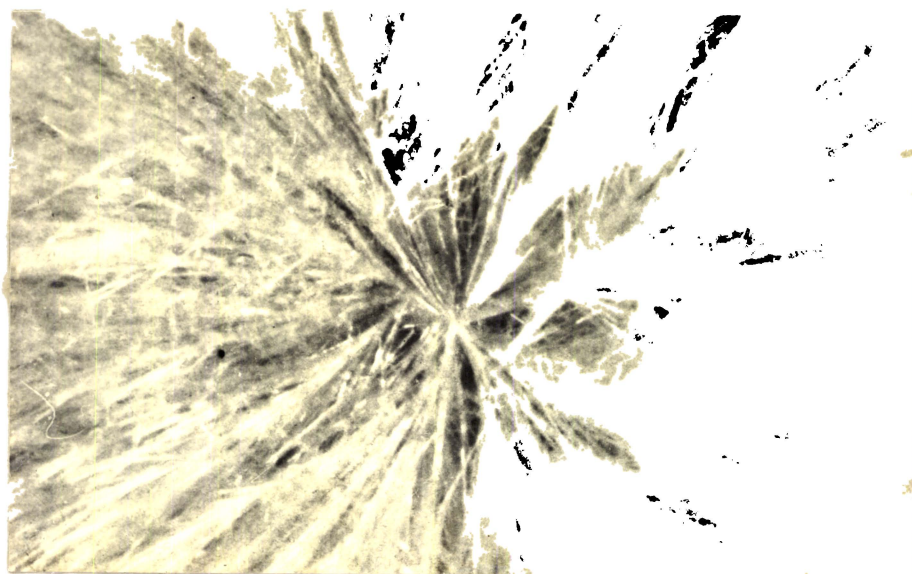


Fig.(47) Cross sectional view of the solution grown spherulite (x 4).

zone so as to melt completely. The ampoule was then lowered slowly by means of a geared motor.

The purity of the material was found to affect the growth seriously. If the commercially available material was used, the impurities segregated at the bottom and was circulated throughout the melt by convection currents. The melt containing impurities had a yellow colour. During crystallisation the impurities were partially rejected into the melt and a dark yellow band was formed at the top of the solidified charge. The impurities were partially incorporated in the crystal giving it a yellow colour. The purified material was colourless in the molten state. To obtain single crystals various tip shapes of growth tubes were used [303]. Of the various tip shapes used, single crystals were obtained with tubes having narrow capillary tips [figure (10)]. Another parameter of importance in obtaining single crystals, was the slope of the tube walls, immediately after the tip. By varying the slope it was found that, an angle of 15° made by the wall with the tube axis, consistently gave good quality single crystals. Higher angles usually resulted in the production of bi-, or tri-crystals. The speed of

descend was varied to different values and a speed of $2-3 \text{ mmh}^{-1}$ was found most suitable for single crystal growth. Under these conditions, the crystals always grew with the $\langle 001 \rangle$ direction parallel to the tube axis. According to Bradley [286] the crystals have excellent cleavages along $\{110\}$ faces. The crystals cleaved well parallel to the tube axis. The crystals were cut perpendicular to the tube axis by the solvent-string cutter described earlier in 6.3(d), using benzene as the solvent. A cut crystal and a cleaved slab are shown in figure (48).

b) Potassium acid phthalate

Potassium acid phthalate possesses a large solubility and large positive temperature coefficient of solubility in water. The solubility curve of potassium acid phthalate is shown in figure (49). The first detailed report on the growth of large single crystals, of this material was made by Bohm et al [292]. They showed that crystals as large as $6.5 \text{ cm} \times 4 \text{ cm} \times 1.5 \text{ cm}$ could be easily grown by the slow cooling of aqueous solutions. In the present study the crystals were grown both by the method of slow cooling and slow evaporation. The seed crystals for the crystal growth was prepared by the evaporation

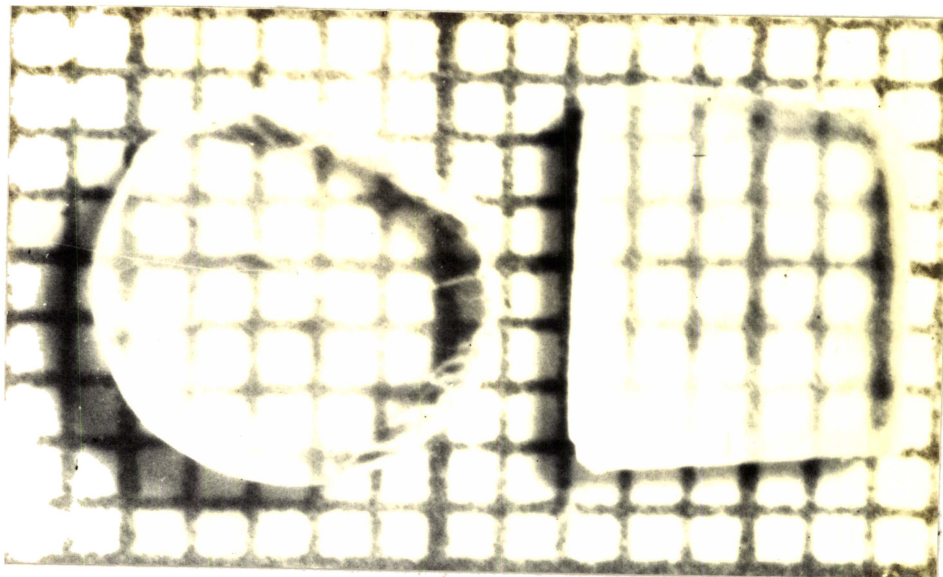


Fig.(48) A cut crystal and a cleaved slab (mm grid).

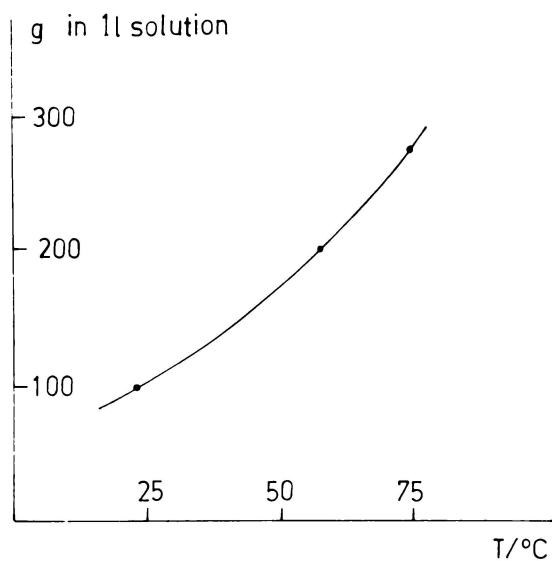


Fig.(49) Solubility curve of potassium acid phthalate in water.

of aqueous solutions placed in a partially covered petri dish. Platelet crystals having {001} faces were found to be the most suitable for growth. The seeds were either fixed by epoxy resin or placed at the bottom of the beaker. A typical crystal grown is shown in figure (50). The grown crystals had the same morphology as the seeds. The crystals exhibited a tendency to grow laterally to develop the {001} faces rather than in a direction normal to it. For the various studies, crystals with larger dimensions in the $\langle 001 \rangle$ direction were necessary. The solutions were doped with various chemicals such as KOH, KNO_3 and thiourea. It was seen that only thiourea was effective in modifying the habit. The addition of thiourea was found to promote growth in the $\langle 001 \rangle$ directions while slowing the growth on other faces. The crystalline morphology was essentially the same as that of crystals grown from pure solutions.

7.3. Dislocation Etch Studies

a) Phthalic anhydride

Various chemicals were tried to find out a suitable etchant for delineating the dislocations in phthalic anhydride. HNO_3 , H_2SO_4 and other acids

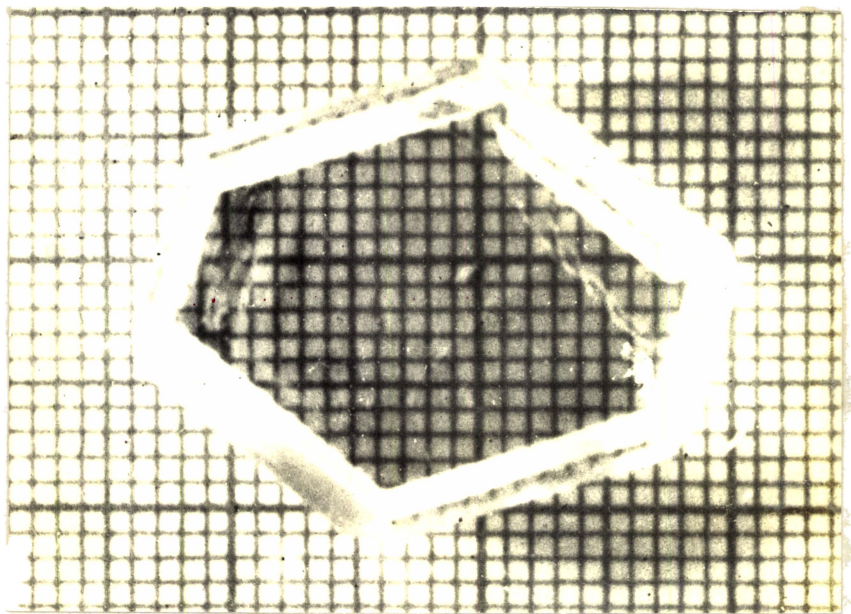


Fig.(50) A typical crystal of potassium acid phthalate (mm grid).

produced excessive reaction and the reaction products were difficult to remove. The various organic acids caused only general dissolution.

Ammonium hydroxide (NH_4OH) have been reported to react with phthalic anhydride to produce phthalamic acid [304]. The reaction is highly efficient with 94 % - 97 % product yield.[305,306]. The suitability of NH_4OH as an etchant was examined by varying the composition of $\text{NH}_4\text{OH} : \text{H}_2\text{O}$ solution. The effect of varying the composition and etching time is shown in table (4). It was seen that well defined etch pits developed for a composition of $\text{NH}_4\text{OH} : \text{H}_2\text{O}$ in the ratio 1 : 3 by volume. The optimum etching time was found to be between 15 to 20 seconds. The etchant was capable of producing etch pits both on the $\{001\}$ and $\{110\}$ faces. A grain boundary revealed on a $\{001\}$ face is shown in figure (51). Successive etching of the same face neither produced new pits nor changed the orientation of earlier pits. The delineation of grain boundaries and the nature of the etch pits on successive etching strongly indicated that the pits were formed at the emergence points of dislocations on these surfaces. The dislocation density was found to be $\sim 10^4 \text{cm}^{-2}$ on $\{001\}$ faces, which was reduced, on annealing at 80°C for 12 hours, to $\sim 10^2 \text{cm}^{-2}$.

Table (4)

The effect of composition variation of the etchant on the etch pit morphology, on {001} and {110} faces

Volume of NH ₄ OH in c.c.	Volume of H ₂ O in c.c.	Etching time in secs.	Remarks	
			{001}	{110}
5	30	5	No pit	No pit
		15	No pit	No pit
		20	No pit	No pit
10	30	5	General disso- lution	No pit
		15	Well defined etch pits	Etch pits observed
		20	Well oriented etch pits	Well ori- ented etch pits
15	30	5	Pit edges gets sli- ghtly curved	Pits get slightly modified
		15	Rapid etching	Rapid etching
		20	Excessive dissolu- tion	General dissolu- tion

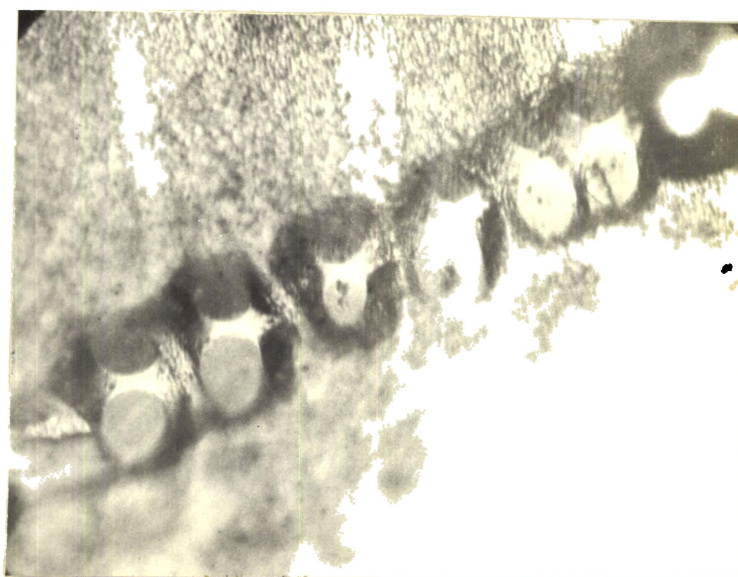


Fig.(51) A grain boundary on {001} face (x 800).

On the $\{110\}$ faces the etch pits exhibited a two fold symmetry. One to one correspondence was observed on matched cleavages and on both sides of thin slabs. A typical 1 : 1 correspondence on matched cleavage surfaces is shown in figure (52).

It was possible to classify the etch pits seen on $\{110\}$ faces into three categories.

- 1) Etch pits exhibiting well-defined planes
[marked A in figure (53)]
- 2) Etch pits having a flat bottom
[marked B in figure (53)]
- 3) Etch pits having a tail
[marked C in figure (53)].

Pits of type A, on successive etching, persisted and got enlarged. They may be formed at the sites of emergence of dislocations perpendicular to the $\{110\}$ faces. Pits of type B disappeared on subsequent etching. These pits may be formed at sites where impurities had segregated, or where the dislocations had moved away, by abrupt bending [307]. Flat bottomed pits have been observed also at points where the dislocations have moved away due to the applied stress [308]. In the C-type pits, the tail developed continuously upon etching. This behaviour indicated that these pits were produced

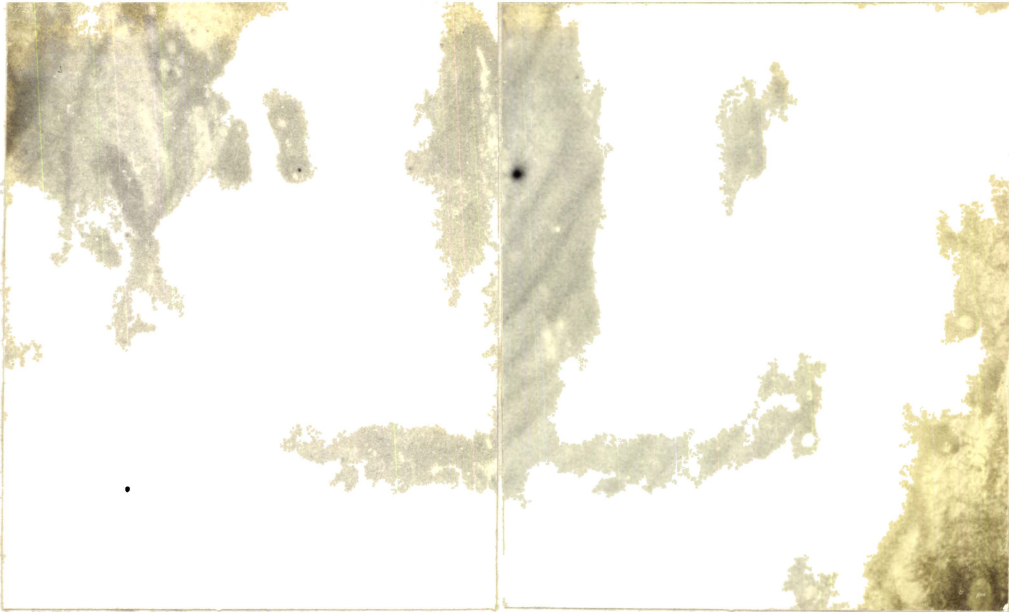


Fig.(52) 1 : 1 correspondence of etch pits on matched cleavage faces of phthalic anhydride (x 180).

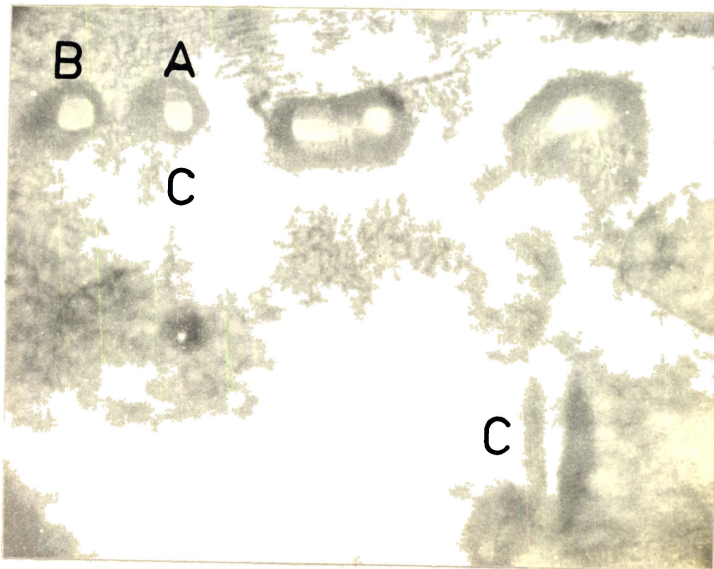


Fig.(53) The etch pits on {110} faces (x 500).

at sites where the dislocations were almost parallel to the $\{110\}$ faces. Dislocations parallel to or almost parallel to the surfaces have been known to exhibit this behaviour [309,310]. The dislocation density on $\{110\}$ faces of unannealed samples were found to be $\sim 10^2 \text{cm}^{-2}$. On annealing at 80° for 12 hours, most of the dislocations were found to disappear. On annealed and unannealed samples large areas completely free of dislocations were seen on both $\{110\}$ and $\{001\}$ faces.

Thermal etching was also tried on phthalic anhydride crystals. The $\{110\}$ faces responded to a stream of hot air and produced etch pits on these faces. But continued etching failed to sustain the original pattern and produced random appearance of new pits. Chemical etching failed to show an 1 : 1 correspondence between the thermally produced etch pits and the chemically produced etch pits.

b) Potassium acid phthalate

Potassium acid phthalate crystals were cleaved along $\{001\}$ planes and various chemical etchants were tried to delineate the dislocations. The various chemical etchants, described in literature and found suitable for delineating dislocations in

other crystals [311], were not successful in potassium acid phthalate crystals. Other etchants prepared by considering the various chemical reactions of the material also proved to be unsuitable.

On etching with water, the surface showed general dissolution rather than etch pits, due to the large solubility of potassium acid phthalate in water. To control the dissolution, acetone was selected as a dilutant due to the miscibility of water and acetone. On the basis of trial and error method, a composition of H_2O in acetone in the ratio 1 : 5 volume was found to produce excellent etch figures on these surfaces, when etched for 5-10 seconds. An interferogram of an etch figure is shown in figure (54). The interferogram clearly showed that the etch figures were pits.

On etching the matched cleavages 1 : 1 correspondence of etch patterns were seen, as shown in figure (55). Very thin cleaved slabs of which both sides were etched showed similar etch patterns. On successive etching no spurious development of pits were observed. The above observations strongly suggested that the etch pits were produced at the emergence points of dislocations on $\{001\}$ faces.

Figure (56) shows an interferogram of an etched $\{001\}$ face. The fringe pattern clearly showed



Fig.(54) FECCO fringes at an etch figure.

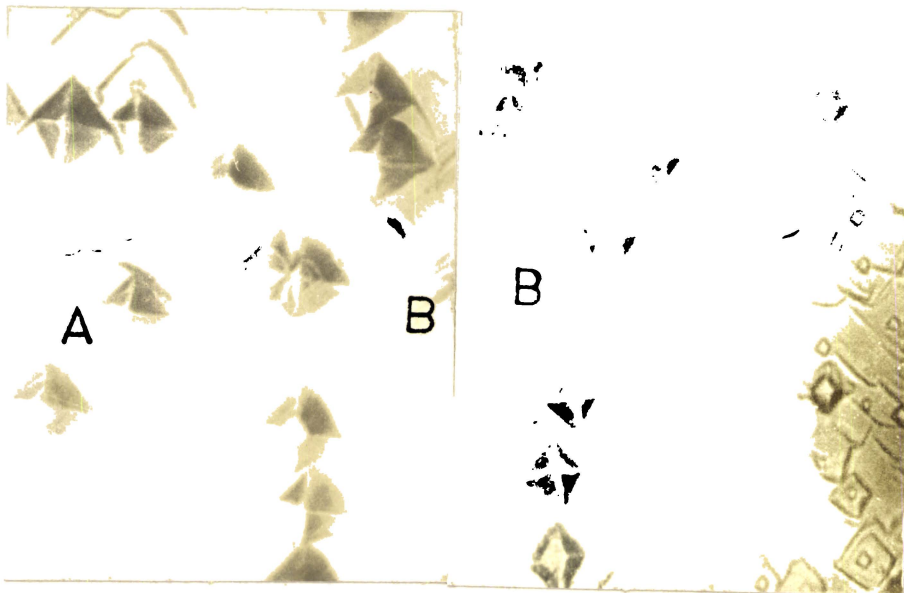


Fig.(55) 1 : 1 correspondence observed on the matched cleavage faces of potassium acid phthalate crystal (x 400).

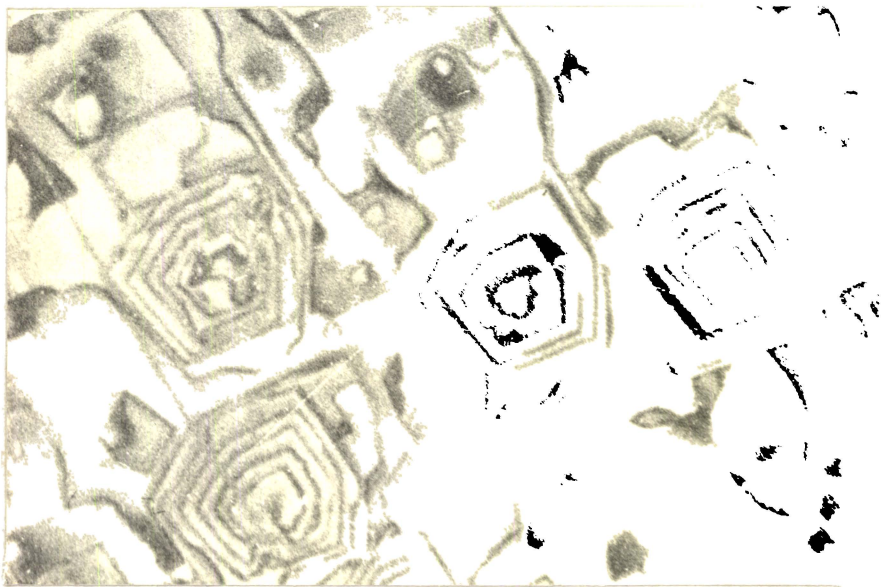


Fig.(56) Fizeau fringes on an etched {001} face of potassium acid phthalate crystal.

the asymmetry of the pit. The pits were observed to be hexagonal with two faces having a curvature. By Weiss zone law, if $[uvw]$ are indices of a zone axis parallel to the face (hkl) which is being etched, then

$$hu + kv + lw = 0 \quad (121)$$

In complex structures the various zone axis which satisfy this condition may have atoms in common. The common atoms may trigger the dissolution from one axis to another. According to Wooster [312] this triggering of dissolution from one direction to another result in etch frames bounded by curved lines. In potassium acid phthalate the curvature of the two adjacent faces of the etch figure was so gradual as to appear as pyramidal in microphotographs.

It was seen that pits like that marked A in figure (55) had no correspondence on the matched face. This type of mismatching have been observed in several crystals [309,313,314] and have been attributed to the bending away of dislocations.

The etch pits on $\{001\}$ cleavages of these crystals exhibited various morphologies. The pits were classified as follows, according to the shape:

- 1) Pyramidal pits with a sharp bottom
(type A and marked A in figure 55)
- 2) Flat bottomed pits
(type B and marked B in figure 55)
- 3) Flat bottomed pits having a small
A-type pit at the center
(type C; figure 57)
- 4) Flat bottomed pits having a row of
smaller pits along a diagonal
(type D; figure 58).

The A-type pits could be further classified as those having flat sides and stepped sides. The A-type pits, in general, were formed at points where the dislocations intersected the surface normally. The flat sided pits were deeper compared to the terraced pits. Similar observations on other crystals have shown that the deeper pits were formed at edge dislocation sites while the terraced shallow pits were formed at screw dislocation sites [315,316,317,318].

The formation of terraced pits have been attributed to the dissolution anisotropy of crystal faces, by Gatos [319]. According to him if the etch rates $R_d > R_v > R_1$, terraced pits will result where

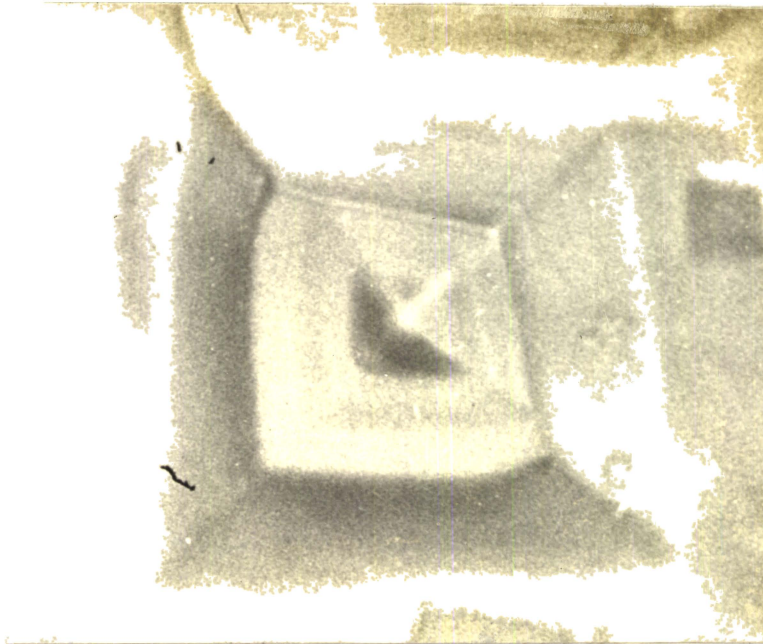


Fig.(57) A flat bottomed pit with a small
A-type pit at the center (x 2800).

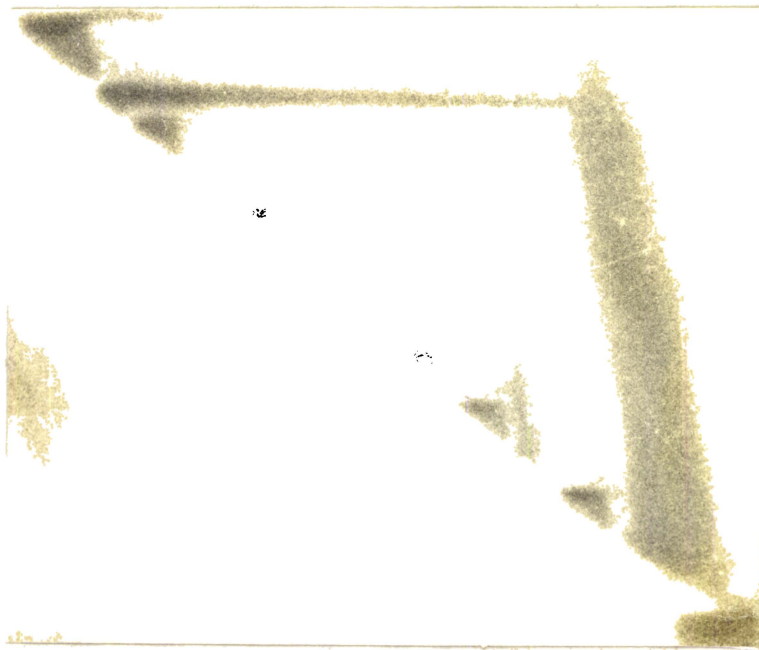


Fig.(58) A flat bottomed pit having a row of
pits along the diagonal (x 2800).

R_d , R_v and R_l are the rates of dissolution along the dislocation line, perpendicular to the surface and parallel to the surface respectively.

The appearance of terraced and flat sided pits on the same surface indicated that the terraced pits were formed at screw dislocation sites. A typical terraced pit is shown in figure (59).

The flat bottomed pit of the type shown in figure (55), were observed on several crystals [307, 308,320,321]. From the abundance of flat bottomed pits, it may be inferred that they are formed neither at points of impurity segregation nor at inclusions [320]. The most reasonable explanation for the occurrence of these pits is the bending away of dislocations at the cleavage plane [314].

Successive etching of the same crystal surface showed interesting features. Two A-type pits existing close together, on etching merged together to form a C-type pit, which on subsequent etching remained as such or split again into two A-type pits. Large number of such pits were observed. In some cases the C-type pits persisted for a long time before splitting into two or more pits. Such behaviour suggested the occurrence of branching and coalescence of



Fig.(59) A terraced pit (x 4000).

dislocations proposed by Read [322]. On sodium chloride Amelinckx [323] has observed that the nodal points of dislocation networks are preferentially decorated, for no apparent reason. Joshi et al [324, 325] have reported the appearance of flat bottomed pits with smaller pits at their centre at the nodal points of dislocations. With the etch/etch procedure for multiple etching it was possible to observe the C-type pits very near the node. It can be reasonably suggested that the mixed character of the dislocations very near the node gives rise to the outer flat bottomed pit while the pit at the centre corresponds to the coalesced part of the dislocation. A schematic diagram of the dislocation branching is shown in figure (60).

In the D-type pits, a row of smaller pits, arranged along the diagonal of a flat bottomed pit were seen. Such a pit is shown in figure (58). The small pits had exactly the same shape as that of the outer pit. On successive etching the number of pits increased or decreased systematically. When etched towards the seed the pits in general decreased in number. Careful observations on these type of pits showed that the small pits were A-type and they changed into C-type pits on successive etching.

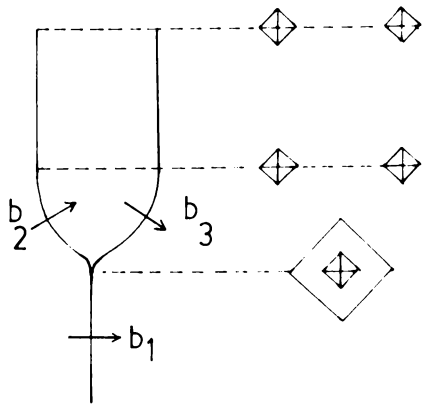


Fig.(60) Schematic diagram of dislocation branching.

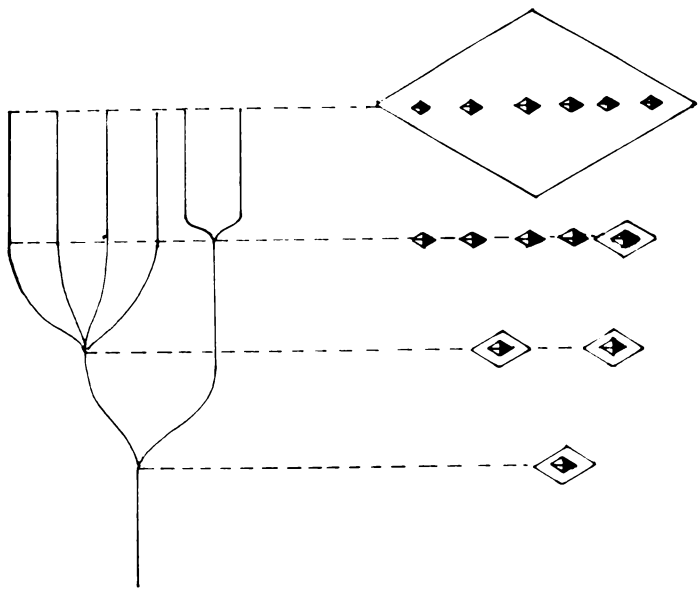


Fig.(61) Schematic diagram of dislocation branching resulting in D-type pits.

Prolonged etching often resulted in a single C-type pit. The systematic reduction in the number of small pits to a single pit, suggested that these pits were produced at the emergence points of dislocation branches, from a single dislocation. Figure (61) shows schematically the branching behaviour which resulted in D-type pits.

The dislocation density was found to be $\sim 10^4 \text{ cm}^{-2}$. The dislocation configuration in these crystals were studied by alternately cleaving and etching. The crystals were etched from the as grown surface towards the seed by cleaving off thin layers. The dislocation density was found to decrease towards the seeds. Figure (62a,b,c) shows the successive stages. The etch pits were observed only at the central portion of the crystals. The majority of the dislocations were traced back to the seed. In several solution grown crystals such dislocation propagation from the seed have been observed [326,327].

Annealing, at different elevated temperatures and for different durations of time, had no effect on the dislocation density. This indicated that the dislocations were immobile, probably due to the branchings and other interactions, of dislocations observed in these crystals.

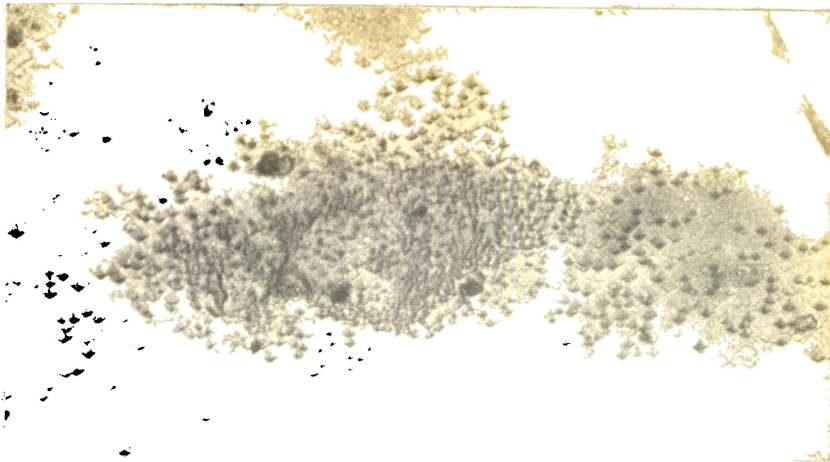


Fig.(62a)

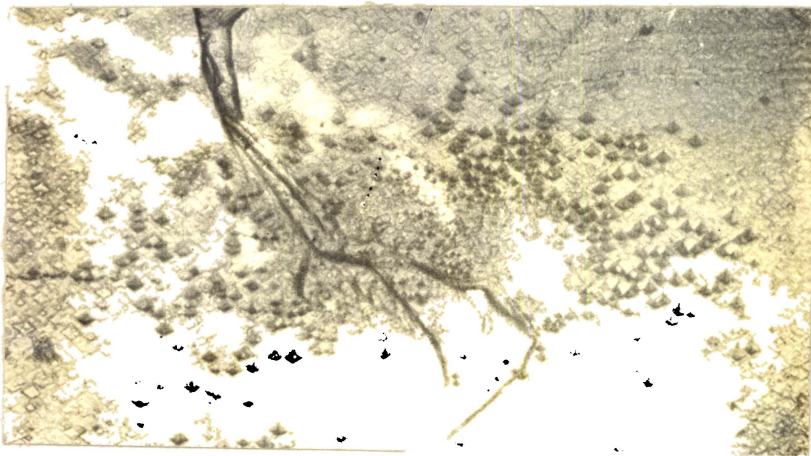


Fig.(62b)



Fig.(62c)

Fig.(62a,b,c) Dislocation distributions on crystal surfaces revealed by the etch/cleave/etch procedure (x 90).

7.4. Investigations on Slip

a) Phthalic anhydride

Phthalic anhydride crystals grown by the Bridgman's method were cleaved along $\{110\}$ planes and cut perpendicular to the $\langle 001 \rangle$ direction. The $\{001\}$ and $\{110\}$ surfaces were indented with the Hanemann's indenter described earlier (6.5). On $\{001\}$ faces the pyramidal indentation produced two sets of parallel lines inclined at 58° or 122° to each other, as shown in figure (63). On $\{110\}$ faces, only one set of slip traces parallel to the C-direction was produced, as shown in figure (64). According to the crystal structure, the projection of 110 planes should appear as lines making 58° or 122° to each other on the $\{001\}$ plane and as parallel lines on $\{110\}$ planes. This strongly indicated that the slip planes involved were $\{110\}$. Figure (65) shows the slip process.

Ball indentations produced cracks on the $\{001\}$ face. Typical cracks are shown in figure (66). The cracks clearly followed the different $\langle 110 \rangle$ directions. The observed slip and crack were typical of the 'cleavage brittle fracture' exhibited by brittle materials [328].

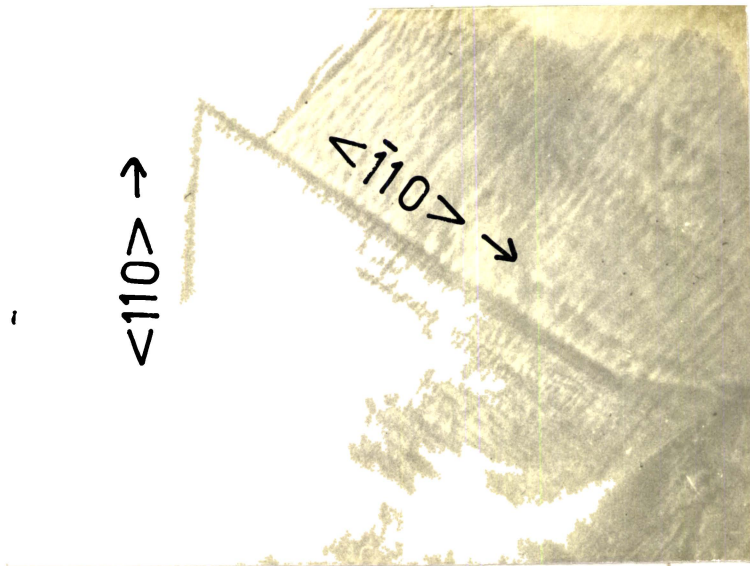


Fig.(63) Slip traces on a {001} face (x 600).

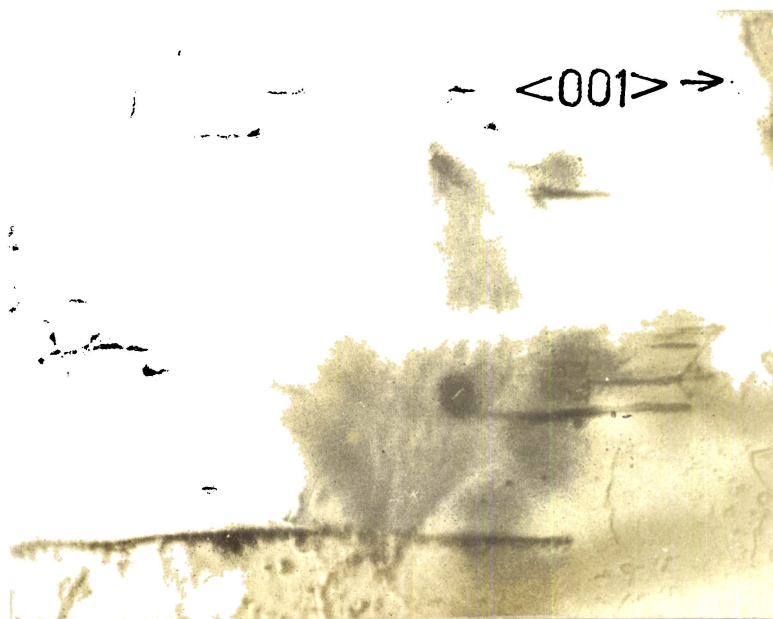


Fig.(64) Slip traces on a {110} face (x 320).

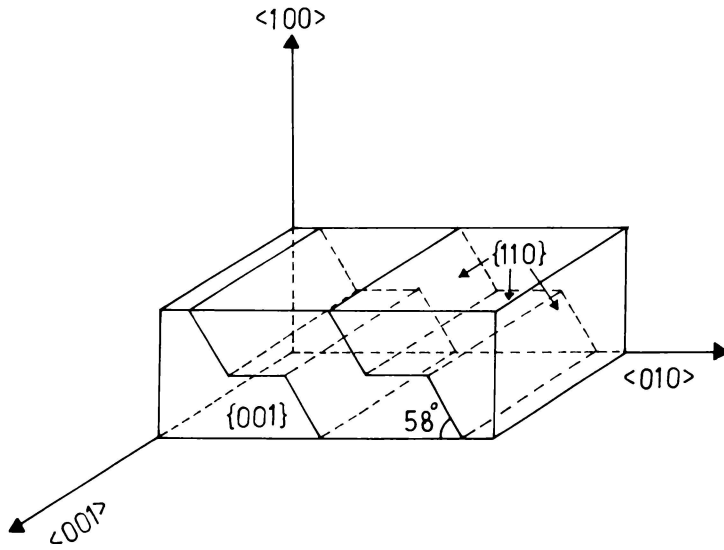


Fig.(65) Schematic representation of the slip process.

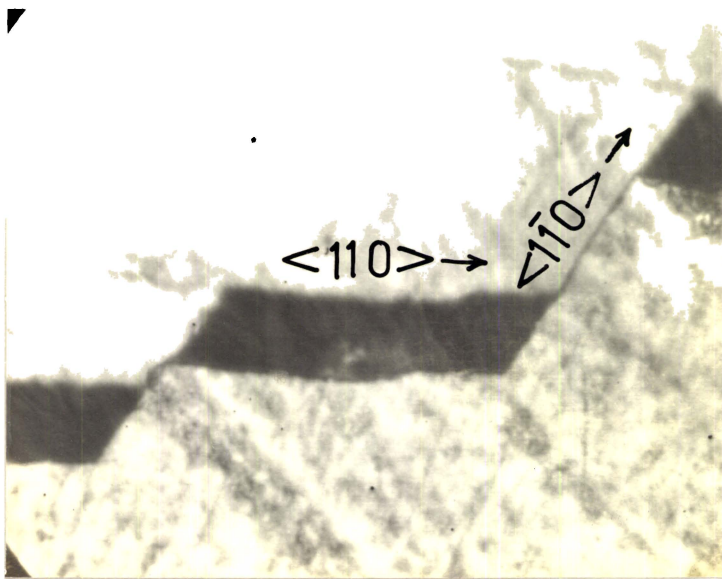


Fig.(66) A typical crack produced on {001} face (x 100).

b) Potassium acid phthalate

The typical indentation mark on {001} faces of potassium acid phthalate is shown in figure (67). The cracks were initiated at very low loads. The circular markings were produced by 'chipping' [329] in the {001} cleavage planes, common in brittle materials having a pronounced cleavage. On {100} and {010} faces, the indentations produced only one set of parallel traces along the $\langle 010 \rangle$ and $\langle 100 \rangle$ directions respectively as shown in figure (68) and figure (69). The {001} slip plane alone is compatible with the traces observed on {001}, {100} and {010} faces. Figure (70) shows the slip process.

7.5. Topography of Crystal Surfaces**a) Phthalic anhydride**

The cleavage faces exhibited the usual river pattern. Detailed examination of the cleavage surfaces, by multiple-beam-interferometry was found impossible due to the low adhesion of reflective metallic coatings on the crystal.

b) Potassium acid phthalate

The cleavage surfaces of potassium acid phthalate crystals exhibited river patterns typical



Fig.(67) Cracks initiated by indentation on {001} face of potassium acid phthalate crystal (x 200).

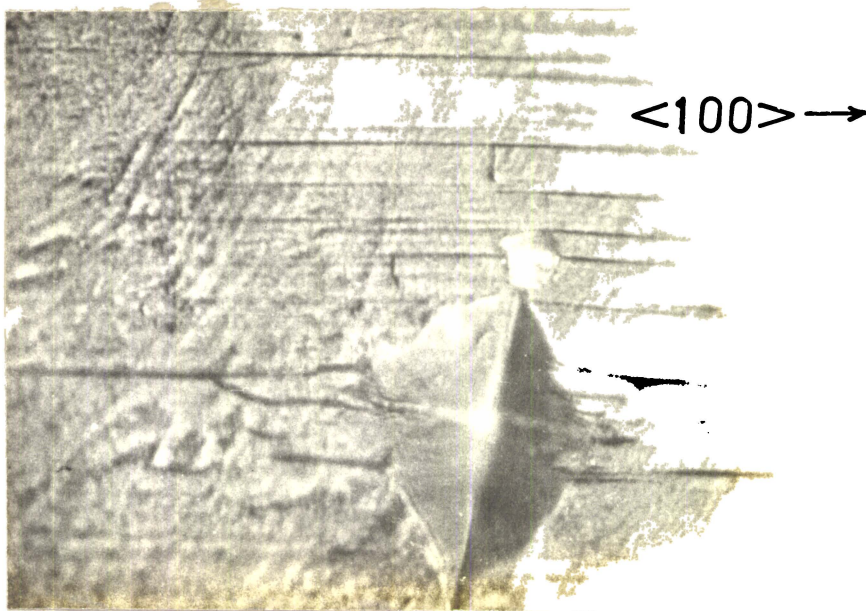


Fig.(68) Slip traces on the {010} face (x 250).

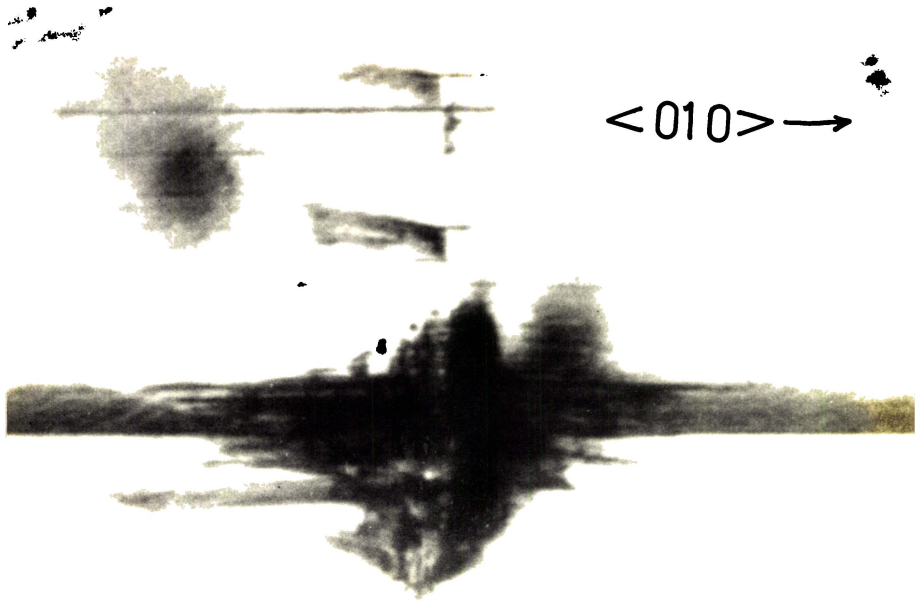


Fig.(69) Slip traces on the {100} face (x 250).

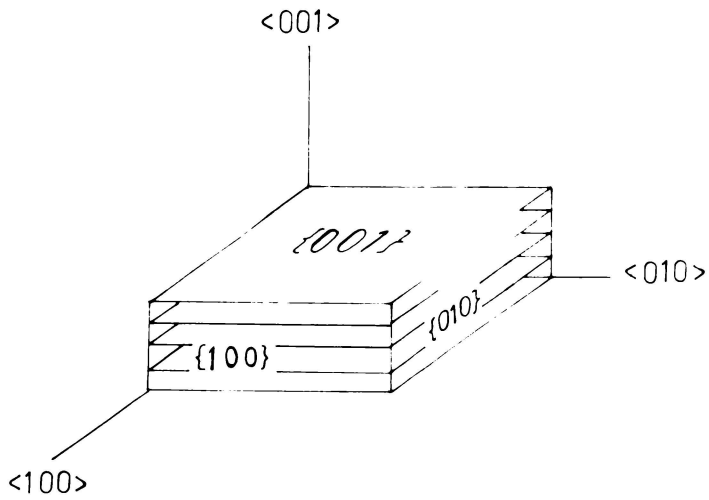


Fig.(70) Schematic diagram of the slip in potassium acid phthalate crystals.

of ionic materials [330,331]. These crystals exhibited good vacuum stability and metals could easily be evaporated on to the crystal surfaces by vacuum evaporation. The cleavage surfaces were examined by multiple-beam-interferometry [279]. A typical interferogram of a cleavage surface, taken with mercury green light is shown in figure (71). The interferogram clearly showed large areas, free of cleavage steps and other irregularities. The cleavage was found perfect, comparable to or better than mica. Figure (72) shows a typical FICO fringe pattern at a step. The cleavage often exhibited 'V' type terminations, level discontinuities and micro-cleavage patterns. Figure (73) shows the microcleavages observed on a cleavage step.

7.6. D.C. Conductivity of Phthalic Anhydride and Potassium Acid Phthalate Crystals

a) Phthalic anhydride

The conductivity of phthalic anhydride crystals were found to be highly anisotropic, the room temperature conductivities being two orders of magnitude higher in the $\langle 001 \rangle$ direction, than in a direction perpendicular to it. The variation of conductivity with temperature is shown in figure (74a,b,c). It was seen that the plot of $\log \sigma$ against $1/T$ was linear.

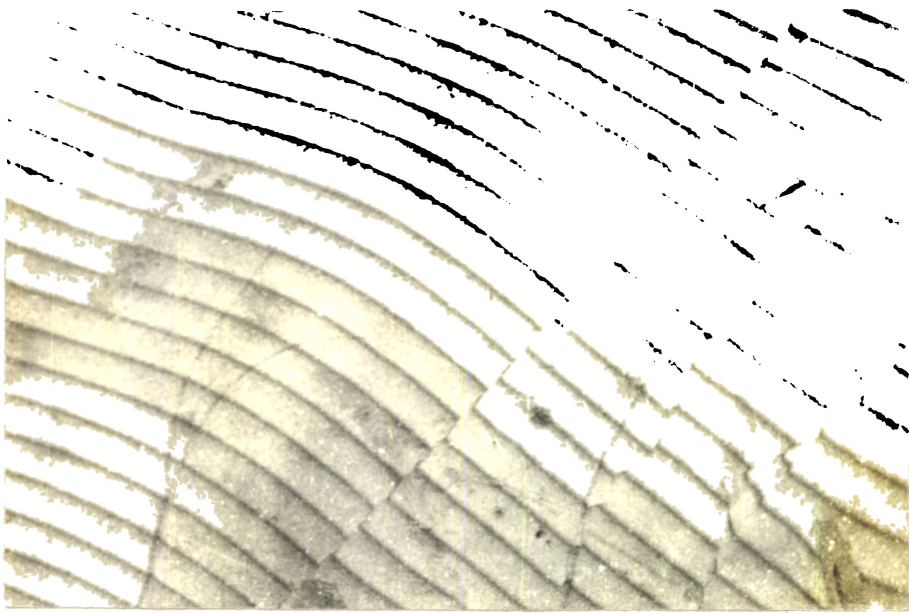


Fig.(71) Fizeau fringes on a cleavage surface.

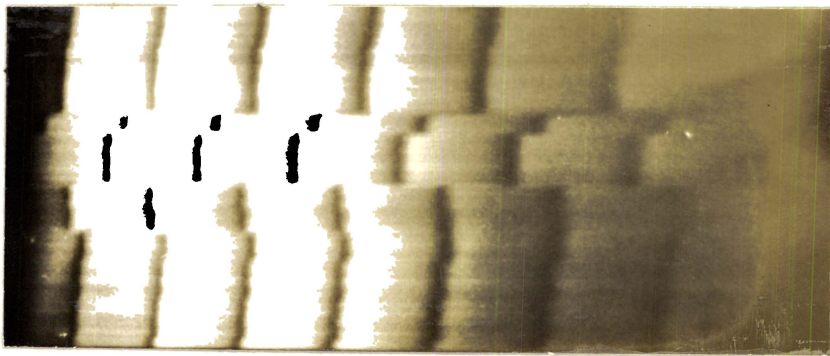
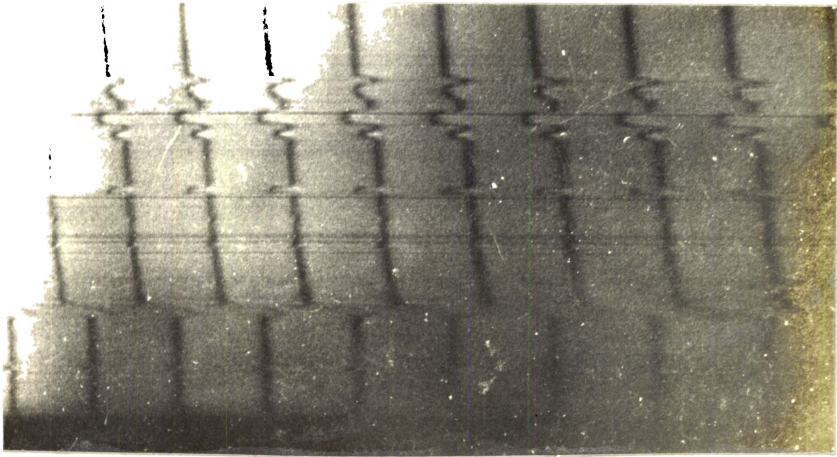


Fig.(72) FICO fringes on a cleavage step.



**Fig.(73) FECO fringes on a cleavage surface,
showing fine structures.**

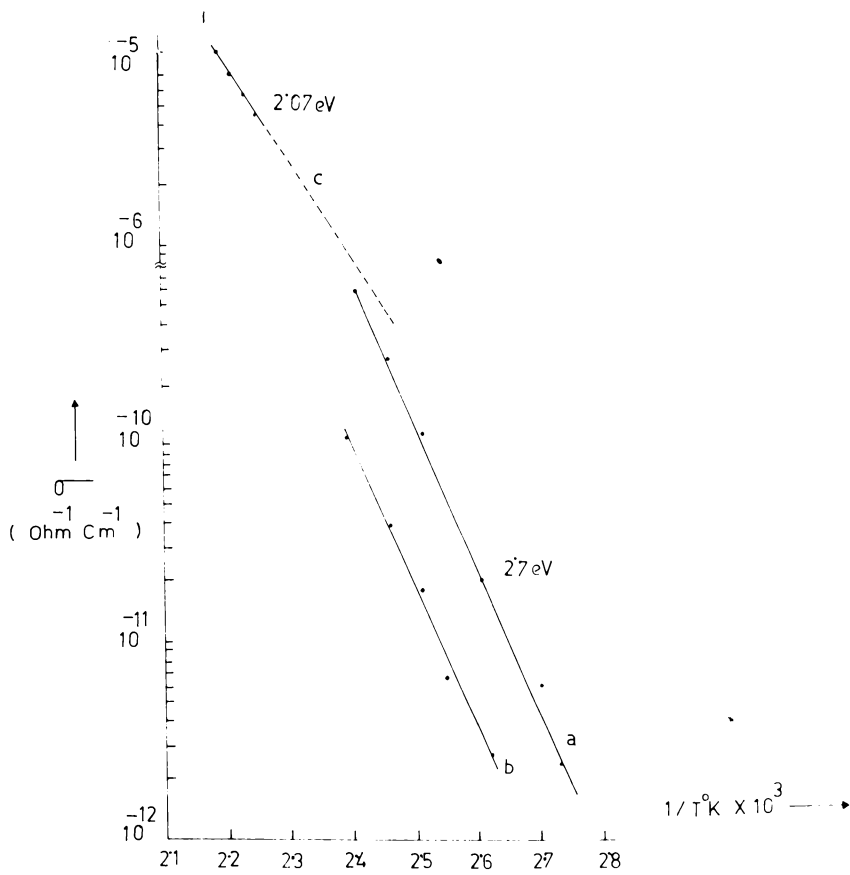
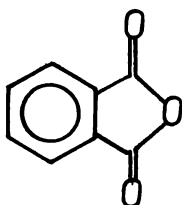


Fig. (74a, b, c) The variation of conductivity with temperature: (a) along c-axis; (b) perpendicular to c-axis; (c) conductivity of the melt.

The anisotropy of conduction could be explained considering the structure of molecules and the crystal. Phthalic anhydride is an aromatic compound with the following chemical structure

$[C_6H_4(CO)_2O]$.



The molecule is almost flat and in the crystal these flat molecules are stacked face-to-face along the 001 direction [286]. The chemical bonding gives rise to 10 π -electrons. The intermolecular bonding can thus be conveniently described by means of π -bonding. In aromatic compounds, like anthracene, the molecular orbital overlap of π -electrons have been found responsible for the observed conduction anisotropy and the maximum overlap of orbitals in a direction perpendicular to the molecular plane have been found to cause an increase in conductivity 5 to 10 times than in a direction parallel to the molecular plane [332]. The molecular overlap have been found to influence the mobility of charge carriers in several materials [333,334,335].

The conductivity variation with temperature yielded a thermal activation energy ~ 2.7 eV, from the relation,

$$\sigma = \sigma_0 \exp(-E/2KT) \quad (122)$$

assuming an intrinsic semiconduction. Though the conductivity exhibits an anisotropy, the activation energy parallel and perpendicular to the $\langle 001 \rangle$ direction remained practically the same.

The conductivity of the molten phthalic anhydride was several orders of magnitude higher than that observed in the solid state, at the same temperature. The variation of the conductivity of the melt with temperature is shown in figure (74c). Similar behaviour has been observed by Reihl [336] in naphthalene. Forster et al [337] have also observed a sharp rise in conductivity in benzene upon melting, the activation energy remaining virtually constant. But in some cases the activation energy has been found to decrease in fusion [338]. A decrease in the activation energy for conduction in the molten state has been found to be due to a fundamentally different transport mechanism operating in the molten state [339]. The observed activation energy of $\sim 2.07\text{eV}$ in the molten state of phthalic anhydride, compared to the value of $\sim 2.7\text{eV}$ in the solid state indicated that the transport mechanism in the molten state was entirely different from that in the solid state.

Various models have been suggested for the electrical conduction in organic crystals. Eley and

Parfit [340] proposed a tunnel model in which the molecules were excited thermally or optically from the normally occupied $N/2^{\text{th}}$ π -orbital to $[(N/2)+1]^{\text{th}}$ π -level. N denotes the number of conjugated π electrons in the molecules. The conduction was limited by the probability of electron/hole tunneling to the corresponding orbital in the adjacent molecule. According to this picture phthalic anhydride with its $10-\pi$ electrons should have an activation energy $\sim 2.5\text{eV}$.

Wilk [341] studied the effect of the number of linearly joined ring systems on the activation energies and found a relation

$$E = (17-n)^2/100 \quad (123)$$

where n denoted the number of rings. For phthalic anhydride $n = 1$ and hence according to this equation, the activation energy should be $\sim 2.56\text{eV}$.

The possible relation between the conduction band and the triplet excited levels was examined by Northrop et al [342] and Rosenberg [343]. The triplet hypothesis [244] envisages the participation of charge carriers in conduction via a triplet excitation. In a singlet state there is no net electronic spin angular momentum, whereas in a triplet state there is a net

positive electronic spin angular momentum. The excited triplet state lies lower in energy than the corresponding singlet excited state. Optical transitions between triplet states and a singlet ground state are forbidden and hence weak. The transitions from the upper singlet state to ground state results in fluorescence and is characterised by short life times of the order of 10^{-8} seconds. The triplet-ground state transitions gives rise to phosphorescence which are weak and have comparatively long life times of the order of 10^{-2} seconds. The carriers can be either thermally or optically excited to the lowest triplet states which by subsequent motion produce the conductivity. The phosphorescence spectra of phthalic anhydride have been studied by Iwata et al [344]. The 0-0 band has been found to occur at 25800 cm^{-1} and the phosphorescence maxima at 23600 cm^{-1} . Hardy et al [345] have also studied the photoluminescence spectrum of phthalic anhydride. The fluorescence have been observed at 29411 cm^{-1} . The phosphorescence have been found to occur at 21276 cm^{-1} . According to those values the energy levels of phthalic anhydride should be like that shown in figure (75). The activation energy for triplet excitation can thus be inferred to be between 2.6eV and 2.9eV.

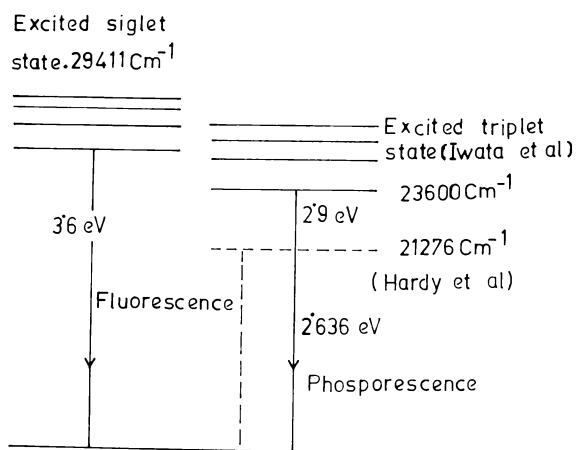


Fig.(75) Energy level diagram of phthalic anhydride crystal.

The observed value of 2.7eV for the thermal activation energy in phthalic anhydride is comparable to 2.64eV of the triplet state. Thus the triplet exciton participation in electrical conduction may be reasonably suspected.

A necessary, but not sufficient, test of the intrinsic nature of the conductivity is a comparison of the observed value of E with the quantity $I_c - A_c$ [346], where I_c and A_c are the ionisation and electron affinity of the molecule in the crystal. For phthalic anhydride, $A_c \sim 2.72\text{eV}$ [347,348], I_c may be calculated from the relation

$$I_c + A_c = I_g + A_g \quad (124)$$

where I_g and A_g are the ionisation potential and electron affinity of the molecule in the gaseous state. $I_g + A_g$ had been observed to be a constant for most of the aromatic molecules and is taken as $\sim 8\text{eV}$ [349]. Hence, $I_c \sim 5.78\text{eV}$. The value of $I_c - A_c \sim 2.56\text{eV}$ is in reasonable agreement with the observed value of 2.7eV for the activation energy. This strongly suggested that the conduction in phthalic anhydride was intrinsic.

b) Potassium acid phthalate

The conductivity variation with temperature is plotted in figure (76a,b,c). The conductivity

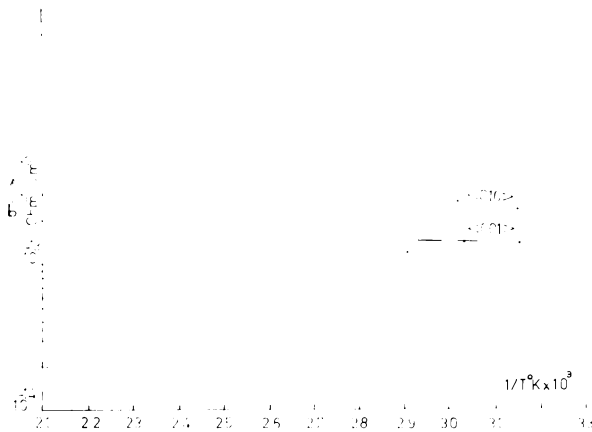


Fig.(76a,b)

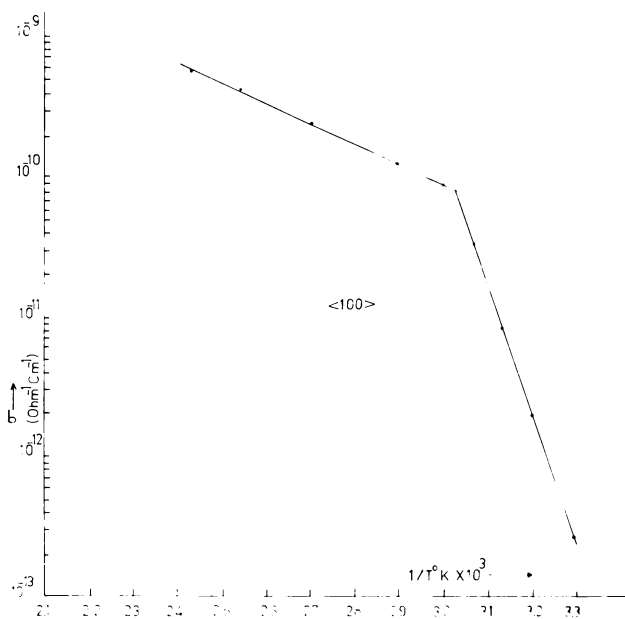


Fig.(76c)

Fig.(76a,b,c) The variation of conductivity with temperature in potassium acid phthalate: (a) along $\langle 010 \rangle$ direction; (b) along $\langle 001 \rangle$ direction; (c) along $\langle 100 \rangle$ direction.

exhibited a strong anisotropy with the crystal direction. The conductivity along the $\langle 100 \rangle$ direction was the largest. Conductivity was less along $\langle 010 \rangle$ and $\langle 001 \rangle$ direction, being lowest along the $\langle 001 \rangle$ direction. The plot of $\log \sigma$ against $1/T$ exhibited a knee typical of ionic crystals. In alkali halides such behaviour have been observed and have been attributed to the difference of mechanism involved in the conduction process at lower and higher temperatures and the observed change in the slope of the $\log \sigma \sim 1/T$ plot has been attributed to the presence of divalent impurities [350,351].

The activation energy of ionic materials change as the temperature is increased. The commonly encountered shapes of the $\log \sigma$ Vs. $1/T$ plots are shown in figure (77). In certain cases the activation energy increases [case(a) of figure (77)] and in others it decreases [case (b) of figure (77)] with increase of temperature. In case (a) the change in activation energy is brought out by a change from extrinsic [portion (i) of curve (a)] to intrinsic [portion (ii) of curve (a)] conductivity [352]. In the case (b) the activation energy is decreased with

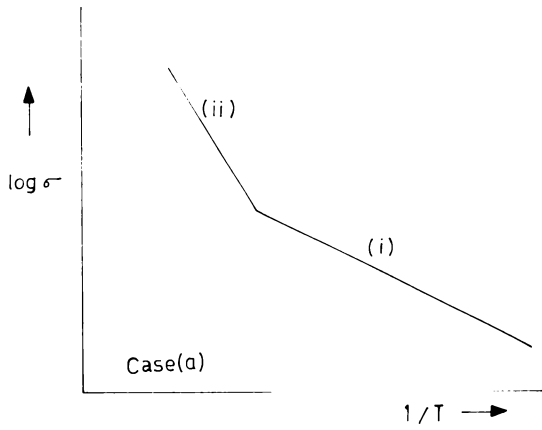


Fig.(77a)

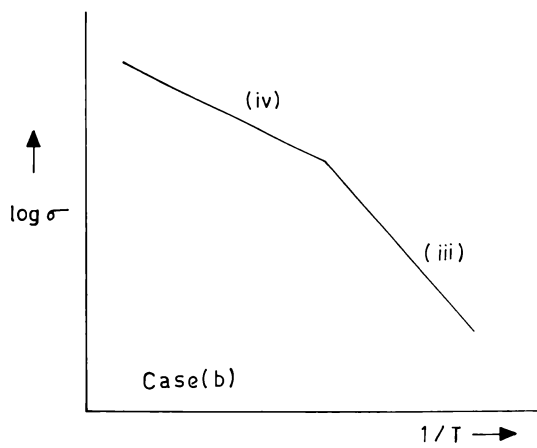


Fig.(77b)

Fig.(77) The commonly encountered shapes of $\log \sigma$ Vs. $1/T$ plots.

the increase of temperature and both the portions (iii) and (iv) corresponds to the extrinsic mode. The change in slope have been found to be caused by a change in the number of excited carriers, n , relative to the number of impurity levels N , less the total number of carriers N_0 . In (iii) $n \ll N - N_0$ and in (iv) $n \gg N - N_0$.

In potassium acid phthalate crystals both these cases have been seen to arise, as can be seen from figure (76a,b,c).

The observed anisotropy of electrical conduction could reasonably be explained on the basis of the crystal structure. The crystal structure is ionic with potassium ions and acid phthalate ions. The phthalate ions have two carboxyl groups one of which is ionised [290,353]. The phthalate ions are stacked along the $\langle 100 \rangle$ axis by an a glide perpendicular to b axis. The phthalate ion chains extending in the $\langle 100 \rangle$ directions are bonded by O-H...O hydrogen bonds. The chains are interconnected by potassium ions each of which is surrounded by six oxygen atoms. The observed conductivity in $\langle 100 \rangle$ axis may be due to the enhanced molecular overlap and hydrogen bonding in the $\langle 100 \rangle$ direction.

Though the presence of the knee can be explained as due to the ionic nature of conductivity the exact mechanism of conduction could not be established.

CONCLUSION

The crystallisation behaviour of phthalic anhydride has been investigated from vapour, solution and melt. Phthalic anhydride crystals grow from vapour in the form of hollow crystals with an opening in the prismatic wall. The faces have been found to grow by filling the space between the side whiskers growing in $\langle 110 \rangle$ directions. A mechanism for the hollow crystal formation has been suggested. The observations of the basal plane growth of crystals in a closed crystal vapour system gives support to the mechanism proposed. The growth and morphological studies of dendrites growing in the $\{001\}$ plane have shown that $\langle 110 \rangle$, $\langle 010 \rangle$ and $\langle 100 \rangle$ are the most active directions of growth in these dendrites, as in the case of hollow crystals and platelet crystals grown from vapour. The growth of platelet crystals has been accounted for, by the filling in process of the space between the dendritic branches. The spherulites grown, from solution and melt, have the substructure of well aligned ribbons with $\{110\}$ faces, with a large number of grain boundaries along the $\langle 001 \rangle$ direction, as revealed by etching. It has been found that the presence of impurities is not a necessary condition for spherulitic growth in this system.

Large single crystals of phthalic anhydride have been grown from melt by the Bridgman method for the first time. $\text{NH}_4\text{OH} : \text{H}_2\text{O}$ (1 : 3 volume) has been found to reveal dislocations on $\{001\}$ faces and on $\{110\}$ cleavages. The slip planes have been identified as $\{110\}$ from the observation of slip traces produced by indentation. The electrical conductivity, measured along the $\langle 001 \rangle$ direction and perpendicular to it, have shown that the conductivity is largest in the $\langle 001 \rangle$ direction.

Potassium acid phthalate crystals have been grown from aqueous solutions. Acetone : water in the ratio 5 : 1 by volume, has been found to be effective in delineating dislocations on the cleavage surfaces of this crystal. The nature and configuration of the dislocations have been revealed by etch/etch and etch/cleave/etch process for multiple etching. The cleavage surfaces have been shown to be perfect, comparable to or better than mica, by multiple beam interferometry. The electrical conductivity has been shown to be predominantly ionic and the conductivity measured along the $\langle 001 \rangle$, $\langle 010 \rangle$ and $\langle 100 \rangle$ directions have shown that the conductivity is largest along the direction.

REFERENCES

1. M.R. Srinivasan, A.H. Rama Rao, H.L. Bhat and P.S. Narayanan, (1978) *Ferroelectrics*, 21, 539.
2. H.L. de Hussel, L.S. de Wainer and M.A.R. de Benyacar, (1978) *Ferroelectrics*, 17, 487.
3. J. Gay, R. Kara and J.P. Mathieu, (1961) *Bull. Soc. Franc. Mineral. Crist.* 84, 187.
4. J. Kommandeur, (1961) *J. Phys. Chem. Solids*, 22, 339.
5. S. Matsuzaki, R. Kuwata and K. Toyoda, (1980) *Solid Stat. Commun.* 33, 403.
6. F.H. Spedding, B.J. Beaudry, J.J. Croat and P.E. Palmer, (1970) *Les Elements Des Terres Rares Vol.1*, (Editions due Centre Nat. de la Recherche Scientifique) p.25.
7. U. Itoh, K. Takeishi and H. Anzai, (1973) *J. Phy. Soc. of Japan*, 35, 810.
8. Z. Burshtein and D.F. Williams, (1977) *Mol. Cryst. Liq. Cryst.* 43, 1.
9. J. Bleay, A.M. Hooper, R.S. Narang and J.W. Sherwood (1978) *J. Crystal Growth*, 43, 589.
10. D.C. Northrop and O. Simpson, (1956) *Proc. Phy. Soc.* A234, 124.
11. K. Hasegawa, (1964) *Jap. J. Appl. Phys.* 3, 633.

12. D.D. Eley, A.S. Fawcett and M.R. Willis, (1968)
Trans. Faraday Soc. 64, 1513.
13. F. Gutman and L.E. Lyons, (1967) 'Organic
Semiconductors' (John Wiley), p.457.
14. M.A. Van Damme - Van Weele, (1973) 'Crystal
Growth, An Introduction', Ed. P. Hartman
(North Holland), p.261.
15. F.A. Khayyat and P. Stanley, (1978) J. Phys. D:
Appl. Phys. 11, 1237.
16. Y. Hase, (1976) J. Mol. Structure 30, 37.
17. S. Iwata, J. Thanaka and S. Nagakura, (1967)
J. Chem. Phys. 47, 2203.
18. R.P. Rastogi, N.B. Singh and R.P. Singh, (1977)
J. Solid State Chem. (USA) 20, 191.
19. H.A. Pohl, 'Modern Aspects of the Vitreous State',
(1962) Ed. J.D. Mackenzie (Butterworth,
London).
20. R. McNeil and D.E. Weiss, (1959) Australian J.
Chem. 12, 12.
21. H.A. Pohl, J.A. Bornmann and W. Itoh (1962)
'Organic Semiconductors' Ed. J.J. Brophy
and J.W. Buttrey (Mc.Millan Co.), p.142.
22. G.E. Hardy, J.C. Baldwin, J.I. Zink, W.C. Kaska,
PO-HSinhu and Dubois, (1977) J. Am. Chem.
Soc. 99, 3352.

23. J.I. Zink and Klmt, (1974) J. Am. Chem. Soc. 96, 4690.
24. A.J. Watson, (1977) Advances in Physics, 26, 887.
25. Y. Okaya, (1965) Acta Cryst. 19, 879.
26. I.S. Rez, (1963) Cesk Casopis Fys. 18, 31.
27. D. Chopra, (1970) Rev. Sci. Instr. 41, 1004.
28. A.J. Bearden and Huffman, (1963) Rev. Sci. Instr. 34, 1233.
29. J.W. Gibbs, (1878) 'Collected Works' (1928) (Longman's Green and Co.), p.325.
30. P. Curie, (1885) Bull. Soc. Franc. Miner. 8, 145.
31. G. Wulff, (1901) Z. Kristallogr. 34, 449.
32. A. Bravais, (1879) 'Entwicklung einer Theorie d. Krystallstruktur' (Leipzig).
33. L. Soehncke, (1879) 'Entwicklung einer Theorie de. Kristall struktur' (Leipzig).
34. W. Kossel, (1927) Nachr. Acad. Wiss. Göttingen Math. Physik K1, 135.
35. I.N. Stranski, (1928) Z. Phys. Chem. 136, 259.
36. W.K. Burton, N. Cabrera and F.C. Frank, (1951) Phil. Trans. Roy. Soc. A243, 299.
37. R. Becker, and W. Döring, (1937) Ann. Phys. 24, 719.
38. F.C. Frank, (1972) J. Crystal Growth, 13/14, 154.
39. M. Ohara and R.C. Reid, (1973) 'Modeling Crystal Growth rates from Solutions' (Prentice-Hall Inc.).

40. W.B. Hillig, (1966) Acta Metall. 14, 1868.
41. N. Hayashi and T. Shichiri, (1974) J. Crystal Growth, 21, 254.
42. F.C. Frank, (1949) Disc. Farad. Soc. 5, 48.
43. L.J. Griffin, (1950) Phil. Mag. 41, 196.
44. I. Sunagawa, (1978) J. Crystal Growth, 45, 3.
45. H. Bethge and K.W. Keller, (1965/66), Optik 23, 462.
46. H. Ishiuki and I. Nakada, (1977) Japan J. Appl. Phys. 16, 1301.
47. D. Aquilano, (1977), J. Crystal Growth, 37, 215.
48. I. Nakada and M. Kubota, (1978), J. Crystal Growth, 43, 711.
49. A.R. Verma, (1953) 'Crystal Growth and Dislocations' (Butterworth's Scientific Publications).
50. S. Amelinckx, (1964) 'Solid State Physics' Supplement Vol.6 (Academic Press).
51. N. Cabrera and M.M. Levine, (1956), Phil. Mag. 1, 450.
52. M.K. Agarwal, H.B. Patel and K. Nagireddy, (1977), J. Crystal Growth, 41, 84.
53. E. Schonhere, G. Muller and E. Winkler, (1978), J. Crystal Growth, 43, 469.
54. S. Maralidhara Rao, (1976), Indian J. Phys. 50, 378.
55. G.S. Duncan, R.H. Hopkins and R. Mazelsky, (1971), J. Crystal Growth, 11, 50.
56. J.R. Carruthers and K. Nassau, (1968), J. Appl. Phys. 39, 5205.

57. Y. Miyasawa, M. Mori and S. Honma, (1978),
J. Crystal Growth, 43, 541.
58. D. Mateika, P. Flisikowski, H. Kohler and
R. Kilian, (1977), J. Crystal Growth, 41, 262.
59. A. Chevy, A. Gousskov and J.M. Besson, (1978),
J. Crystal Growth, 43, 756.
60. S.J. Bass and P.E. Oliver, (1968), J. Crystal
Growth, 3, 286.
61. E. Buchler, (1978), J. Crystal Growth, 43, 584.
62. G.F. Reynolds, (1969) 'Physics and Chemistry of
Organic Solids' Eds. D. Fox, M. Labes and
A. Weissberger (Wiley-Interscience).
63. J.N. Sherwood and S.J. Thomson, (1960), J. Sci.
Instru. 37, 242.
64. K.J. Bachmann, (1976), J. Crystal Growth, 33, 177.
65. A.G. Fischer, (1975) 'Crystal Growth', Ed. Pamplin
(Pergamon).
66. A.G. Fischer, (1961) Bull. Am. Phys. Soc. II, 6, 17.
67. W.G. Pfann, (1952) Trans. AIME 194, 747.
68. W.G. Pfann, (1966) 'Zone Melting, 2nd Edn.
(Wiley, N.Y.).
69. D. Fischer, (1973) Materials Res. Bull. 8, 385.
70. T. Tanaka, E. Bannai, S. Kawai and T. Yamane,
(1975), J. Crystal Growth, 30, 193.

71. J.M. Quenisset and R. Nastain, (1975), *J. Crystal Growth*, 30, 169.
72. E.S. Johnson, (1975), *J. Crystal Growth*, 30, 249.
73. D.B. Gasson and B. Cockayne, (1970), *J. Mat. Science* 5, 100.
74. J.L. Richards, P.B. Hart and L.M. Gallone, (1963), *J. Appl. Phys.* 34, 3418.
75. J.R. Arthur and J.J. Lepore, (1969) *J. Vac. Sci. Tech.* 6, 545.
76. W.W. Piper, S.J. Polich, (1961) *J. Appl. Phys.* 32, 1278.
77. B. Honingman, (1954), *Z. Electrochem.* 58, 322.
78. H. Heyer, (1974) 'Crystal Growth', Ed. H.S. Peisel, (Pergamon Press).
79. J. Nishizawa and H. Nitura, (1978), *J. Crystal Growth*, 45, 82.
80. J.J. Tietjen and J.A. Amick, (1966) *J. Electrochem. Soc.* 113, 724.
81. J. Bloem and L.J. Giling, (1978) 'Current Topics in Materials Science' Ed.E. Kaldis (North Holland), p.150.
82. T. Kobayashi and H. Takei, (1978), *J. Crystal Growth*, 45, 29.
83. R. Madar, F. Weiss and R. Fruchart, (1978), *J. Crystal Growth*, 45, 37.

84. J. A. James and R.C. Kell, (1975) 'Crystal Growth'
Ed. B.R. Pamplin (Pergamon Press).
85. E.M. Hampton, B.S. Shah and J.N. Sherwood,
(1974), J. Crystal Growth, 22, 22.
86. A.E. Robinson, (1949), Disc. Farad. Soc. 5, 315.
87. C. Forno, (1974), J. Crystal Growth, 21, 61.
88. M. Delfino, J.P. Dougherty, W.K. Zwicker and
M.M. Choy, (1976), J. Crystal Growth, 36, 267.
89. M. Delfino, (1976), J. Crystal Growth, 32, 378.
90. J. Flicstein and M. Schieber, (1974), J. Crystal
Growth, 24/25, 603.
91. R.A. Laudise and J.W. Nielsen, (1961) Solid State
Physics, Vol.12, Eds. F. Seitz and D.Turnbull.
92. R.A. Laudise and A.A. Ballman, (1961), J. Phys.
Chem. 65, 1396.
93. R. Uhrin, R.F. Belt and R.C. Puttbach, (1974),
J. Crystal Growth, 21, 65.
94. A. Baronnet, M. Amouric, B. Chabot and F. Corny,
(1978), J. Crystal Growth, 43, 255.
95. R.A. Laudise, (1963) 'The Art and Science of
Growing Crystals' Ed. J.J. Gilman (John Wiley).
96. A. Rau and A. Rabenau, (1967) Solid State Commun.
5, 331.
97. E.D. Kolb, A.J. Caporaso and R.A. Laudise, (1968),
J. Crystal Growth, 3/4, 422.

98. D. Elwell and B.W. Neate, (1971), *J. Mat. Sci.* 6, 1499.
99. D. Elwell, (1975), 'Crystal Growth', Ed. B.R. Pamplin (Pergamon Press).
100. B.M. Wanklyn, (1975), 'Crystal Growth', Ed. B.R. Pamplin, (Pergamon Press).
101. J.W. Nielsen and R.R. Monchamp, (1970), Phase Diagrams, Ed. Allen M. Alper (Academic Press).
102. S.B. Austerman, (1977), *J. Crystal Growth*, 42, 284.
103. H. Komatsu, S. Homma, S. Kimura, Y. Miyazawa and I. Shinds, (1974), *J. Crystal Growth*, 24/25, 633.
104. K. Watanabe and Y. Sumiyoshi, (1977), *J. Crystal Growth*, 41, 1.
105. M.S. Joshi and A.V. Antony, (1980), *Bull. Mater. Sci.* 2, 31.
106. K. Sanghwal and A.R. Patel, (1974), *J. Crystal Growth*, 23, 282.
107. M.S. Joshi and A.V. Antony, (1978), *J. Mater. Sci.* 13, 939.
108. A.R. Patel and A. Venkateswara Rao, (1978), *J. Crystal Growth*, 43, 351.
109. H.K. Henisch, (1970), 'Crystal Growth in Gels', (The Pennsylvania State University Press).

110. R.J. Haüy, (1784), 'Essay d'une theorie Sur la Structure de Cristaux' (Paris).
111. J.F.C. Hessel, (1831), 'Krystallometrie oder Krystallonomie und Kristallographie' (Leipzig).
112. R.M. Aliev, (1969) 'Growth of Crystals', Vol.7, Ed. N.N. Sheftal (Consultants Bureau), p.60.
113. G. Friedel, (1907), Bull. Soc. Franc. Minera, 30, 326.
114. J.D.H. Donnay and D. Harker, (1937), Ame. Miner. 22, 446.
115. J.D.H. Donnay and G. Donnay, (1961), Compt. Rend. Acad. Sci. (Paris), 252, 908.
116. P. Hartman, (1973) 'Crystal Growth : An Introduction', Ed. P. Hartman (North Holland), p.367.
117. K. Hamamura and K. Takenouchi, (1979), J. Crystal Growth, 46, 804.
118. S. Motojima, Y. Takahashi and K. Sugiyama, (1978), J. Crystal Growth, 44, 106.
119. S. Ito, N. Yoneda, S. Shimada, A. Tsunashima, K. Kodaira and T. Matsushita, (1979), J. Crystal Growth, 47, 310.
120. K. Nakahigashi and Y. Shimomura, (1975), J. Crystal Growth, 28, 367.
121. I. Yamai and H. Saito, (1978), J. Crystal Growth, 45, 511.

122. N. Zelinger, J. Flicstein and A. Zangvil, (1977), *J. Crystal Growth*, 42, 253.
123. Y. Smooha and Y. Komen, (1977), *J. Crystal Growth*, 38, 149.
124. J. Kasahara, K. Kajiwara and T. Yamada, (1977), *J. Crystal Growth*, 38, 23.
125. O. Nittono, H. Hasegawa and S. Nagakura, (1977), *J. Crystal Growth*, 42, 175.
126. E. Schonherr and E. Winckler, (1976), *J. Crystal Growth*, 32, 117.
127. F.C. Frank, (1953), *Phil. Mag.* 44, 854.
128. J.D. Eshelby, (1953) *Phy. Rev.* 91, 755.
129. S. Amelinckx, W. Botinck, W. Dekeyser and F. Seitz, (1957) *Phil. Mag.* 8, 355.
130. G.W. Sears, (1955) *Acta Metall.* 3, 361 and 367.
131. S. Amelinckx, (1962), 'Growth and Perfection of Crystals', Eds. R.H. Doremus, B.W. Roberts and D. Turnbull (John-Wiley).
132. P.B. Price, (1960), *Phil. Mag.* 5, 873.
133. R.S. Wagner, W.C. Ellis, K.A. Jackson and S.M. Arnold, (1964), *J. Appl. Phys.* 35, 2993.
134. R.S. Wagner and W.C. Ellis, (1965), *Trans. Met. Soc. AIME*, 233, 1053.
135. R.S. Wagner and C.J. Doherty, (1968), *J. Electro Chem. Soc.* 115, 93.

136. E.I. Givargizov, (1978) 'Current Topics in Material Science' Vol.1, Ed. E. Kaldis, (North-Holland), p.87.
137. E.I. Givargizov, (1975) *Kristall und Technik*, 10, 473.
138. J.J. Nickl and W. Just, (1971), *J. Crystal Growth*, 11, 11.
139. C.A. May and J.S. Shah, (1970), *Phil. Mag.*21, 599.
140. K. Nakahigashi and Y. Shimomura, (1975), *J. Crystal Growth*, 28, 367.
141. R.S. Wagner, (1970) 'Whisker Technology' Ed.A.P. Levitt, (Wiley).
142. W.W. Webb and N.P. Bertolone, (1960), *J. Appl. Phys.* 31, 207.
143. K. Yoshida, (1964), *Jap. J. Appl. Phys.*3, 565.
144. T. Tomita, (1974), *J. Crystal Growth*, 24/25, 331.
145. Y.S. Park and D.C. Reynolds, (1967), *J. Appl. Phys.* 38, 756.
146. B. Wanklyn, (1969), *J. Crystal Growth*, 5, 279.
147. A. Gaumann and P. Bohac, (1972), *J. Crystal Growth*, 15, 304.
148. S. Simov, (1976), *J. Mat. Science*, 11, 2319.
149. E. Landvay and P. Kovacs, (1970), *J. Crystal Growth*, 4, 61.
150. K. Kumar, (1974), (1974) *J. Crystal Growth*, 26, 200.

151. C. Paorici, (1969), *J. Crystal Growth*, 5, 315.
152. C. Paorici, (1970), *J. Mat. Science*, 5, 918.
153. M. Maeda, F. Goto and K. Miyata, (1964), *Jap. J. Appl. Phys.* 3, 426.
154. H. Iwanaga and N. Shibata, (1974), *J. Crystal Growth*, 24/25, 357.
155. M.N. Chandrasekharaiiah and M.N. Krishna, (1969), *J. Crystal Growth*, 5, 213.
156. H. Frijisaki, M. Takahashi, H. Shoji and Y. Tanabe, (1963), *Jap. J. Appl. Phys.* 2, 665.
157. D.O. McKee and J.T. McMullan, (1975) *J. Crystal Growth*, 30, 143.
158. E.J. Soxman, (1963), *J. Appl. Phys.* 34, 948.
159. F.C. Frank, (1958) 'Growth and Perfection of Crystals' Eds. R.H. Doremus, B.W. Roberts and D. Turnbull (John-Wiley).
160. S.D. Sharma and L.K. Malhotra, (1971), *J. Crystal Growth*, 8, 285.
161. S. Amelinckx (1953), *Phil. Mag.* 44, 337.
162. G.G. Lemmalain, M.O. Klifa and A.A. Chernov, (1964), *Kristallogr.* 9, 213.
163. H. Iwanaga and N. Shibata, (1978), *J. Crystal Growth*, 43, 71.
164. B. Chalmers, (1964) 'Principles of Solidification', (John-Wiley).

165. K.A. Jackson, E.R. Uhlman and J.D. Hunt, (1966),
III TMS-AIME 236, 149.
166. M. Kahlweit, (1969), J. Crystal Growth, 5, 391.
167. C. Zener, (1946), TMS-AIME, 167, 550.
168. W.A. Tiller, K.A. Jackson, J.W. Rutter and
B. Chalmers, (1953) Acta Metall. 1, 428.
169. W.W. Mullins and R.F. Sekerka, (1963), J. Appl.
Phys. 34, 323.
170. S.R. Coriell, S.C. Hardy and R.F. Sekerka, (1971),
J. Crystal Growth, 11, 53.
171. S.R. Coriell, D.T.J. Hurle and R.F. Sekerka, (1976),
J. Crystal Growth, 32, 1.
172. R.T. Delves, (1975) 'Crystal Growth', Ed. B.R. Pamplin
(Pergamon Press).
173. K.A. Jackson, (1958) 'Liquid Metals and Solidification',
(ASM Cleveland).
174. R.D. Townsend and J.S. Kirkclady, (1968) ASM.
Trans. 61, 605.
175. G.P. Ivatsov, (1958) 'Growth of Crystals', Ed.
N.N. Sheftal (Consultants Bureau Inc).
176. D.E. Temkin, (1960), Dokl. Akad. Nauk. SSSR, 132, 1307.
177. R. Trivedi, (1970), Acta Metall. 18, 287.
178. G.E. Purdy, (1971) Metal Sci. J. 5, 81.
179. J.S. Langer, (1980), Rev. Mod. Phys. 52, 1.
180. M.E. Glicksman, Schaefero and J.D. Ayers, (1976)
Metall. Trans. 7, 1747.

181. G.E. Nash and M.E. Glicksman, (1974) *Acta Metall.* 22, 1283.
182. J.S. Langer and H. Muller-Krumbhaar, (1978), *Acta Metall.* 26, 1681.
183. J.S. Langer, R.F. Sekerka and T. Frijioka, (1978), *J. Crystal Growth*, 44, 414.
184. A. Johannsen, (1939) 'A Descriptive Petrography of Igneous Rocks', 2nd Ed. (University of Chicago, Illinois).
185. H.D. Keith and F.J. Padden Jr., (1963) *J. Appl. Phys.* 34, 2409.
186. G. Gross, R.B. Stephens and D. Turnbull, (1977), *J. Appl. Phys.* 48, 1139.
187. B. Wunderlich, (1973) 'Macromolecular Physics', Vol.1 (Academic Press).
188. H.D. Keith, F.J. Padden, N.M. Walter and H.W. Wyckoff, (1959), *J. Appl. Phys.* 30, 1485.
189. J. George and S.K. Premachandran, (1979), *J. Crystal Growth*, 46, 297.
190. J.P. Hirth and J. Lothe, (1967) 'Theory of Crystal Dislocations', (Clarendon Press, Oxford).
191. J. Weertman and J.R. Weartman, (1964) 'Elementary Dislocation Theory', (MacMillan, New York).
192. W. Bollmann, (1970), 'Crystal Defects and Crystal-line Interfaces', (Springer-Verlag).

193. F.C. Frank and W.T. Read, (1950), Phys. Rev. 79, 722.
194. W.L. Bragg, (1940), Proc. Phy. Soc. (London), 52, 54.
195. J.M. Burgers (1940), Proc. Phy. Soc. (London), 52, 23.
196. J. Friedel, (1967) 'Dislocations' (Addison-Wesley).
197. F.C. Frank, (1950), Proc. Phys. Soc. A62, 131.
198. R. Peierls, (1940), Proc. Phy. Soc. 52, 34.
199. F.R.N. Nabarro and P.J. Jackson, (1958), Phil. Mag. 3, 1105.
200. V.A. Phillips, (1971) 'Modern Metallographic Techniques and Their Applications', (Wiley-Interscience).
201. H.C. Gatos, (1975) 'Crystal Growth and Characterisation' Eds. R.Ueda and J.B. Mullin (North-Holland).
202. J.J. Gilman, (1960), 'The Surface Chemistry of Metals and Semiconductors' Ed.H.C.Gatos (John Wiley).
203. S. Amelinckx, (1964), 'Direct Observation of Dislocations' (Solid State Physics Supplement) Vol.6, Eds. F. Seitz and D. Turnbull (Academic Press).
204. P.F. Kane and G.B. Larrabee, (1970), 'Characterisation of Semiconductor Materials' (McGraw-Hill).

205. N. Cabrera, (1960), 'The Surface Chemistry of Metals and Semiconductors', Ed.H.C. Gatos, (John-Wiley), p.71.
206. H. Nishikawa, (1973), Japan J. Appl. Phys. 12, 1647.
207. A.R. Patel and A. Venkateswara Rao, (1979), J. Crystal Growth, 47, 213.
208. W.A. Wooster, (1976), Kristal und Technik, 11, 615.
209. A. Koma, E. Takimoto and S. Tanaka, (1970), Phys. Stat. Solidi, 40, 239.
210. V. Hari Babu and K.G. Bensigir, (1967), J. Phys. Soc. Japan, 23, 860.
211. K. Somaiah and V. Hari Babu, (1979), J. Crystal Growth, 46, 711.
212. J. George and P.K. Sarangadharan, (1977), J. Phys. D : Appl. Phys. 10, 1467.
213. J. George and P.K. Sarangadharan, (1978), Presented at the IXth National Conference on Crystallography, India, held at Sardar Patel University, Gujarat, India.
214. J.D. Livingston, (1961), General Electric Research Laboratory Report No.61-RL-2620M.
215. J.J. Gilman, W.G. Johnston and G.W. Sears, (1958), J. Appl. Phys. 29, 747.
216. W.C. Dash, (1958), J. Appl. Phys. 29, 705.

217. Y. Ito and Y. Furuhashi, (1974) Phys. Stat. Sol(a) 23, 147.
218. K. Sato, K. Yokoyama, H. Kouchi and M. Okada, (1978) Jap. J. Appl. Phys. 17, 1483.
219. T.M. Hedges and J.W. Mitchell, (1953) Phil. Mag. 44, 223.
220. S. Amelinckx, Gevers. R, G. Remnaut and Van Landuyut, (1970), 'Modern Diffraction and Imaging Techniques in Material Science', (North-Holland).
221. H.J. Meyer and H. Dabringhans, (1978), 'Current Topics in Materials Science', Ed. E. Kaldis, (North-Holland).
222. K.W. Keller, (1975) 'Crystal Growth and Characterisation' Ed. R.Ueda and J.B. Mullin (North-Holland).
223. A.R. Lang (1973), 'Crystal Growth : An Introduction', Ed. P. Hartman (North-Holland).
224. W. Berg, (1931) Naturwissenschaften, 19, 391.
225. G. Borrmann, H. Hartwig and H. Irmeler, (1958), Z. Naturforsch, 13a, 423.
226. C.S. Barrett, (1945), Trans. AIME. 161, 15.
227. W.W. Webb, (1969) 'Direct Observation of Imperfections in Crystals', Eds. J.B. Newkirk and J.H. Wernick, (Interscience, New York).

228. A.R. Lang, (1958) *J. Applied Phys.* 29, 597;
(1959) *Acta Cryst.* 12, 249.
229. N. Kato, (1975) 'Crystal Growth and Characterisation' Eds. R. Ueda and J.B. Mullin (North-Holland).
230. D.B. Bolt, (1975) 'Crystal Growth', Ed. B.R. Pamplin, (Pergamon Press).
231. A. Authier, (1977) 'Crystal Growth and Materials', Eds. E. Kaldis and H.J. Scheel (North-Holland).
232. A. Izrael, J.F. Petroff, A. Authier and Z. Malek, (1972), *J. Crystal Growth*, 16, 131.
233. R.A. Duokett and A.R. Lang, (1973), *J. Crystal Growth*, 18, 135.
234. K. Naukkarinen, (1976) Thesis for the Degree of Doctor of Technology, Helsinki University of Technology, Helsinki, Finland.
235. T. Tuomi, K. Naukkarinen, E. Laurila and P. Rabe, (1973) *Acta Polytech. Scand.* Ph100, 1.
236. T. Tuomi, K. Naukkarinen, P. Rabe, (1974), *Phys. Stat. Sol. (a)* 25, 93.
237. P.B. Hirsch, A. Howie and M.J. Whelan, (1960), *Phil. Trans. Roy. Soc.* A252, 499.
238. P.B. Hirsch, A. Howie, R.B. Nicholson, D.W. Pashley and M.J. Whelan, (1965) 'Electron Microscopy of Thin Crystals', (Butterworth, London).

239. D.R. Clarke, (1970), *J. Mat. Sci.* 5, 689.
240. P. Morin, M. Pitaval, D. Besuard and G. Foutaine, (1979) *Phil. Mag.* A.40, 511.
241. M. Tajima, Y. Okada and Y. Tokumaru, (1978), *Jap. J. Appl. Phys. Supplement*, 17-1.
242. B. Rosenberg, (1958) *J. Chem. Phys.* 29, 1108.
243. D.C. Northrop and O. Simson, (1956) *Proc. Roy. Soc. (London)* A234, 124.
244. D.J. Carswell, J. Ferguson and L.E. Lyons, (1954) *Nature* 173, 736.
245. D.D. Eley, (1959) *Research (London)*, 12, 293.
246. D.J. Kommandeur, (1967) *Physics and Chemistry of the Organic Solid State*, Vol.II, Eds. D. Fox, M.M. Labes and A. Weissberger.
247. H. Kallmann and M. Pope, (1960), *J. Chem. Phys.* 32, 300.
248. H. Inokuchi and H. Akamatu, (1961) *Solid Stat. Phys.* 12, 108.
249. A. Bradley and J.P. Hammes, (1963), *J. Electrochem. Soc.* 110, 543.
250. P.J. Reucroft, O.N. Rudyj and M.M. Labes, (1963), *J. Am. Chem. Soc.* 85, 2059.
251. A. Many, E. Harnik and D. Gerlich, (1955), *J. Chem. Phys.* 23, 1733.
252. H. Kallmann, (1958) *Disc. Farad. Soc.* 27, 240.

253. G.H. Heilmeyer, G. Warfield and S.E. Harrison,
(1963), J. Appl. Phys. 34, 2278.
254. O.H. LeBlanc. Jr., (1963), J. Chem. Phys. 39, 2395.
255. H. Frohlich and G.L. Sewell, (1959) Proc. Phys.
Soc. (London) 74, 643.
256. R.G. Kepler, (1960), Phys. Review, 119, 1226.
257. O.H. LeBlanc Jr. (1960), J. Chem. Phys. 33, 626.
258. J. Riga, J.J. Verbist, F. Wudl and A. Kruger,
(1978) J. Chem. Phys. 69, 3221.
259. J. Gavis, (1964), J. Chem. Phys. 41, 3787.
260. C.M. Huggins and A.H. Sharbaugh, (1963), J. Chem.
Phys. 38, 393.
261. P.L. Kronick, and M.M. Labes, (1961) J. Chem. Phys.
35, 2016.
262. J. Ehlers, K. Kepp, R. Kippenhahn, H.A. Weidenmuller
and J. Zittartz (Eds.), (1977) 'Organic Conductors
and Semiconductors', (Springer-Verlag).
263. R.J. Warmack and T.A. Callcott, (1975) Phys. Rev.
B. 12, 3336.
264. Y. Matsunaga, (1965), J. Chem. Phys. 42, 1982.
265. A. Taniguchi, S. Kanda, T. Nogaito, S. Kusabayashi,
H. Mikawa and K. Ito, (1964), Bull. Chem. Soc.
Japan, 37, 1386.
266. F. Gutmann and E. Lyons, (1967) 'Organic Semi-
conductors' (John Wiley and Sons).

267. H.A. Pohl, D.A. Opp, (1962), J. Phys. Chem. 66, 2121.
268. M.J. Rice, (1977) Solid Stat. Commun. 21, 757.
269. W.J. Gunning, S.K. Khanna, A.F. Garito and A.J. Heeger, (1977) Solid Stat. Commun. 21, 765.
270. H. Arend and W. Huber, (1972), J. Crystal Growth, 12, 179.
271. H.J. Guggenheim and D. Bahnck, (1974), J. Crystal Growth, 26, 29.
272. M.L. Kaplan, (1976), J. Crystal Growth, 33, 161.
273. H. Anzai, (1976), J. Crystal Growth, 33, 185,
274. R.C. Sangster and J.W. Irvine, (1956) J. Chem. Phys. 24, 670.
275. J.A. James and R.C. Kell, (1975) 'Crystal Growth', Ed. B.R. Pamplin (Pergamon Press), p.557.
276. J.C. Brice, (1973), 'Growth of Crystals from Solution' (North-Holland), p.292.
277. J. George and S.K. Premachandran, (1978), J. Crystal Growth, 43, 126.
278. S. Tolansky, (1948) 'Multiple Beam Interferometry', (Clarendon Press, Oxford).
279. S. Tolansky, (1955) 'An Introduction to Interferometry' (Longmans Green, London).
280. S. Tolansky, (1970), 'Multiple Beam Interference Microscopy of Metals' (Academic Press).

281. S. Tolansky, (1949), 'Multiple-Beam Interferometry of Surfaces and Films' (Oxford).
282. P. Groth, (1910), *Chemische Kristallographie*, 4, 712.
283. M.B. Williams, W.P. Van Meter and W.C. McCrone, (1952), *Analyt. Chem.* 24, 911.
284. O.N. Pandey, (1954), *Science and Culture*, 20, 254.
285. K.C. Banerji, (1956), *Proc. Natn. Acad. Sci. India*, 25A, 115.
286. R.S. Bradley, (1958), 'Growth and Perfection of Crystals', Eds. R.H. Doremus, B.W. Roberts and D. Turnbull (Wiley), p.133.
287. H.E. Buckley, (1951), 'Crystal Growth', (Wiley).
288. P. Groth, (1917), *Chemische Kristallographie*, 4, 724.
289. Y. Okaya and Pepinsky, (1957), *Acta Cryst.* 10, 324.
290. Y. Okaya, (1965), *Acta Cryst.* 19, 879.
291. G. Bohm and K. Ulmer, (1971), *J. Crystal Growth*, 10, 175.
292. G.W. Sears, (1955), *Acta. Metall.* 3, 361.
293. R.G. Crystal and D. Hansen, (1967), *J. Appl. Phys.* 38, 3103.
294. I.L. Hay and A. Keller, (1965), *Kolloid. Z.Z. Polymere*, 204, 43.
295. M.C. Coughlin and B. Wunderlich, (1972), *J. Polymer Sci. Part B*, 10, 57.

296. Keith and Padden Jr., (1963), *J. Appl. Phys.*
34, 2409.
297. P. Hartman, (1963), 'Physics and Chemistry of
Organic Solid State', Eds. D. Fox, M.M. Labes
and A. Weissberger, Vol.I (Interscience
Publishers), p.404.
298. K.A. Jackson and J.D. Hunt, (1965), *Acta Metall.*
13, 1212.
299. J. George and S.K. Premachandran, (1979), *J.*
Phys. D : Appl. Phys. 12, 1129.
300. J.L. Stevenson, (1977), *J. Crystal Growth*, 37, 118.
301. R. Doherty, (1975), 'Crystal Growth', Ed.B.R.
Pamplin (Pergamon Press), p.581.
302. J. Beynon and Saunders, (1960), *Brit. J. Appl.*
Phys. 11, 128.
303. G.F. Reynolds, (1969), *Physics and Chemistry of*
Organic Solid State, Vol.I, Eds. D. Fox,
M. Labes and A. Weissberger (Interscience
Publishers).
304. G. Dahlgren and N.L. Simmerman, (1965), *J. Phys.*
Chem. 69, 3626.
305. E.H. Huntress and S.P. Mulliken, (1941), 'Identi-
fication of Pure Organic Compounds' (John
Wiley), p.148.
306. I.L. Finar, (1973), *Organic Chemistry*, Vol.I,
(McGraw-Hill), p.777.

307. A. Sagar and J.W. Faust, (1966), Phys. Letts. 23, 406; (1967), J. Appl. Phys. 38, 2240; (1967), J. Appl. Phys. 38, 482.
308. J.J. Gilman and W.G. Johnston, (1962), 'Solid State Physics', Vol.13, Eds. F. Seitz and D. Turnbull (Academic Press).
309. V.P. Bhatt and G.R. Pandya, (1973), J. Phys. Q: Solid State Phys. 6, 36.
310. W.C. Dash, (1958), J. Appl. Phys. 29, 705.
311. S. Amelinckx, (1964), 'Direct Observation of Dislocations', (Academic Press), p.40.
312. W.A. Wooster, (1976), Kristall und Technik, 11, 615.
313. S. Amelinckx, (1960), J. Appl. Phys. 31, 1359.
314. M.S. Joshi and M.A. Ittyachen, (1969), Indian J. Pure and Appl. Phys. 7, 678.
315. M.S. Joshi and M.A. Ittyachen, (1969), Indian J. Pure and Appl. Phys. 7, 624.
316. F.W. Young, (1961), J. Appl. Phys. 32, 192.
317. S. Mendelson, (1961), J. Appl. Phys. 32, 1579.
318. J.W. Davisson and S. Levinson, (1966), J. Appl. Phys. 37, 4888.
319. H.C. Gatos, (1975), 'Crystal Growth and Characterisation', Ed. R. Ueda and J.B. Mullin, (North-Holland), p.313.
320. W.J.P. Van Enckevort and W.H. Van Der Linden, (1979), J. Crystal Growth, 47, 196.

321. K. Sato and M. Okada, (1977), *Nature*, 269, 399.
322. T.W. Read, (1954), 'Dislocations in Crystals', (McGraw Hill), p.207.
323. S. Amelinckx, (1956), *Phil. Mag.* 8, 269.
324. M.S. Joshi and M.A. Ittyachen, (1969), *Indian J. Pure and Appl. Phys.* 7, 678.
325. M.S. Joshi, M.A. Ittyachen and P.N. Kotru, (1978), *Pramana*, 10, 601.
326. S.H. Emara, B.R. Lawn and A.R. Lang, (1969), *Phil. Mag.* 19, 7.
327. S. Gits Leon, F. Lefauchaux and M.C. Robert, (1978), *J. Crystal Growth*, 44, 345.
328. S.F. Pough, (1967), *Brit. J. Appl. Phys.* 18, 129.
329. J.H. Westbrook, (1973), 'The Science of Hardness Testing and its Applications', Eds. J.H. Westbrook and H. Conrad (American Society for Metals), p.491.
330. J.J. Gilman, C. Knudsen and W.P. Walsh, (1958), *J. Appl. Phys.* 29, 601.
331. J.J. Gilman and D.W. Stauff, (1958), *J. Appl. Phys.* 29, 120.
332. H. Mette and H. Pick, (1953), *Z. Physik*, 134, 566.
333. M. Matsumoto and T. Tsukada, (1964), *Bull. Chem. Soc. Japan*, 37, 1545.
334. Y. Yamamoto, K. Yoshino and Y. Inuishi, (1979), *J. Phy. Soc. Japan*, 47, 1887.

335. G.H. Heilmair and G. Warfield, (1963), Phys. Rev. 132, 2010.
336. H. Riehl, (1959), 'Electrical Conductivity in Organic Solids', Eds. Kallmann and M. Silver, (Interscience).
337. E.O. Forster, (1962), J. Chem. Phys. 37, 1021.
338. P.K. Mitskevich and M.I. Bashmakova, (1964), Russian J. Phys. Chem. 6, 869.
339. O.H. LeBlanc Jr., (1962), J. Chem. Phys. 37, 916.
340. D.D. Eley and G.D. Parfitt, (1955), Trans. Faraday Soc. 51, 1529.
341. M. Wilk, (1960), Z. Elektrochem. 64, 930.
342. D.C. Northrop and O. Simpson, (1956), Proc. Roy. Soc. London, A234, 124.
343. B. Rosenberg, (1958), J. Chem. Phys. 29, 1108; (1959), J. Chem. Phys. 31, 238; (1961), J. Chem. Phys. 34, 812; (1961), J. Chem. Phys. 35, 982; (1962), J. Chem. Phys. 37, 1371.
344. S. Iwata, J. Thanaka and S. Nagakura, (1967), J. Chem. Phys. 47, 2203.
345. G.E. Hardy, J.C. Baldwin, J.I. Zink, W.C. Kaska, P.H. Lin and L. Dubois, (1977), J. Am. Chem. Soc. 99, 3552.
346. F. Gutman and L.E. Lyons, (1967) 'Organic Semiconductors', (John Wiley), p.361.

347. R. Foster, (1969), 'Organic Charge-Transfer Complexes', (Academic Press), p.52.
348. M.E. Peover, (1962), Trans. Farad. Soc. 58, 2370.
349. F. Gutman and L.E. Lyons, (1967), 'Organic Semiconductors', (John Wiley), p.358.
350. K. Saibabu and T. Chiranjivi, (1980), J. Phys. C : Solid State Phys. 13, L587.
351. M. Samoc, C. Gilbert, J.B. Webb and D.F. Williams, (1980), J. Phys. C : Solid State Phys. 13, 4419.
352. F. Gutman and L.E. Lyons, (1967), 'Organic Semiconductors', (John Wiley), p.368.
353. Y.H. Park and B.W. Lau, (1971), J. Korean Phys. Soc. 4, 39.

ACKNOWLEDGEMENTS

I am deeply indebted to Professor Joy George for introducing me into the fascinating field of crystals. I should like to express my gratitude to him for the constant encouragement and invaluable guidance I have received, without which it would not have been possible to bring the present work to a successful culmination.

I wish to extend my sincere thanks to Professor K. Sathianandan, Head of the Department of Physics for providing excellent laboratory and library facilities and for his interest in the work.

I am extremely thankful to all members of the faculty, office staff and technical personnel for their friendly assistance throughout the period of research,

I am especially thankful to Fr.E.C. Joy and Mr.P.K. Sarangadharan for the many discussions, which have inspired me much.

I am happy to acknowledge the cooperation and companionship extended to me by all fellow research scholars--especially, Mr.M.K. Radhakrishnan, Mr.A.V.Alex, Mr.K.S. Joseph, Miss Susy Abraham, Fr.George Pittappilly, Mr.T.I. Palson and Mr.B. Pradeep.

It would be impossible to name everyone to whom I would like to convey thanks for making my stay in the campus pleasant and memorable.

I wish to thank the University of Cochin for awarding me a junior research fellowship in the early stages of the present work. I would also like to acknowledge the Council of Scientific and Industrial Research for the award of a junior research fellowship from 1976-'78 and a senior research fellowship thereafter.

- G 2586 -